A THEORETICAL STUDY ON ENHANCEMENT OF HEAT TRANSFER IN A SOLAR AIR HEATER COLLECTOR BY USING POROUS MEDIA

Özgür ÇEKMER

İzmir Institute of Technology
July, 2011

A THEORETICAL STUDY ON ENHANCEMENT OF HEAT TRANSFER IN A SOLAR AIR HEATER COLLECTOR BY USING POROUS MEDIA

A Thesis Submitted to
the Graduate School of Engineering and Sciences of
İzmir Institute of Technology
in Partial Fulfilment of the Requirements for the Degree of

MASTER OF SCIENCE

in Energy Engineering

by
Özgür ÇEKMER

July, 2011

İZMİR

We approve the thesis of **Özgür ÇEKMER**

_____
Assoc.Prof.Dr. Moghtada MOBEDI
Supervisor

_____
Prof.Dr.M. Barış ÖZERDEM
Co-Supervisor

_____
Prof.Dr. Zafer İLKEN
Committee Member

_____
Assoc.Prof.Dr. Serhan KÜÇÜKA
Committee Member

6 July 2011

_____
Assoc.Prof.Dr. Gülden GÖKÇEN AKKURT
Head of the Department of
Energy Engineering

_____
Prof.Dr.Durmuş Ali DEMİR
Dean of the Graduate School of
Engineering and Sciences

ACKNOWLEDGEMENTS

I would like to express my sincere gratitude to my supervisor Dr. Moghtada MOBEDI for his valuable advises. I also would like to thank my co-advisor, Dr. M. Barış ÖZERDEM, for his contributions.

My continual advisor, Dr. Şule ERGÜN, deserves the best words for her everlasting supports.

I would like to thank my grandmother, my grandfather, and my sister. Special words are deserved by my mother, Gülsüm KÜPELİ (the best physicist I have ever known) for being a great mentor to me.

I would like to express the great contribution of my wife, Hayriye BOZKURT ÇEKMER (the best engineer I have ever known), to my thesis and myself. I would like to thank her for drawing my figures, breathing with me on my hardest days and her supports from the beginning, till the end.

ABSTRACT

A THEORETICAL STUDY ON ENHANCEMENT OF HEAT TRANSFER IN A SOLAR AIR HEATER COLLECTOR BY USING POROUS MEDIA

In this study; a theoretical work is performed on heat and fluid flow in a solar-air heater collector partially filled with porous medium. The most of the efforts are paid to understand the characteristics of heat and fluid flow in a duct filled with the porous media. Various porous–clear media configurations are investigated. The buoyancy effects are neglected. The air flow in the channel is assumed to be incompressible, laminar, and hydrodynamically fully developed. For the porous regions, Darcy and Darcy-Brinkman models are used to obtain the velocity profile. In all chapters, dimensionless forms of the governing equations for the heat and the fluid flow are used. In the chapters with asymmetric cases, three different Nusselt numbers are defined; two individual Nusselt numbers for the upper and the lower wall, and an overall Nusselt number. The study is mainly focused on heat transfer enhancement by using porous media and only for a few cases pressure-drop analyses are performed. It is concluded that the use of a porous medium affects the heat transfer significantly, and the rate of effect is influenced by the thickness and location of porous media. Finally, a two-dimensional study including thermally entrance region for an air-solar collector with partially filled porous medium is performed. It is observed that the outlet and mean temperature along the channel are significantly affected by upper wall energy loss, and thickness and conductivity of the porous medium.

ÖZET

GÖZENEKLİ ORTAM KULLANILARAK HAVA ISITICILI GÜNEŞ KOLEKTÖRLERİNDE ISI GEÇİŞİNİN ARTIRILMASI ÜZERİNE TEORİK BİR ÇALIŞMA

Bu tezde; kısmen gözenekli ortam doldurulmuş bir hava ısıtıcılı güneş kolektörünün akışkan ve ısı akışı üzerine, teorik bir çalışma yapılmıştır. Gözenekli yapı karakteristiğinin anlaşılmasına ağırlık verilmiş ve bir kanalda farklı boş - gözenekli ortam yapılandırmaları incelenmiştir. Serbest taşınım etkileri ihmal edilmiş, dolayısıyla temel ısı transferi biçimi zorlamalı taşınım olarak kabul edilmiştir. Hava akışı; sıkıştırılamaz, laminar, ve ısıl ve hidrodinamik açıdan tam gelişmiş kabul edilmiştir. Gözenekli ortamlardaki hız dağılımının eldesi için Darcy ve Brinkman-Darcy modelleri kullanılmıştır. Nusselt sayısının ve sıcaklık dağılımının eldeleri için enerji dengesi denklemi kullanılmıştır. Tezin bütün bölümlerinde, ısı ve momentum akışı için uygulanan denklemlerin boyutsuz formları kullanılmıştır. Asimetrik durumlar içeren bölümlerde, üç ayrı Nusselt sayısı elde edilmiştir; alt ve üst duvar için iki Nusselt sayısı ve genel Nusselt sayısı. Bütün bu analizler, ağırlıklı olarak gözenekli ortam kullanılarak ısı geçişinin artırılması üzerine yapılmıştır ve sadece birkaç durum için basınç düşümü hesapları yapılmıştır. Çalışma; gözenekli yapının ısı geçişini önemli ölçüde etkilediği ve bu etkilerin; gözenekli yapının; kalınlığı ve kanal içindeki yeri ile değiştiği sonucuna varmıştır. Son olarak, kısmen gözenekli yapıyla dolu bir hava-güneş kolektöründeki ısı ve momentum akışı incelenmiştir. Kolektör kanalının sonunda, akışkan sıcaklığının gözenekli ortam kullanıldığında önemli ölçüde arttığı gözlenmiştir.

TABLE OF CONTENTS

LIST OF FIGURES ix

LIST OF TABLES xii

LIST OF SYMBOLS xiii

CHAPTER 1. INTRODUCTION 1
1.1.Solar Energy 1
1.2. Solar Air Heater 2
1.3. Heat Transfer Enhancement 3
1.4. Porous Media 5
1.5. Heat Transfer Enhancement by Using Porous Media 6
1.6. Literature Survey 7
1.7. Aim of the Present Study 11

CHAPTER 2.HEAT AND FLUID FLOW IN POROUS MEDIA 14
2.1. Fluid Flow in Porous Media 14
2.1.1. Darcy's Law 15
2.1.2. Brinkman-Extended Darcy's Law 16
2.1.3. Forchheimer Extended Darcy's Law 16
2.1.4. Brinkman-Forchheimer Extended Darcy's Law 17
2.2. Heat Flow in Porous Media 18

CHAPTER 3.FULLY DEVELOPED FLOW IN A CHANNEL WITH CLEAR FLUID: SYMMETRIC AND ASYMMETRIC HEAT FLUX BOUNDARY CONDITIONS 19
3.1. The Concept of Fully Developed Condition 19
3.1.1. Hydrodynamically Fully Developed Flow 19
3.1.2. Thermally Fully Developed Flow 21
3.2 First Case: Symmetric Heat Fluxes at the Walls 22
3.2.1. Fluid Flow Analysis 22
3.2.2. Heat Flow Analysis 24
3.3. Second Case: Asymmetric Heat Fluxes at the Walls 28
3.3.1. Fluid Flow Analysis 28
3.3.2. Heat Flow Analysis 28

CHAPTER 4.FULLY DEVELOPED HEAT AND FLUID FLOW IN A POROUS CHANNEL: SYMMETRIC HEAT FLUX BOUNDARY CONDITIONS 35
4.1. Problem Definition 35
4.2. Fluid Flow Analysis 36
4.3. Heat Flow Analysis 38
4.4. Pressure Drop Calculations 42
4.5. Analysis of Heat Transfer and Pressure Drop 42

CHAPTER 5. FULLY DEVELOPED HEAT AND FLUID FLOW IN A POROUS CHANNEL: ASYMMETRIC HEAT FLUX BOUNDARY CONDITIONS ... 44

5.1. Problem Definition 44
5.2. Fluid Flow Analysis 45
5.3. Heat Flow Analysis 47

CHAPTER 6. FULLY DEVELOPED HEAT AND FLUID FLOW IN A PARTIALLY POROUS CHANNEL: SYMMETRIC HEAT FLUX BOUNDARY CONDITIONS 52
6.1. Problem Definition 52
6.2. Fluid Flow Analysis 52
6.3. Heat Flow Analysis 56
6.4. Pressure Drop Calculations 62
6.5. Analysis of Heat Transfer and Pressure Drop 63

CHAPTER 7. FULLY DEVELOPED HEAT AND FLUID FLOW IN AN ASYMMETRIC PARTIALLY POROUS CHANNEL: SYMMETRIC CONSTANT HEAT FLUXBOUNDARY CONDITIONS 65
7.1. Problem Definition 65
7.2. First Approach: Brinkman-Extended Darcy Law 66
7.2.1. Fluid Flow Analysis 66
7.2.2. Heat Flow Analysis 71
7.3. Second Approach: Darcy Law 78
7.3.1. Fluid Flow Analysis 78
7.3.2. Heat Flow Analysis 80
7.4. Pressure Drop Calculations 86
7.5. Analysis of Heat Transfer and Pressure Drop 87

CHAPTER 8. HEAT AND FLUID FLOW IN A SOLAR AIR HEATER COLLECTOR PARTIALLY FILLED WITH POROUS MEDIA 89
8.1. Problem Definition 89
8.2. Fluid Flow Analysis 90
8.3. Heat Flow Analysis 92
8.4. Pressure Drop Calculations 95
8.6. Numerical Solution Procedure 97

CHAPTER 9. RESULTS AND DISCUSSION 99
9.1. Results for Flow in a Clear Channel 99
9.2. Results for Flow in a Porous Channel with Symmetrical Heating 101
9.3. Results for Flow in a Porous Channel with Asymmetric Heating 105
9.4. Results for Chapter 6: Flow in a Symmetrically Filled Partial Porous Channel 111
9.5. Results for Flow in an Asymmetrically Filled Partial Porous Channel 119
9.6. Results for Flow in a Solar Air Heater 127

CHAPTER 10. CONCLUSION 135

REFERENCES 137

APPENDICES
APPENDIX A. THE COMPATIBILITY CONDITION 140
APPENDIX B. THE NUMERICAL SOLUTION PROCEDURE 142

LIST OF FIGURES

Figure **Page**

Figure 1.1. The schematic view of a simple solar collector 2
Figure 1.2. A solar air heater collector used in the study of G. Alvarez et al. 3
Figure 1.3. Another solar air heater used by Sreekumar who made the techno-economic analysis of it. 3
Figure 1.4. A surface is getting cooled by a fluid 4
Figure 1.5. Heat transfer enhancement by using fins. 4
Figure 1.6. Schematic demonstration of a porous medium 5
Figure 1.7. An example porous medium: A typical fuel array for a PWR. 5
Figure 1.8. Microscopic vs. Macroscopic View 6
Figure 1.9. The schematic view of the channel in the forced convection, porous media study of Hooman 7
Figure 1.10 Satyamurty and Bhargavi performed a numerical study to find the optimum porous medium fracture for Nusselt number. 9
Figure 1.11.A physical demonstration of the tube that Yang et al. studied. 9
Figure 1.12. A double-pass solar collector used in the study of Sopian et al. 10
Figure 1.13. One of the results of the experimental study of Sopian et al. 10
Figure 1.14. The physical demonstration of the domain in the study of Al-Nimr 11
Figure 1.15. The schematic view of a solar collector wanted to be investigated.. 12
Figure 3.1. Hydrodynamic entrance and fully developed regions in a channel 20
Figure 3.2. Shear force acted on a fluid molecule 20
Figure 3.3. Thermal entrance and fully developed regions in a channel 21
Figure 3.4. Schematic view of the problem 22
Figure 3.5. Total energy of the fluid is conserved. 25
Figure 3.6. Schematic demonstration of the considered problem.. 28
Figure 3.7. Total energy of the fluid is conserved. 30
Figure 4.1. Schematic view of the channel that the fluid flows 35
Figure 4.2. Total energy of the fluid is conserved. 40
Figure 5.1.Schematic view of the channel that the fluid flows through. 44
Figure 5.2. Signs of the individual Nusselt numbers 51
Figure 6.1. The schematic view of the channel which is wanted to be investigated 52
Figure 6.2. Upper clear region of the channel 54
Figure 6.3. Lower clear part of the channel 55
Figure 6.4. Porous part of the channel 55
Figure 6.5. Total energy of the fluid is conserved. 58
Figure 7.1. The schematic view of the channel which is wanted to be investigated 65
Figure 7.2. The schematic view of the dimensionless channel wanted to be investigated 68
Figure 7.3. Upper clear region of the channel 68
Figure 7.4. Lower clear part of the channel 69
Figure 7.5. Porous part of the channel 69
Figure 7.6. Total energy of the fluid is conserved. 72
Figure 8.1. Physical demonstration of the solar air heater collector, which is wanted to be investigated 89
Figure 8.2. Energy balance for the clear fluid region 92

Figure 8.3. Energy balance for the porous region 93
Figure 8.4. The energy balance for the upper wall..... 94
Figure 8.5. The nodes used in the numerical solution..... 94
Figure 9.1. Normalized velocity distribution of a fluid in a clear channel..... 100
Figure 9.2. Dimensionless temperature distribution of a fluid in a clear channel..... 100
Figure 9.3. Dimensionless velocity distributions for the flows with four different darcy numbers 101
Figure 9.4. Normalized velocity distribution for fully porous channel for different Darcy number 102
Figure 9.5. Dimensionless temperature vs. Y-axis for the flows with four different Darcy numbers 102
Figure 9.6. Nusselt number variation with darcy 103
Figure 9.7. Logarithmic plot of Nu vs. Da 103
Figure 9.8. Logarithmic plot of heat transfer increment ratio vs. Da..... 104
Figure 9.9.Logarithmic plot of pressure drop increment ratio vs. Da 104
Figure 9.10.Logarithmic plot of overall performance..... 105
Figure 9.11. Nusselt number variation with darcy 107
Figure 9.12. Individual Nusselt number variations with darcy for Da=100..... 108
Figure 9.13. Variation of individual Nusselt number with absolute value of heat flux ratio when Da = 01, 0.01 and 0.001 a) lower plate, b) upper plate..... 110
Figure 9.14. Critical heat flux ratio variation with darcy number..... 110
Figure 9.15. Normalized velocity distributions for flows with different Darcy numbers in a channel with different porous thicknesses..... 112
Figure 9.16. Dimensionless temperature profiles for flows with different Darcy numbers in a channel with different porous thicknesses 114
Figure 9.17. The heat transfer increment ratio for flows with different Darcy numbers in a channel with different conductivity ratios 115
Figure 9.18. The pressure drop ratio for flows with different Darcy number flows in a channel..... 116
Figure 9.19. The overall performances for flows with different Darcy numbers in a channel with different conductivity ratios 117
Figure 9.20. The heat transfer increment ratio vs. conductivity ratio 118
Figure 9.21. The overall performances vs. conductivity ratio 119
Figure 9.22. Normalized velocity distribution for M=1.1, ξ1=0.5 and ξ2=0.5 by (a) first approach: Darcy's Law (Beaver-Joseph boundary conditions are used at the interfaces), and (b) second approach: Brinkman Extended Darcy's Law (Shear stresses are accepted to be equal at the interfaces)..... 120
Figure 9.23. Normalized velocity distribution for ξ1=0.5 and ξ2=1 (a) first approach (b) second approach..... 121
Figure 9.24. Two individual and overall Nusselt number variation with porous location when M=1.1 and porous length=1 124
Figure 9.25. Two individual and overall Nusselt number variation with porous location when M=5 and porous length=1 125
Figure 9.26. Two individual and overall Nusselt number variation with porous location when M=10 and porous length=1 126
Figure 9.27. The velocity distribution in the case of the maximum lower plate Nusselt number..... 127

Figure 9.28. (a)Velocity distributions for three different darcy numbers, (b) temperature distribution for Da=0.01, (c) mean temperature along the X-axis for Da=0.01, (d) outlet temperature distribution along the Y-axis for Da=0.01 128
Figure 9.29. Comparison of outlet temperatures with three Nusselt number flows..... 129
Figure 9.30. Comparison of mean temperatures with three Nusselt number flows 129
Figure 9.31. Comparison of outlet temperatures with three porous media with different conductivity ratios (Nu=0.01)..... 130
Figure 9.32. Comparison of mean temperatures with three porous media with different conductivity ratios (Nu=0.01)..... 131
Figure 9.33. Comparison of outlet temperatures with three different porous media thicknesses..... 132
Figure 9.34. Comparison of mean temperatures with three different porous media thicknesses..... 132
Figure 9.35. Performance analysis of the solar air heater collector assisted by a porous medium with kr=10000. (a)Heat transfer increment ratio against the porous thickness ($0 \leq \xi \leq 1.6$) (a)Pressure drop increment ratio against ξ, (c)Overall performance against ξ..... 134

LIST OF TABLES

Table **Page**

Table 9.1. Comparison of the analytical and numerical results for the Nusselt numbers of a flow in a porous medium when Da = 0.01 106

Table 9.2. Comparison of the Nu, Nu_l and Nu_u variation for a clear fluid and a porous medium for Da=1000 106

Table 9.3. Nusselt numbers for flows in various media (a) M=1.1, (b) M=10 113

Table 9.4. Conductivity ratios for specified fluid-solid combinations 114

Table 9.5. Nusselt numbers for various porous medium locations for dimensionless porous length of 1 122

Table 9.6. Nusselt numbers for various porous medium locations for dimensionless porous length of 0.5 122

Table 9.7. Nusselt numbers for various conductivity ratios for dimensionless porous length of 1 123

LIST OF SYMBOLS

C Forchheimer constant

C_p specific heat at constant pressure, *J/kg K*

Da Darcy number

g gravitational acceleration, m/s^2

G pressure gradient in x-direction

h convective heat transfer coefficient

H half height of channel, *m*

k thermal conductivity, *W/m K*

k_{eff} effective thermal conductivity, *W/m K*

k_r thermal conductivity ratio

K permeability, m^2

L length of the channel, *m*

M dimensionless viscosity ratio parameter

Nu Nusselt number

Ppressure, *Pa*

PePeclet number

Re Reynolds number

q''_l lower wall subjected heat flux, W/m^2

q''_uupper wall subjected heat flux, W/m^2

q''_μ average wall heat flux, W/m^2

q_r heat flux ratio

S porous media shape parameter

T temperature, *K*

T_{wl} lower wall temperature, K

T_{wu} upper wall temperature, K

$T_{w\mu}$ average wall temperature, *K*

u velocity component along the x-direction, *m/s*

U dimensionless velocity component along dimensionless X-direction

$u_m$average velocity, *m/s*

$U_m$dimensionless average velocity

$\hat{u}$ dimensionless normalized velocity

x coordinate along the axis of the channel, m

y coordinate normal to the surfaces of the channel, m

X,Y dimensionless coordinates

Greek letters

β a coefficient

ε porosity

ξ dimensionless porous thickness

μ dynamic viscosity of fluid, $kg/m\,s$

μ_{eff} effective dynamic viscosity, $kg/m\,s$

ρ density, kg/m^3

v kinematic viscosity of fluid, m^2/s

θ dimensionless temperature

CHAPTER 1

INTRODUCTION

1.1. Solar Energy

The global demand of energy is rapidly growing day by day. Current fossil reserves have short lifetime (coal: 148 years, petroleum: 43 years, natural gas: 61 years(DOE, 2011)) and their possible extinction in the near future will affect the human kind in a negative way if any new resources are not found. Furthermore, the effects of greenhouse gas emission imply the carbon-free energy technologies to be improved. Therefore, all energy sources must be used to compensate the world's growing energy demand in a reducing-carbon-emission path.

Since the Big Bang; the main source of the energy in the universe has been fusion. Fusion can be defined as the joining of two or more nuclei together and compound a new nucleus. The mass of the new nucleus is less than the summation of the masses of the previous nuclei. This lost mass turns into energy. All the stars live by thermonuclear fusion, so does the sun.

The sun produces 10^{26} *joules* of energy in each second and radiates it to the space. In each second, approximately, *1500 jou*les of solar energy reaches to the one meter-squared area of the earth. This energy corresponds to *1.5 kW* of power per meter-square. This means that; the solar energy collection in five hours throughout the world is equal to the total energy obtained by primary energy resources consumed annually by the humankind (Baede et al., 2007). However, there is still a problem exists about solar energy. Not all of this power can be captured and used as electrical energy by current technologies. Therefore, in this area, the studies are mainly focused on enhancement techniques of the solar energy capturing devices to increase the energy gain.

This study aims the heat transfer enhancement of a solar air heater, which is defined in Section 1.3, by using porous media.

1.2. Solar Air Heater

A solar air heater is a system that utilizes solar energy to heat air passing throughout the collector. A schematic demonstration of a simple solar-air heater is shown in Figure 1.1.

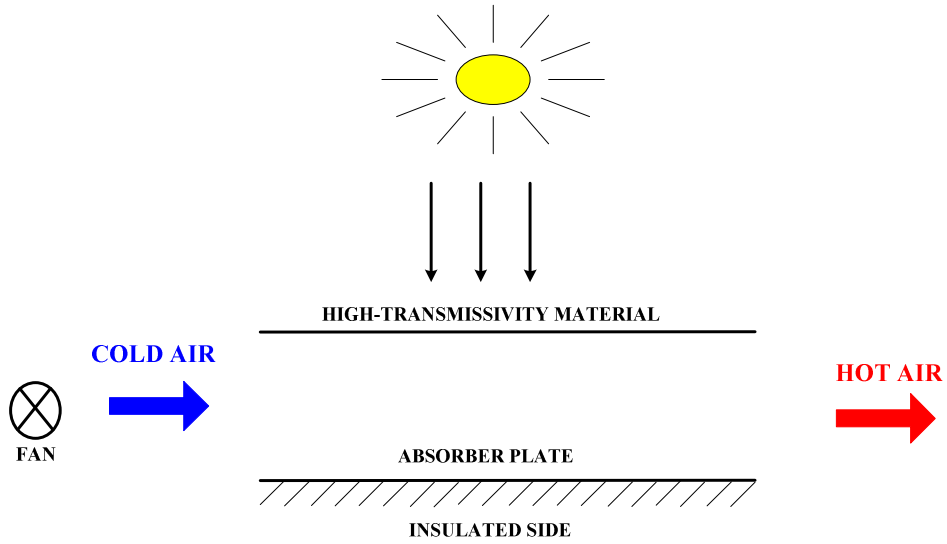

Figure 1.1. The schematic view of a simple solar collector

The system can be thought as a parallel plate and the upper plate should be made by a high-transmissivity material such as glass to transmit all of the solar radiation heat flux into the absorber plate in the channel. As its name indicates, the absorber plate should absorb high amount of solar irradiation. Because, the lower plate of the air-solar collector is well insulated, the absorb heat is conducted directly to the air. Generally a fan is used to provide flowing of air through the solar collector. In the most of solar air heaters, the dominant heat transfer mode is the forced convection. Two samples of air-solar heaters used in the studies of Alvarez et al. (2004) and Sreekumar (2010) are shown in the Figures 1.2 and 1.3, respectively.

Figure 1.2. A solar air heater collector used in the study of G. Alvarez et al.
(Source: G. Alvarez et al., 2010)

Figure 1.3. Another solar air heater used by Sreekumar who made the techno-economic analysis of it.
(Source: Sreekumar, 2010)

1.3. Heat Transfer Enhancement

The Newton's Law of Cooling can be applied for the Figure 1.4 as in Equation (1.1).

$$q = hA(T_s - T_\infty) \tag{1.1}$$

In this equation, q is the total heat transfer, h is convective heat transfer coefficient, A is heat transfer area, T_s and T_∞ are the temperatures of the surface and the fluid respectively. It is assumed that the surface is hotter than the fluid. As seen in Equation (1.1), for cooling systems; increasing the heat transfer coefficient, reducing

the fluid temperature, and increasing the heat transfer area, combined or individually, are different paths to enhance the total heat transfer rate.

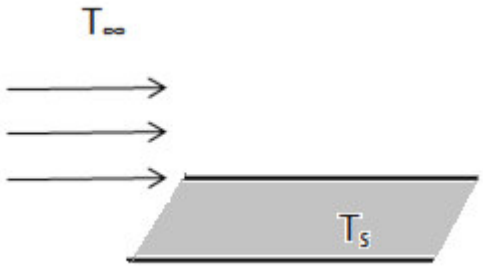

Figure 1.4. A surface is getting cooled by a fluid

It is obvious that the enhancement techniques are used for reducing the thermal resistance, hence increasing the heat transfer rate. These techniques can be categorized in two groups: Active techniques and passive techniques. Active techniques like surface vibration, jet impingement, fluid vibration etc. require direct input of external power whereas passive techniques do not. They perform surface or geometrical modifications to the flow channel or incorporate an insert, material, or additional device. The most common passive technique is surface extension. Generally fins are used to increase the heat transfer area as shown in Figure 1.5. It is clear that the heated or cooled surface area is increased; hence the total heat transfer is increased by using fins. Left figure illustrates an external flow on a smooth surface without fins and the right one is demonstrating the heat transfer area increment by using cylindrical fins.

Figure 1.5. Heat transfer enhancement by using fins.

Porous media approach is another passive heat transfer technique explained in Sections 1.4 and 1.5.

1.4. Porous Media

A porous medium is defined as a material consisting of a solid matrix with an interconnected void as shown in Figure 1.6. Water flowing through the rocks and stones, blood flowing into the lungs, and Helium gas flows over the fuel pebbles in a Pebble Bed Modular Reactor (PBMR) are all examples of porous media.

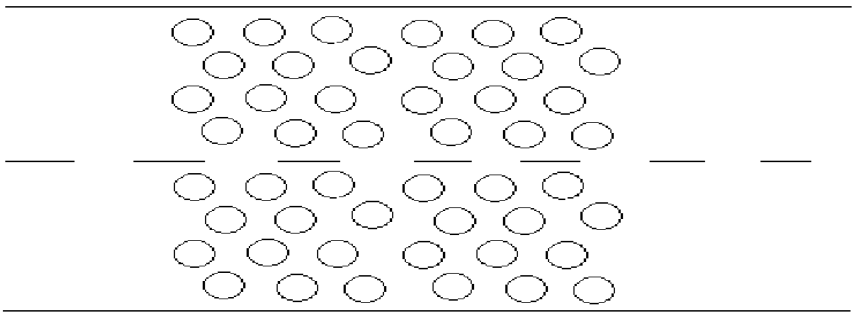

Figure 1.6. Schematic demonstration of a porous medium

The existence of several application areas of porous media approach is known. A typical pressurized water reactor (PWR) fuel array (Figure 1.7) is one of the examples of porous media and its thermal-hydraulic analysis can be made by using porous media approach. Thermal insulation of buildings, other nuclear energy systems (as PBMR), geothermal engineering, energy storage and recovery systems, storage of fruits, vegetables and grain, petroleum reservoirs, and catalytic reactors are some of the other application areas of this approach.

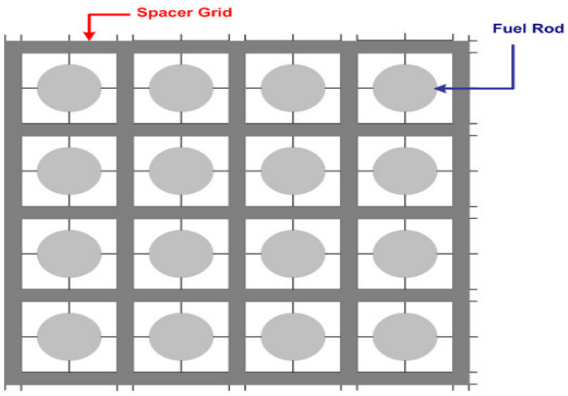

Figure 1.7. An example porous medium: A typical fuel array for a PWR. The coolant (water) flows through the channels with fuel bundles.

1.5. Heat Transfer Enhancement by Using Porous Media

A rigid and permeable solid influences the heat transfer significantly. This truth inspires the studies of porous media.

Using porous media enhances the heat transfer because of several reasons. First of all, the heat transfer area is increased by using porous media. Hence, the total heat transfer will increase as seen in Equation (1.1). Furthermore, porous media provide mixing of flow and generate fluctuations in the flow. It is well known that, fluctuations in the flow increase the heat transfer. Finally, high conductive porous medium increases diffusion in parallel and transverse direction of the flow.

Beyond all these advantages, there is a significant drawback of using porous media; it increases the pressure drop along the channel. Therefore, the fan (or pump) that forces the fluid into the channel needs more power to do its job.

To begin thermal-hydraulic analysis of a system that is assisted by porous media, a basic assumption must be mentioned first. It may not be appropriate to approach to heat and fluid flow in a porous media microscopically. It is impossible to follow fluid flows between the particles, and take their velocities into consideration (Figure 1.8.a) for whole domain. Instead, the volume averaged velocities and pressures are used to overcome this complexity. This method is named as “macroscopic approach”. For a flow in a parallel plate channel filled with porous media, flow in parallel and transverse directions should be considered when a microscopically approach is taken into account. However, from macroscopic point of view, flow through the porous channel is unidirectional for the specified direction (Figure 1.8.b).

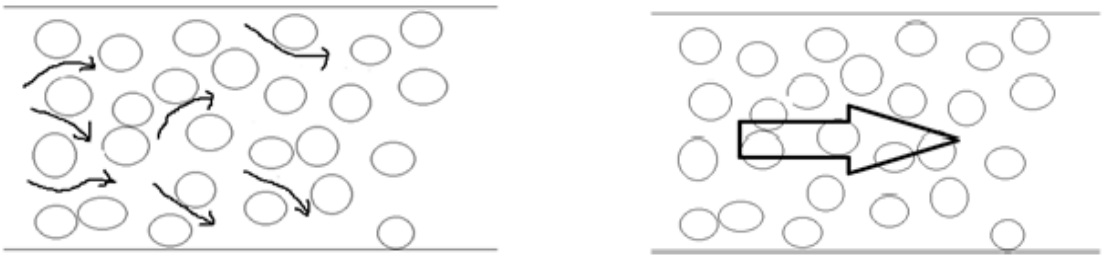

(a) (b)

Figure 1.8. Microscopic vs. Macroscopic View

1.6. Literature Survey

Several studies on internal flows in parallel plate with clear channels, channels filled with porous media, channels filled partially with porous media, studies of solar air heaters with and without porous media are summarized in this section.

Convective heat transfer in porous media has broad technological applications such as application in oil recovery, water supply management in hydrogeology, geothermal exploitation, ground heat storage, building thermal insulation, nuclear waste disposals, radioactive waste management, ground water flow modeling. It is also a subject of interest in environmental and geophysics sciences. A wide application of the porous media on many practical applications can be found in the well-known books of Nield and Bejan (2006), Ingham and Pop (2005), Vafai (2005, 2010), Pop and Ingham (2001), Bejan et al. (2004) and Vadasz (2008). They provide significant information on porous media application as well as formulation of heat and fluid flow in porous media.

Literature survey showed that several studies on heat and fluid flow in ducts filled with porous medium have been performed due to importance of the subject. Most of the studies have been performed on channels with symmetrical boundary conditions. For instance, Hooman (2008) analytically investigated fully developed forced convection in a porous medium bounded by two isoflux parallel plates as shown in Figure 1.9, on the basis of Darcy-Brinkman-Forchheimer model. The related momentum and energy equations were solved by an asymptotic technique and they declared that the value of Nusselt number is sensitive to the magnitude of shaping factor, and it improves with an increase in shaping factor value.

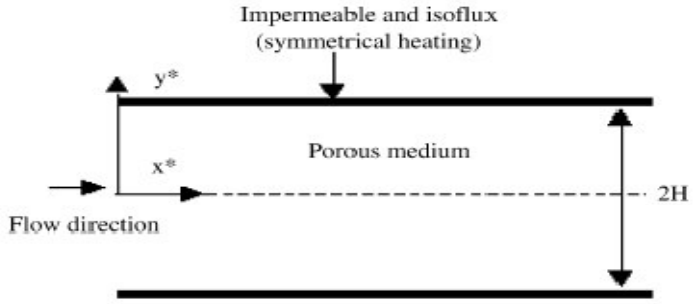

Figure 1.9. The schematic view of the channel in the forced convection, porous media study of Hooman (Source: Hooman, 2010)

Nield et al. (2004) studied the effects of viscous dissipation and flow work for a forced convection flow in a channel filled by a saturated porous medium with the walls either held with uniform temperature or subjected to uniform heat flux. The Darcy-Brinkman model was used and the governing equations were solved analytically, in their study. Fully developed flow through the straight porous channels for different flow mechanisms was considered by Awartani and Hamdan (2005) to study the effects of the porous matrix and the microscopic inertia on the velocity profiles. They obtained velocity profiles for the Darcy–Lapwood–Brinkman and the Darcy–Forchheimer–Brinkman models, and compared the achieved results with the corresponding solutions of the Navier–Stokes flow for Poiseuille, Couette and Poiseuille–Couette flow regimes. Further studies on heat and fluid flow in channels under symmetrical boundary conditions can be found in the literature (Hooman and Ranjbar-Kani, 2003;Tada and Ichimiya, 2007; Degan et al., 2002;Kaviani, 1985).

A survey of the literature reveals that number of studies on heat and fluid flow in channels with asymmetric boundary conditions are limited. For the channels with clear fluid, the well-known book of Shah and London (1978) provides useful information for scientists concern on asymmetric internal heating or cooling duct problems. They investigated the effects of asymmetric boundary conditions for parallel plate channel and circular ducts. Recently, Nield (2004) performed a theoretical study on heat and fluid flow in a parallel plate channel with asymmetric temperature and asymmetric heat flux boundary conditions. He declared that the individual wall Nusselt numbers may not provide sufficient information on heat transfer rate from the walls since the value of Nusselt number becomes infinite when heat flux ratio takes the value of 26/9. Hence, he defined an overall Nusselt number based on average heat flux and average wall temperature. He found that Nusselt number is independent of the heat flux ratio for the symmetrical flows.He also found that the value of overall Nusselt number is 140/17 for Poiseuille flow in a parallel plate channel.

There are several studies on partially filled porous channels and ducts encountered in the literature. Transient forced convection in the developing region of a channel was investigated numerically by Alkam et al. (2001). They used Forcheimer-Brinkman extended Darcy model to construct the governing equations for momentum. After the energy analysis, it was found that the maximum Nusselt number can be obtained when the channel was fully filled with porous medium. They also stated that, in the developing region, the Darcy number has more significant effects on the flow

than that in the fully developed region. Satyamurty and Bhargavi (2010) performed a numerical study of a flow in a partially porous channel (Figure 1.10). Both walls were hold symmetrically at constant temperatures. They found an optimum porous medium fracture of 0.8 for the Nusselt number.

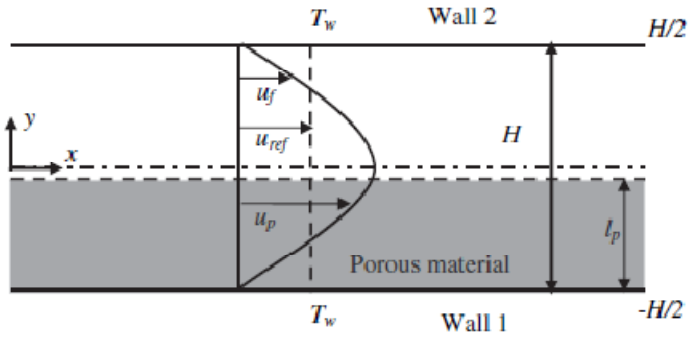

Figure 1.10.Satyamurty and Bhargavi performed a numerical study to find the optimum porous medium fracture for Nusselt number. (Source: Satyamurty and Bhargavi, 2010)

A study on forced convection in a tube with partially filled porous media was performed by Yang et al. (2009). A constant heat flux is subjected to the tube's wall. The physical demonstration of the domain is illustrated in Figure 1.11. Darcy model was used for the momentum equations. The optimum porous fractions for the Nusselt number change between 0.8 and 0.9 for different Darcy numbers.

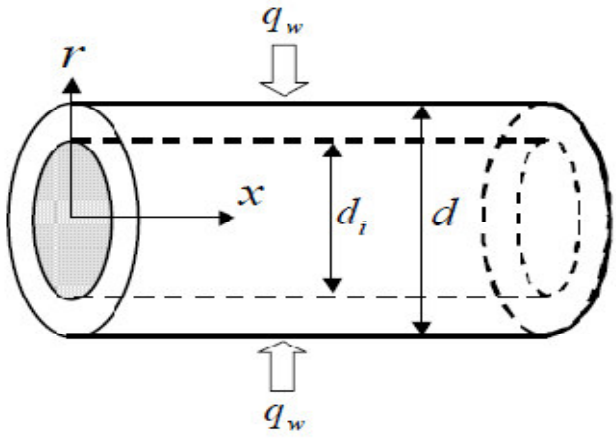

Figure 1.11.A physical demonstration of the tube that Yang et al. studied.di is the diameter of the porous material, remaining part is clear medium. (Source: Yang et al., 2009)

Further studies on heat and fluid flow analyses for internal flow through partially porous filled media can be found in the literature (Kuznetsov and Nield, 2010; Najjari and Nasrallah, 2008; Ould-Amer et al., 1998; Alkam and Al-Nimr, 1998).

There are several studies on the heat transfer analysis of solar air heaters in the literature, but reported studies on heat transfer enhancement by using porous media application for solar-air heater collectors are very limited. An experimental study was performed by Sopian et al. (1999) to investigate the outlet temperature variation of a double-pass solar collector when one pass is filled with a porous medium as shown in Figure 1.12. The study concluded that the presence of porous media in the second channel increases the outlet temperature and the thermal efficiency of the systems. One of their results is shown in Figure 1.13. As it can be seen, thermal efficiency of the flow in the channel with porous medium is greater than it is with clear one.

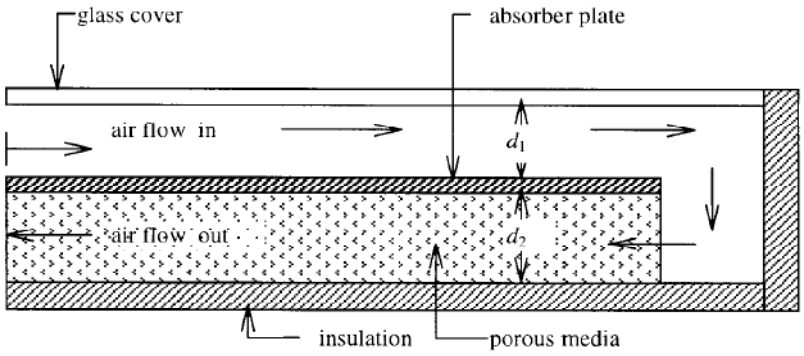

Figure 1.12.A double-pass solar collector used in the study of Sopian et al.
(Source: Sopian et al., 2009)

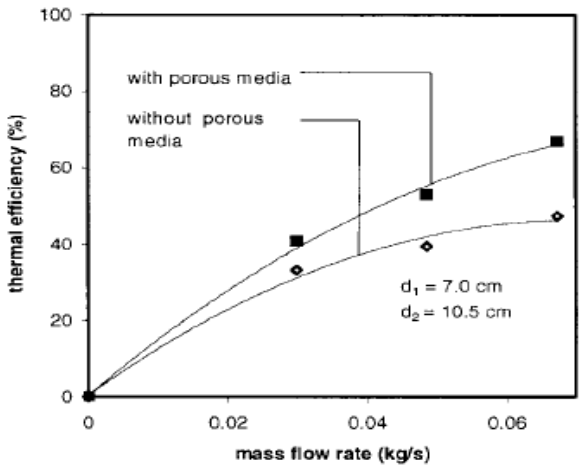

Figure 1.13.One of the results of the experimental study of Sopian et al.
(Source: Sopian et al., 2009)

The heat transfer characteristics and performance of the double-pass flat plate solar air heater with and without porous media were studied numerically by Naphon (2005). They used constant convective heat transfer coefficients in and out of the channel. The solar air heater with the porous media provided 25.9% higher thermal efficiency than that without porous media. There are several further studies performed on full porous solar-air heaters such as Sopian et al. (2009), Prasad et al. (2009), Thakura et al. (2003).

The reported studies of solar collectors with partially filled porous media are limited in literature. Al-Nimr and Alkamm (1998) performed a numerical study on the heat transfer enhancement of a solar collector partially filled with porous substrate as shown in Figure 1.14. Darcy-Brinkman-Forchheimer model was used for the momentum balance in porous region. At the interface of the porous and clear regions, continuous shear stress approach was applied. They concluded that the insertion of the porous substrate increases the Nusselt number up to 25 times and the optimum porous thickness is found to be 0.5.

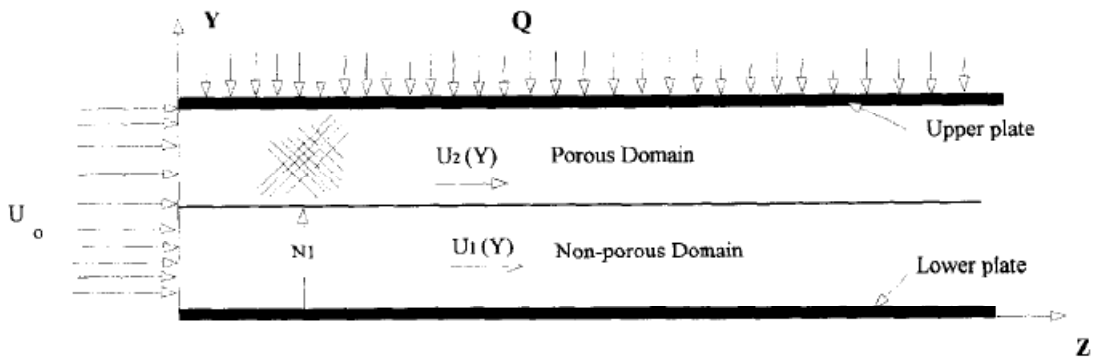

Figure 1.14. The physical demonstration of the domain in the study of Al-Nimr and Alkamm (1998)

1.7. Aim of the Present Study

The present study is aimed to theoretically investigate the enhancement of heat transfer by using porous media in a solar-air collector shown schematically in Figure 1.15. It is clear that the problem is unsteady. However, due to slow variation temperature during the day, and the complex mechanism of heat and fluid flow in a porous structure, the steady-state analysis is performed. Both pressure-drop and heat

transfer effects are investigated to obtain an optimum porous-clear media configuration in the channel of solar air heater collector.

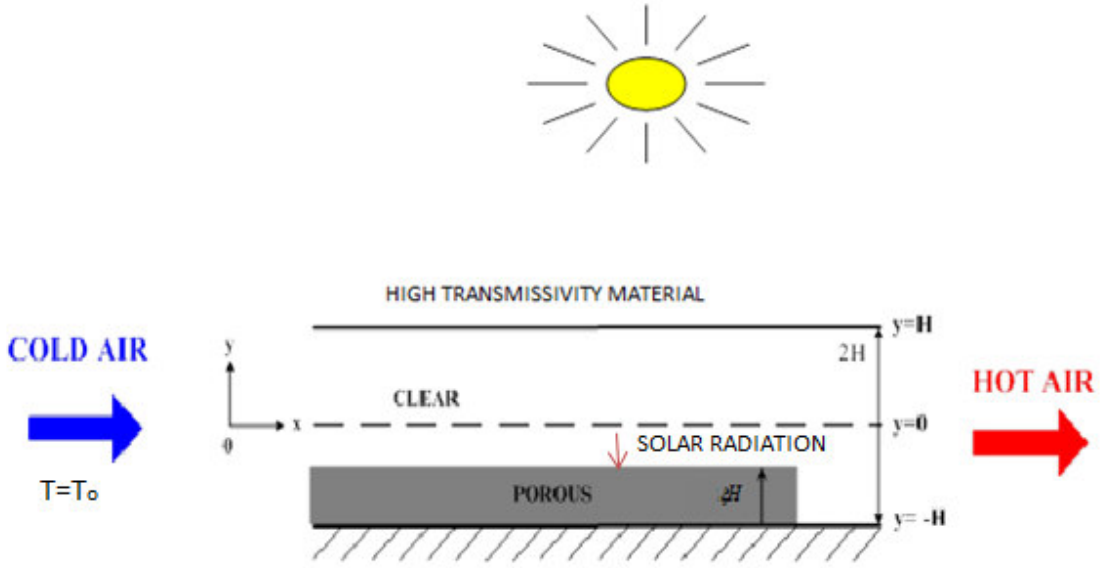

Figure 1.15. The schematic view of a solar collector wanted to be investigated. For this system; ξ takes values from 0 to 1.

Glass is known as a high-transmissivity material and let the thermal radiation directly pass through it. The radiation heat flux is absorbed at the porous-clear media interface. Air flows in a channel with a length of *2H*. *2ξH* of this channel is filled with porous media. The flow is laminar, incompressible, and the dominant heat transfer mode is forced convection and the buoyancy effects are neglected $(Gr/Re^2<<1)$.

The present study is started with analyzing of heat and fluid flow in a clear channel that does not contain any porous medium. Then, a theoretical base is presented by analyzing energy and momentum equations used in porous media. Further studies are performed to understand the mechanisms of heat and fluid flow in fully and partially filled porous channels.

In this thesis, all the governing equations are made dimensionless. The Nusselt number, has a significant importance, on analyzing heat transfer is calculated for all chapters. The main purpose is to increase Nusselt number and consequently increasing the heat transfer.

The Nusselt number is defined as the dimensionless convective heat transfer coefficient or the dimensionless temperature gradient at the surface. It is related to dimensional convection heat transfer coefficient by the following relation.

$$Nu = \frac{hL_c}{k} \Rightarrow \quad h = \frac{Nu\, k}{L_c} \tag{1.2}$$

Here, k is the conductivity of the fluid if the channel has no porous medium at the surface. For the latter case, it will be the effective conductivity of the porous medium and the fluid (Equation 2.10). L_c is the characteristic length and in our case, it is the channel height, $2H$. h is the convective heat transfer coefficient.

In Chapter 2, the mathematical formulations of heat and fluid flow in porous media are stated and explained.

In this thesis; six different cases are analyzed. In all cases, the velocity profiles and the Nusselt numbers are derived and the pressure drop effects are investigated. First, the analyses for flows in a clear channel with two different boundary conditions are investigated in Chapter 3. The individual Nusselt numbers at the lower and upper walls are obtained for the case with asymmetric heat fluxes. A fluid flow in a fully filled porous channel with symmetric heat flux boundary conditions is studied in Chapter 4. In Chapter 5, the same case as the previous chapter except the boundary conditions is investigated. In this case, both walls are subjected to heat fluxes, which are different from each other. As in the asymmetric heating case in Chapter 3, the individual Nusselt numbers at the lower and upper walls are analyzed. A flow in a channel with partially and symmetrically located porous medium is investigated in Chapter 6. In Chapter 7, the flow in a channel with partially and asymmetrically located porous medium with symmetric heat flux boundary conditions are investigated. The overall and individual Nusselt numbers found after the calculations are studied. Finally, a solar air heater is analyzed in Chapter 8. All the results are discussed in Chapter 9 and the thesis is concluded in Chapter 10.

CHAPTER 2

HEAT AND FLUID FLOW IN POROUS MEDIA

2.1. Fluid Flow in Porous Media

Mathematical formulation of the fluid flow in a porous medium is presented in this chapter. A basic law named as "Darcy Law" can be accepted as the starting point of the porous media approach. By modifying this equation; the governing equations and their solutions for the fluid flow in porous media for different cases can be obtained.

The macroscopic approach, which is briefly mentioned in Chapter 1, is used in the derivations of the governing equations for the flow. On this purpose, the local Darcian velocity is defined as:

$$< \boldsymbol{u} >= \frac{1}{V}\int_{V_f} \boldsymbol{u}\, dV \tag{2.1}$$

where V_f is the volume space which the fluid occupies. The symbol V shows the total volume. Darcian velocity vector (superficial velocity or apparent velocity) can also be defined as follows where Q indicates the volumetric flow rate in m^3/s, and A is the cross-sectional area in m^2.

$$< \boldsymbol{u} >= \frac{Q}{A} \tag{2.2}$$

Another velocity vector, named "pore velocity vector" is defined as shown in Equation (2.3) and it is related to Darcian velocity as shown in Equation (2.4).

$$< \boldsymbol{u} >^f = \frac{1}{V_f}\int_{V_f} \boldsymbol{u}\, dV \tag{2.3}$$

$$< \boldsymbol{u} >^f = \frac{< \boldsymbol{u} >}{\varepsilon} \tag{2.4}$$

In the right hand side of the Equation (2.4), the term ε is called "porosity" and it is defined as the ratio of the volume occupied by the fluid to the total volume.

$$\varepsilon = \frac{V_f}{V} \tag{2.5}$$

2.1.1. Darcy's Law

Darcy stated that the volume-averaged fluid velocity through a column of porous medium is directly proportional to the pressure gradient established along the column and the permeability of the space, and inversely proportional to the viscosity of the fluid. The governing equation for momentum, Equation (2.6), and the velocity profile, Equation (2.7) are shown below where μ stands for the dynamic viscosity.

$$\frac{\mu}{K} < \boldsymbol{u} >= -\frac{d < P >^f}{dx} \tag{2.6}$$

$$< \boldsymbol{u} >= \frac{K}{\mu}\left(-\frac{d < P >^f}{dx}\right) \tag{2.7}$$

In Equation (2.6), a new variable is introduced, which is called permeability (K). The permeability is an empirical constant whose dimension is m^2. It depends on the geometric structure of the porous medium. When the permeability increases, the flow resembles the flow in a clear medium; as water flows in an empty channel. For a channel with clear flow, the governing equations for fluid flow are the continuity equation for the mass conservation, and the Navier-Stokes equations for the momentum balance.

In three-dimensional case, the Darcy Equation turns into the following form:

$$\frac{\mu}{K} < \boldsymbol{u} >= \rho_f \boldsymbol{g} - \nabla < P >^f \tag{2.8}$$

2.1.2. Brinkman-Extended Darcy's Law

Darcy equation is not applicable for some cases. As an example; for an internal flow, the Darcy equation cannot be used, because some additional terms as the one for the boundary effects must be included in the momentum conservation equation. The boundary frictional effects cannot be ignored for the flows of small porous media. Introducing a new variable, "effective dynamic viscosity", μ_{eff}, which depends on the fluid and the structure of the porous medium, Darcy equation can be modified as follows.

$$\mu_{eff}\frac{d^2<\boldsymbol{u}>}{dy^2}-\frac{\mu}{K}<\boldsymbol{u}>=\frac{d<P>^f}{dx} \tag{2.9}$$

The effective dynamic viscosity can be written as follows:

$$\mu_{eff}=\varepsilon\mu_f+(1-\varepsilon)\mu_s \tag{2.10}$$

In three-dimensional form, this equation becomes into the form as Equation (2.11). This equation is known as the Brinkman-extended Darcy equation.

$$\mu_{eff}\nabla^2<\boldsymbol{u}>-\frac{\mu}{K}<\boldsymbol{u}>+\rho_f\boldsymbol{g}=\nabla<P>^f \tag{2.11}$$

As the permeability increases, the Equation (2.11) reduces to the momentum equation for the two-dimensional flow of a fluid in a clear channel, which is written below.

$$\mu\frac{d^2<\boldsymbol{u}>}{dy^2}-\frac{d<P>^f}{dx}=0 \tag{2.12}$$

2.1.3. Forchheimer Extended Darcy's Law

For flows at high velocities, Darcy's law may not appropriate. Darcy equation only depends on the pressure gradient and the viscous force. For high velocity flows,

the inertial effects should be taken into consideration. Therefore, a modification must be made to the Darcy equation to overcome this difficulty. Equation (2.13) is the convenient form of the Equation (2.6) named as Forchheimer-extended Darcy's law.

$$-\frac{C}{\sqrt{K}}\rho_f <\boldsymbol{u}>^2-\frac{\mu}{K}<\boldsymbol{u}>=\frac{d<P>^f}{dx} \tag{2.13}$$

In the left hand side of the Equation (2.13), the first term indicates the inertial contribution or form drag (A. Nakayama, 1995), and the second term stands for the viscous contribution or the frictional drag. The new term, *C*, is the Forchheimer constant. In three-dimensional form and with taking the gravitational force into account, this law can be written as follows:

$$-\frac{\mu}{K}<\boldsymbol{u}>-\frac{C}{\sqrt{K}}\rho_f|<\boldsymbol{u}>|<\boldsymbol{u}>+\rho_f\boldsymbol{g}=\nabla<P>^f \tag{2.14}$$

2.1.4. Brinkman-Forchheimer Extended Darcy's Law

All the modifications of the Darcy's law can be generalized as in Equation (2.15).

$$\mu_{eff}\frac{d^2<\boldsymbol{u}>}{dy^2}-\frac{C}{\sqrt{K}}\rho_f <\boldsymbol{u}>^2-\frac{\mu}{K}<\boldsymbol{u}>=\frac{d<P>^f}{dx} \tag{2.15}$$

Finally, the general modified Darcy's law can be written as three-dimensional form with gravitational force as follows.

$$\mu_{eff}\nabla^2<\boldsymbol{u}>-\frac{\mu}{K}<\boldsymbol{u}>-\frac{C}{\sqrt{K}}\rho_f|<\boldsymbol{u}>|<\boldsymbol{u}>+\rho_f\boldsymbol{g}=\nabla<P>^f \tag{2.16}$$

Equation (2.16) is called as the Brinkman-Forchheimer extended Darcy's Law, and it is the most general form of the momentum conservation equation for a flow in a porous medium.

2.2. Heat Flow in Porous Media

The total energy of the fluid should be conserved as stated in the first law of thermodynamics. In the case of a two-dimensional fluid flow through a porous medium; if the fluid and the solid porous material are in thermal equilibrium *(T_s= T_f= T)*, then the governing equation for the energy balance can be written in the following form.

$$\rho C_p \left(< u > \frac{\partial < T >}{\partial x} + < v > \frac{\partial < T >}{\partial y} \right) = k_{eff} \left(\frac{\partial^2 < T >}{\partial x^2} + \frac{\partial^2 < T >}{\partial y^2} \right) \qquad (2.17)$$

In this equation, k_{eff} is the effective conductivity of the fluid and solid porous material and, can be written as in Equation (2.18), and it should be noted that the viscous dissipation effects are neglected.

$$k_{eff} = \varepsilon k_f + (1 - \varepsilon) k_s \qquad (2.18)$$

In the studies performed in this thesis, the viscous dissipation term is neglected. The working fluid is Newtonian and the flow is thermally fully developed. Furthermore, the temperature gradient in y-direction is much greater than it is in x-direction. Then, in most of the analysis, the following form of the energy equation is used for a flow in a porous channel.

$$\rho C_p < u > \frac{\partial < T >}{\partial x} = k_{eff} \frac{\partial^2 < T >}{\partial y^2} \qquad (2.19)$$

The above equation is almost the same equation with the energy equation of a fluid flow in a clear channel except the thermal conductivity in the right hand side is the effective thermal conductivity of the fluid and the porous structure.

From Chapter 3, the averaging quantities; $< T >$, $< P >$, $< u >$, and $< v >$will be designated without brackets but the reader should keep in mind that these quantities are the volume average values.

CHAPTER 3

FULLY DEVELOPED FLOW IN A CHANNEL WITH CLEAR FLUID: SYMMETRIC AND ASYMMETRIC HEAT FLUX BOUNDARY CONDITIONS

An incompressible, fully developed flow in a clear channel is investigated in this chapter. The fluid is assumed to be Newtonian. The flow is laminar, hence Reynolds number of the flow is assumed to be less than the critical Reynolds number as *2300*. Thermally and hydro-dynamically fully developed flow is explained to start our analysis. After the fundamental discussion on heat and fluid flow in a fully developed channel, the considered problem is defined. The following section is presented to explain the heat and fluid flow governing equations to obtain the velocity and temperature fields. Although heat and fluid flow for fully developed in a clear channel are discussed in different references such as Incropera and DeWitt (1996), Shahand London (1978), continuity, momentum and energy equations are solved for both symmetric and asymmetric channels by using Nield (2004) to show the accuracy of the employed method particularly for asymmetric boundary conditions in this study.

3.1. The Concept of Fully Developed Condition

The following two sections are written to explain the fully-developed phenomena for both hydrodynamic and thermal considerations.

3.1.1. Hydrodynamically Fully Developed Flow

After the fluid enters in a duct or a channel, viscous effects become important and a boundary layer develops until they meet each other (at the point of $x_{fd,h}$), as shown in Figure 3.1. After this point, the velocity profile is not changed along the channel and the flow is named as hydrodynamically fully developed flow.

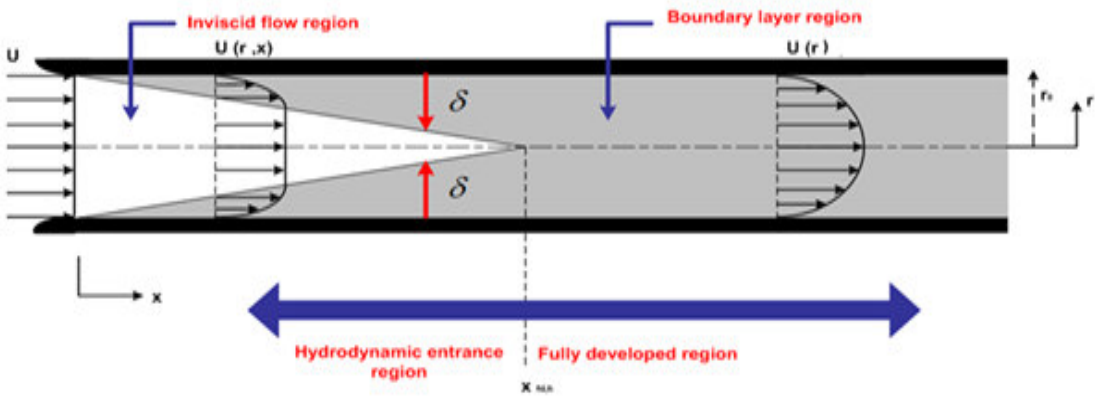

Figure 3.1. Hydrodynamic entrance and fully developed regions in a channel

This boundary layer in the channel is caused by a phenomenon called as **no-slip condition**. This condition can be defined simply as follows: The closest fluid molecule to the wall sticks to solid molecule. This means that, if the solid is stationary, then this molecule will be stationary, too. If the solid (in this case it is the wall) moves with a velocity of *V*, then the stuck fluid molecule will move with the same velocity, *V*. -In our case, the walls of the channel are stationary. Hence, the fluid molecule closest to the wall is stationary. Furthermore, this molecule tries to stop the closest fluid molecule to it and slows its neighbors down. Since the fluid flows, all the fluid molecules get forced to be moved (Figure 3.2). These opposite forces cause a shear stress near the boundaries and the area that the shear stress occurs enlarges with the x-direction. The cause of the existence of the boundary layer is this shear stress.

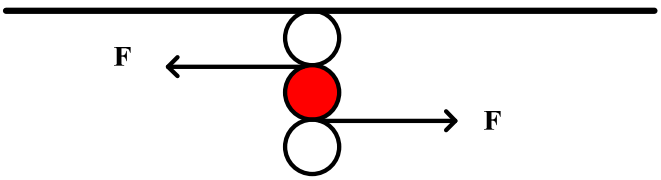

Figure 3.2. Shear force acted on a fluid molecule

In hydro-dynamically fully developed region, the condition stated in Equation (3.1) should be satisfied.

$$\frac{\partial u}{\partial x} = 0, \qquad v = 0 \tag{3.1}$$

In Equation (3.1), u is the x-component and v is the y-component of the fluid velocity.

3.1.2. Thermally Fully Developed Flow

After the fluid enters into a channel, a thermal boundary layer occurs. These boundary layers meet each other at $x_{fd,t}$ as shown in Figure 3.3. After this point the flow is called thermally fully developed flow.

The **no-temperature jump condition** is responsible for the development of this boundary layer. This condition states that the temperature of the closest fluid particle to the wall is as the same as the temperature of the wall. If the wall temperature is less than the fluid inlet temperature, then the fluid particles near the surface tend to cool the neighbour fluid particle. That situation continues towards y-direction of the channel until the two fluid particles have the same temperature. At some distance, two boundaries intercept. After this point the dimensionless temperature does not change with x-direction. This condition can be written as in Equation (3.2).

$$\frac{\partial}{\partial x}\left[\frac{T - T_w}{T_m - T_w}\right] = 0 \tag{3.2}$$

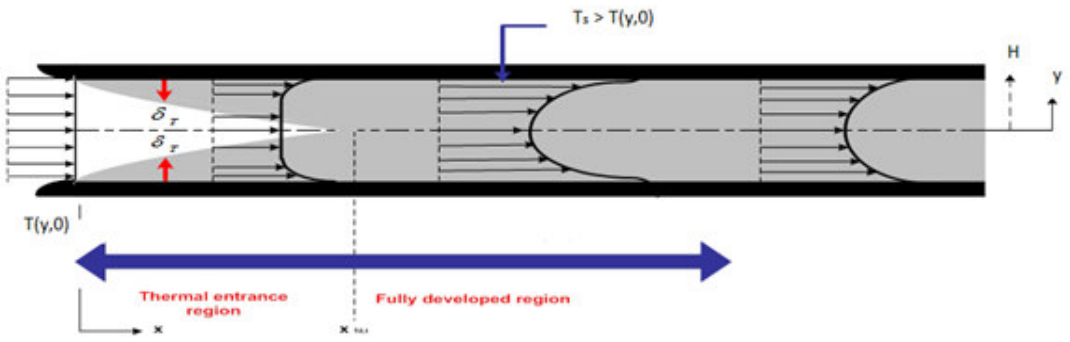

Figure 3.3. Thermal entrance and fully developed regions in a channel

3.2 First Case: Symmetric Heat Fluxes at the Walls

In this case, thermally and hydro-dynamically fully developed, laminar flow in a channel whose walls are subjected to heat fluxes is investigated. The heat fluxes at the walls are constant and equal to each other. The schematic demonstration is shown in Figure 3.4.

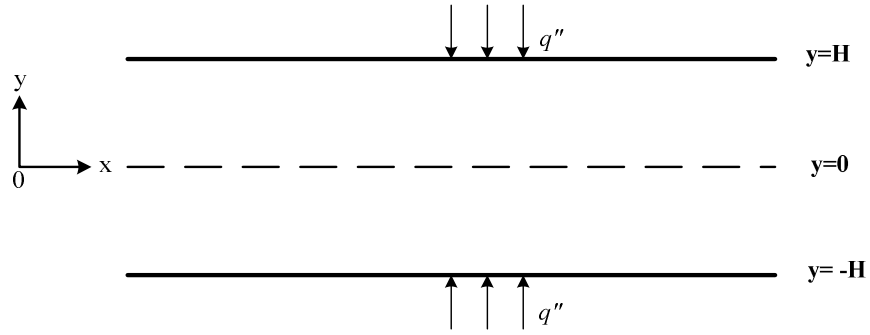

Figure 3.4. Schematic view of the problem

3.2.1. Fluid Flow Analysis

To obtain the velocity profile, the well-known Navier-Stokes equations should be solved. These equations are shown in Equations (3.3) and (3.4).

$$u\frac{\partial u}{\partial x}+v\frac{\partial u}{\partial y}=-\frac{1}{\rho}\frac{\partial P}{\partial x}+\nu\left(\frac{\partial^2 u}{\partial x^2}+\frac{\partial^2 u}{\partial y^2}\right) \tag{3.3}$$

$$u\frac{\partial v}{\partial x}+v\frac{\partial v}{\partial y}=-\frac{1}{\rho}\frac{\partial P}{\partial y}+\nu\left(\frac{\partial^2 v}{\partial x^2}+\frac{\partial^2 v}{\partial y^2}\right) \tag{3.4}$$

Since the flow is hydro-dynamically fully-developed, then the Equation (3.1) can be applied to x-momentum and y-momentum equations.

$$\mu\frac{\partial^2 u}{\partial y^2}-\frac{\partial P}{\partial x}=0 \tag{3.5}$$

$$\frac{1}{\rho}\frac{\partial P}{\partial y} = 0 \tag{3.6}$$

The above equations show that pressure field is only the function of *x*, hence it does not change with *y*. To solve Equation (3.5), two boundary conditions are needed. No-slip condition, explained in subsection 3.1.1, is used.

$$u(\pm H) = 0 \tag{3.7}$$

Equation (3.5) can be made dimensionless to reduce the number of parameters by using the following dimensionless parameters. After some mathematical manipulation, Equation (3.5) can be made dimensionless as given by Equation (3.9).

$$Y = \frac{y}{H}, \qquad G = -\frac{dP}{dx}, \qquad U = \frac{\mu u}{GH^2} \tag{3.8}$$

$$\frac{d^2U}{dY^2} + 1 = 0 \tag{3.9}$$

Boundary conditions should also be dimensionless,

$$U(\pm 1) = 0 \tag{3.10}$$

The ordinary differential equation given by Equation (3.9) under boundary conditions presented by Equation (3.10) is solved and the equation of the velocity profile for the problem demonstrated in Figure 3.4 is found as:

$$U(Y) = \frac{1}{2}(1 - Y^2) \tag{3.11}$$

The mean velocity can be defined and found for velocity profile of Equation (3.11).

$$U_m = \frac{\int_{-1}^{1} U(Y)dY}{\int_{-1}^{1} dY} = \frac{\int_{-1}^{1} U(Y)dY}{2} = \frac{1}{3} \tag{3.12}$$

The normalized velocity is defined as the ratio of the velocity and the mean velocity and it can be calculated as follows.

$$\hat{u} = \frac{U}{U_m} = \frac{\frac{1}{2}(1 - Y^2)}{\frac{1}{3}} = \frac{3}{2}(1 - Y^2) \tag{3.13}$$

.

3.2.2. Heat Flow Analysis

Total energy of the fluid should be conserved as stated in the first law of thermodynamics and the related energy conservation equation for a flow in a channel can be written as in Equation (3.14).

$$(\rho C_p)_f \left(u\frac{\partial T}{\partial x} + v\frac{\partial T}{\partial y}\right) = k_f \left(\frac{\partial^2 T}{\partial x^2} + \frac{\partial^2 T}{\partial y^2}\right) + \mu\Phi \tag{3.14}$$

In this equation, μ is the dynamic viscosity of the fluid, Φ is the viscous dissipation term, and k_f is the conductivity of the fluid.

As stated in previous section, velocity component in y direction, *v,* is zero in our case. Furthermore, neglecting viscous dissipation, and assuming that the temperature gradient in y-direction is much greater than it is in x-direction, the energy equation can be written as in Equation (3.15).

$$(\rho C_p)_f u\frac{\partial T}{\partial x} = k_f \frac{\partial^2 T}{\partial y^2} \tag{3.15}$$

Reminding the dimensionless parameters defined in Equation (3.8), and introducing a new dimensionless parameter named as dimensionless temperature, Equation (3.16), the energy equation becomes into the form written below:

$$\theta = \frac{T - T_w}{T_m - T_w} \tag{3.16}$$

$$(\rho C_p)_f u\left[\theta\left(\frac{\partial T_m}{\partial x} - \frac{\partial T_w}{\partial x}\right) + (T_m - T_w)\frac{\partial \theta}{\partial x} + \frac{\partial T_w}{\partial x}\right] = k_f (T_m - T_w)\frac{\partial^2 \theta}{\partial y^2} \tag{3.17}$$

The walls are getting heated by constant heat fluxes. Therefore, the gradient of wall heat flux with respect to x-direction should be taken zero.

$$\frac{dq"}{dx} = \frac{d[h(T_w - T_m)]}{dx} = 0 \qquad => \frac{\partial T_w}{\partial x} = \frac{\partial T_m}{\partial x} \tag{3.18}$$

As mentioned before, it is accepted that the flow in the channel is thermally fully developed *(∂θ/∂x=0)*.Using this condition and the equation Equation (3.18), the energy equation becomes as:

$$(\rho C_p)_f u \frac{\partial T_m}{\partial x} = k_f (T_m - T_w) \frac{\partial^2 \theta}{\partial y^2} \tag{3.19}$$

In Equation (3.19), two dependent variables as the mean temperature and the wall temperature exist. Both of them are not known. Therefore, further manipulations are required to obtain dimensionless temperature field. To find a definition for the mean temperature gradient in x-direction, an energy balance can be applied for a control volume shown in Figure 3.5.

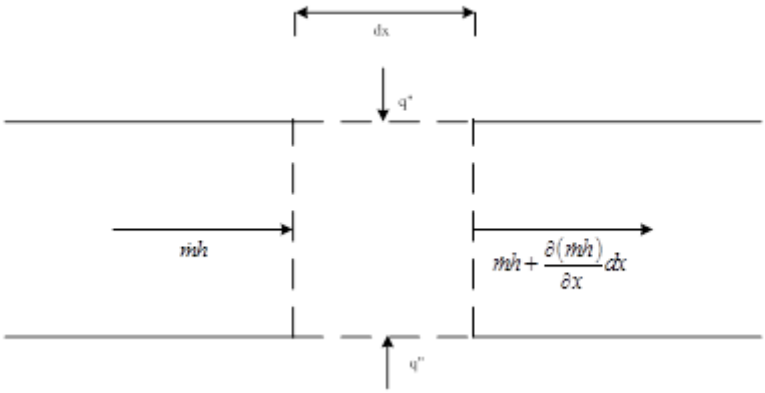

Figure 3.5. Total energy of the fluid is conserved. $h=C_pT_m$ is specific enthalpy and □ $=2H\rho u_m$ is the mass flow rate of the fluid

After performing an energy balance, the following equation is obtained.

$$2H\rho u_m C_p T_m + 2q"dx = 2H\rho u_m C_p T_m + \frac{\partial(2H\rho u_m C_p T_m)}{\partial x} dx \tag{3.20}$$

The final result of the energy balance is that the gradient of mean temperature is equal to the ratio of the heat flux to the multiplication of fluid density, specific heat, mean velocity, and characteristic length. This relation can be written as.

$$\frac{dT_m}{dx} = \frac{q"}{\rho C_p u_m H} \tag{3.21}$$

After substituting Equation (3.21) into Equation (3.19), the energy equation can be obtained as:

$$\frac{u}{u_m}\frac{q"}{H} = k_f(T_m - T_w)\frac{\partial^2\theta}{\partial y^2} \tag{3.22}$$

Equation (3.13) is the definition of the dimensionless normalized velocity and it can be seen that it exists in the left hand side of Equation (3.22). Furthermore, convective heat flux from the wall to the fluid can be formulated as written in Equation (3.23). Using these two relations and applying the dimensionless parameters defined in Equations (3.8) and (3.16) to the equation (3.22), the energy equation takes the following form, shown in Equation (3.24).

$$q" = h(T_w - T_m) \tag{3.23}$$

$$\frac{\partial^2\theta}{\partial Y^2} + \hat{u}\frac{hH}{k_f} = 0 \tag{3.24}$$

Nusselt number can be defined as the dimensionless convective heat transfer coefficient or the dimensionless temperature gradient at the surface and it can be related to the channel height, convective heat transfer coefficient and the conductivity of the fluid as in Equation(3.25). By using this relation, the final form of the dimensionless energy equation is obtained as in Equation 3.26.

$$Nu = \frac{h\ 2H}{k_f} \tag{3.25}$$

$$\frac{\partial^2\theta}{\partial Y^2} + \frac{1}{2}\hat{u}Nu = 0 \tag{3.26}$$

Two boundary conditions are needed to solve this second order ordinary differential equation. The dimensional forms of these boundary conditions are.

$$T(\pm H) = T_w \tag{3.27}$$

It must be mentioned that the wall temperatures are functions of x-direction and they are not constants. They are also not known. When these boundary values are inserted into the dimensionless temperature equation defined as in Equation (3.16), the following dimensionless boundary conditions are obtained.

$$\theta(\pm 1) = 0 \tag{3.28}$$

Now, the energy equation can be solved by using the dimensionless boundary conditions. After solving Equation (3.26) by using Equation (3.28), the following result is obtained.

$$\theta(Y) = \frac{1}{16}Nu(Y^4 - 6Y^2 + 5) \tag{3.29}$$

The Nusselt number for the flow in a clear channel should be found to compare the heat transfer with other channel designs containing porous media. To find the Nusselt number, the compatibility condition, Equation (3.30) must be applied.

$$\int_{-1}^{1} \theta\hat{u}dY = 2 \tag{3.30}$$

The detailed derivation of the compatibility condition is explained in Appendix A. Using the compatibility condition, the Nusselt number is found as:

$$Nu = 4.1176 \tag{3.31}$$

3.3. Second Case: Asymmetric Heat Fluxes at the Walls

The only difference of the present case than the previous one is that the wall heat fluxes are different with each other. The schematic view of the problem is shown in Figure 3.6. In this case, besides the overall Nusselt number, two individual Nusselt numbers will also be investigated for the upper and lower walls.

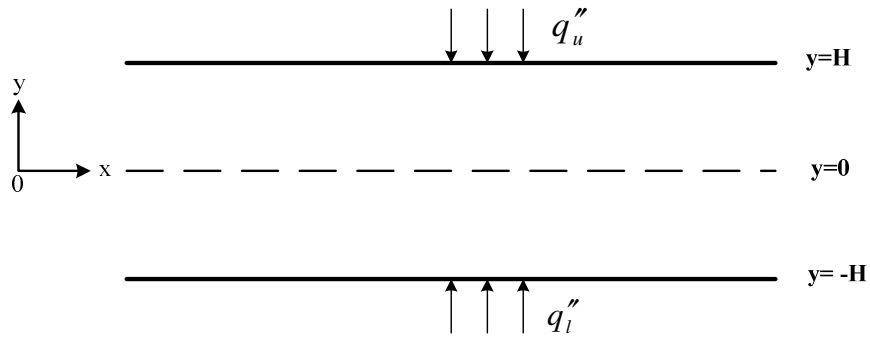

Figure 3.6.Schematic demonstration of the considered problem. Both walls are subjected to different heat fluxes.

3.3.1. Fluid Flow Analysis

Since the governing equation and the boundary conditions do not get affected with any change in heat flux at the walls, then the normalized velocity profile is as the same as it was in the previous section.

$$\hat{u} = \frac{3}{2}(1 - Y^2) \tag{3.13}$$

3.3.2. Heat Flow Analysis

The governing equation for the energy balance in this case, is also as the same as it was in the case with symmetric heat flux boundary conditions.

$$(\rho C_p)_f u \frac{\partial T}{\partial x} = k_f \frac{\partial^2 T}{\partial y^2} \tag{3.15}$$

Three new parameters should be introduced at the beginning of the energy analysis of the problem in this case.

$$T_{w\mu} = \frac{T_{wl}+T_{wu}}{2}, \qquad q"_{\mu} = \frac{q"_{l}+q"_{u}}{2}, \qquad \theta = \frac{T-T_{w\mu}}{T_m-T_{w\mu}} \tag{3.32}$$

Inserting the dimensionless temperature stated in Equation (3.32), into the energy equation, Equation (3.15), the following equation is obtained.

$$\begin{aligned}(\rho C_p)_f u\left[\theta\left(\frac{\partial T_m}{\partial x}-\frac{\partial T_{w\mu}}{\partial x}\right)+(T_m-T_{w\mu})\frac{\partial \theta}{\partial x}+\frac{\partial T_{w\mu}}{\partial x}\right] \\ = k_f(T_m-T_{w\mu})\frac{\partial^2\theta}{\partial y^2}\end{aligned} \tag{3.33}$$

Since the wall heat fluxes are constants, they should not be changed with x-direction. Then, the gradients of the wall heat fluxes with respect to *x* are zero. These manipulations are shown in Equation (3.34).

$$\begin{aligned}\frac{dq"_l}{dx}=0 \quad &=> \frac{d[h_l(T_{wl}-T_m)]}{dx}=0 \quad => \frac{dT_{wl}}{dx}=\frac{dT_m}{dx} \\ \frac{dq"_u}{dx}=0 &=> \frac{d[h_u(T_{wu}-T_m)]}{dx}=0 => \frac{dT_{wu}}{dx}=\frac{dT_m}{dx}\end{aligned} \tag{3.34}$$

If the temperature gradients of the upper and lower walls are added to each other, the following result will be obtained.

$$\frac{dT_{wl}}{dx}+\frac{dT_{wu}}{dx}=\frac{d(T_{wu}+T_{wl})}{dx}=2\frac{dT_{w\mu}}{dx}=2\frac{dT_m}{dx}$$

$$\frac{dT_{w\mu}}{dx}=\frac{dT_m}{dx} \tag{3.35}$$

Inserting Equation (3.35) into Equation (3.33), and remembering the thermally fully developed condition, which states the dimensionless temperature gradient in x-direction is zero, the energy equation turns into the form stated below.

$$(\rho C_p)_f u\frac{\partial T_m}{\partial x}=k_f(T_m-T_{w\mu})\frac{\partial^2\theta}{\partial y^2} \tag{3.36}$$

The next step is performing an energy balance for a differential control volume shown in Figure 3.7.

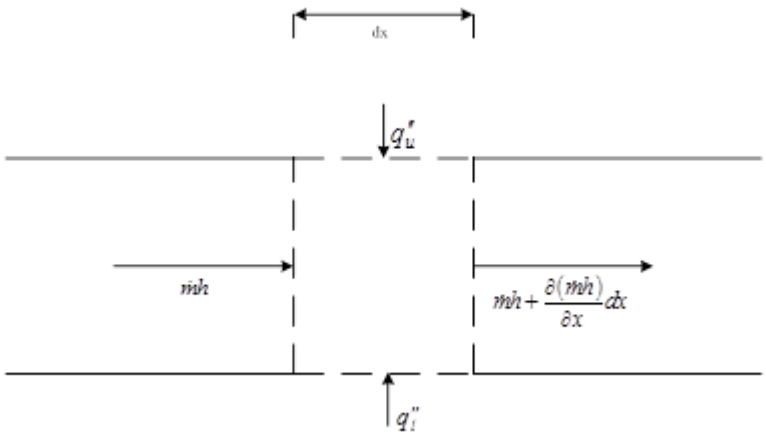

Figure 3.7. Total energy of the fluid is conserved. $h=C_pT_m$ is specific enthalpy and $\dot{m}=2H\rho u_m$ is the mass flow rate of the fluid

The energy entering the control volume shown in Figure 3.7 must be equal to the energy leaving the boundaries, since there is no heat generation in the control volume. Equation (3.37) is obtained for the mean temperature gradient in x-direction after the following manipulations.

$$2H\rho u_m C_p T_m + q''_l dx + q''_u dx = 2H\rho u_m C_p T_m + \frac{\partial\left(2H\rho u_m C_p T_m\right)}{\partial x}dx$$

$$\frac{q''_l + q''_u}{2} = H\rho u_m C_p \frac{dT_m}{dx}$$

$$\frac{dT_m}{dx} = \frac{q''_\mu}{H\rho u_m C_p} \tag{3.37}$$

The Nusselt number for the flow in a channel with the length of $2H$ was defined in the previous case with symmetric boundary conditions, as in Equation (3.25), and the average heat flux is written as in Equation (3.38).

$$Nu = \frac{h\,2H}{k_f} \tag{3.25}$$

$$q''_\mu = h\left(T_{w\mu} - T_m\right) \tag{3.38}$$

Inserting Equations (3.37) and (3.38) into Equation (3.36), and applying the equations for dimensionless parameter Y, the normalized velocity $\hat{u}$ (Equations (3.4) and (3.13)), and the Nusselt number, the energy equation becomes into the final form as written in Equation (3.39).

$$\frac{\partial^2\theta}{\partial Y^2} + \frac{1}{2}\hat{u}Nu = 0 \tag{3.39}$$

To solve the energy equation written in Equation (3.39), two boundary conditions are needed. Before stating the boundary conditions, one new parameter must be defined, as shown in Equation (3.40).

$$\beta = \frac{T_{wl} - T_{wu}}{2\left(T_m - T_{w\mu}\right)} \tag{3.40}$$

Now, it can be seen that at the lower wall, the dimensionless temperature is β where as it is -β for the upper wall.

$$\theta(1) = -\beta, \qquad \theta(-1) = \beta \tag{3.41}$$

After solving the energy equation by using the boundary conditions stated above, the following solution for the dimensionless temperature profile is obtained.

$$\theta(Y) = -\beta Y + \frac{Nu}{16}(Y^4 - 6Y^2 + 5) \tag{3.42}$$

The Nusselt number is still an unknown. To find it, the compatibility condition stated in Equation (3.30) should be used. The derivation of the compatibility condition is explained in Appendix A.

$$\int_{-1}^{1} \theta\hat{u}dY = 2 \tag{3.30}$$

After solving the compatibility condition for the Nusselt number, the following result is obtained.

$$Nu = 4.1176 \tag{3.43}$$

This result for the overall Nusselt number will be discussed in Chapter 9 (the results and discussion).

In this section, unlike the previous one with symmetric boundary conditions, further analysis should be performed for the individual Nusselt numbers at the walls. To do this, the analysis must be started from a foundation of a new definition for β. The heat fluxes at the walls can be written as follows.

$$\begin{aligned} q"_l &= -k\frac{\partial T}{\partial y}\Big|_{y=-H} = -\frac{k(T_m - T_{w\mu})}{H}\frac{\partial \theta}{\partial Y}\Big|_{Y=-1} \\ q"_u &= -k\frac{\partial T}{\partial y}\Big|_{y=H} = -\frac{k(T_m - T_{w\mu})}{H}\frac{\partial \theta}{\partial Y}\Big|_{Y=1} \end{aligned} \tag{3.44}$$

Dividing the lower heat flux to the upper one, and solving it for β, the following result is obtained;

$$\beta = \frac{Nu}{2}\frac{(1+q_r)}{(1-q_r)} \tag{3.45}$$

where, q_r is the ratio of the upper and lower wall heat fluxes.

At this point, the individual Nusselt numbers at the lower and upper walls can be investigated. To do this, the heat fluxes at both walls can be used again. The walls are assumed to be so thin that the conduction resistance can be neglected. Hence, the wall heat fluxes directly convected to the fluid and the following equations for the upper and lower walls can be written as follows.

$$\begin{aligned} q"_l &= -k\frac{\partial T}{\partial y}\Big|_{y=-H} = h(T_{wl} - T_m) \\ q"_u &= -k\frac{\partial T}{\partial y}\Big|_{y=H} = h(T_{wu} - T_m) \end{aligned} \tag{3.46}$$

The dimensionless parameters, defined in Equations (3.4) and (3.14), are used to continue our analysis of individual Nusselt numbers. For the upper wall, the analysis can be performed as follows:

$$-\frac{k(T_m - T_{w\mu})}{H}\frac{\partial\theta}{\partial Y}\Big|_{Y=1} = h(T_{wu} - T_m) \Rightarrow \frac{\partial\theta}{\partial Y}\Big|_{Y=1} = \frac{hH(T_m - T_{wu})}{k(T_m - T_{w\mu})}$$

$$= \frac{h\ 2H(T_m - T_{wu})}{2k(T_m - T_{w\mu})} = \frac{1}{2}Nu_u\frac{(T_m - T_{wu})}{(T_m - T_{w\mu})}$$

$$= \frac{1}{2}Nu_u\frac{\left(T_m - \frac{T_{wu}}{2} - \frac{T_{wu}}{2} + \frac{T_{wl}}{2} - \frac{T_{wl}}{2}\right)}{(T_m - T_{w\mu})}$$

$$= \frac{1}{2}Nu_u\frac{\left(T_m - T_{w\mu} + \frac{T_{wl} - T_{wu}}{2}\right)}{(T_m - T_{w\mu})}$$

Finally, the dimensionless temperature gradient at the upper surface can be written as follows.

$$\frac{\partial\theta}{\partial Y}\Big|_{Y=1} = \frac{1}{2}Nu_u(1 + \beta) \tag{3.47}$$

After further mathematical manipulations, Nu_u can be written as in Equation (3.48). Similarly, the dimensionless heat transfer coefficient of the lower wall can be stated as in Equation (3.49).

$$Nu_u = -\frac{70}{26 + 9q_r} \tag{3.48}$$

$$Nu_l = \frac{70}{26 + 9/q_r} \tag{3.49}$$

As seen above, when the boundaries are subjected to equal heat fluxes, then Nu_u and Nu_lbecomes *-70/17* and *70/17*, respectively. All these results will be discussed in Chapter 9.

3.4. Pressure Drop Calculations

Pressure drop calculations are essential in all cases, which are studied in this thesis, since the power needed by fan (or pump) is directly proportional to pressure drop. To achieve an opinion about the pressure drop in the channel, the definition of the

friction factor is used. Friction factor for a channel in which fluid flows with a mean velocity of u_m can be defined as:

$$f = \frac{\left(-\frac{dP}{dx}\right) 2H}{\frac{1}{2}\rho u_m^2} \tag{3.50}$$

For a fully developed flow in a channel, the pressure gradient along the x-axis is constant and this negative gradient is denoted by *G*, as stated in Equation (3.8). Then the Equation (3.50) becomes as follows:

$$f = \frac{4GH}{\rho u_m^2} \tag{3.51}$$

Using the definition of the dimensionless velocity defined in Equation (3.8), the following equation is obtained for the friction factor.

$$f = \frac{4}{U_m} \frac{\mu}{\rho u_m H} \tag{3.52}$$

or

$$f\,Re = \frac{8}{U_m} \tag{3.53}$$

Since the dimensionless mean velocity is found as *1/3* as shown in Equation (3.13), then the multiplication of the friction factor and Reynolds number of a fluid flowing in a clear channel is calculated as *24*. This result can be used for comparison of pressure drops in a clear channel and channels, which are partially or fully filled with porous media.

CHAPTER 4

FULLY DEVELOPED HEAT AND FLUID FLOW IN A POROUS CHANNEL: SYMMETRIC HEAT FLUX BOUNDARY CONDITIONS

In this section, Brinkman-Darcy equation and energy equation are solved for a channel filled with porous media under symmetric boundary condition. Nusselt number and friction coefficient based on Darcy are obtained analytically. The calculation of Nusselt Number is reported in literature by some researchers such as Nield and Bejan(2006). However, in this study, the method proposed by Nield is used to solve energy equation and approve the accuracy of our methods. Moreover, three different parameters as heat transfer increment ratio, pressure drop increment ratio and overall performance are defined to find out feasibility of the use of porous media for enhancement of heat transfer in channels.

4.1. Problem Definition

Thermally and hydrodynamically fully developed, laminar flow in a channel, which is fully filled with porous material, is investigated in this chapter. The channel height is *2H* as shown in Figure 4.1.

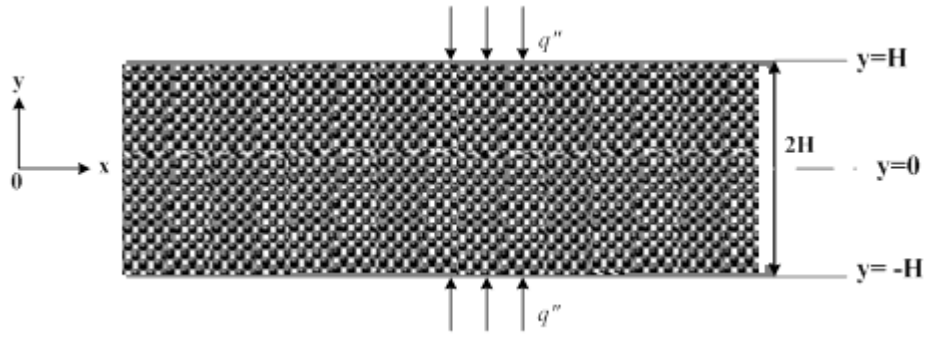

Figure 4.1. Schematic view of the channel that the fluid flows

The walls are subjected to constant heat fluxes, which are equal to each other. The basic purpose of this chapter is to investigate the effects of the Darcy number on heat transfer. Darcy number can be defined as the dimensionless permeability and it is formulated as in Equation (4.1).

$$Da = \frac{K}{H^2} \tag{4.1}$$

In Equation (4.1), *K* represents the permeability of the porous medium. As its name indicates; when the permeability of the porous medium is high, then the channel permits more fluid to flow. When *K* is small, the fluid flow requires stronger fan or pump power.

Another characteristic parameter of the porous media is the viscosity ratio, which is the ratio of the effective viscosity of fluid and the porous structures, and the dynamic viscosity of the fluid. The viscosity ratio is formulated as in Equation (4.2).

$$M = \frac{\mu_{eff}}{\mu_f} \tag{4.2}$$

As expressed above the main reason of writing this chapter is to observe the effects of Darcy number on heat transfer rate, specifically on Nusselt number. Momentum equation is also solved to understand the Darcy effects on the velocity profile. For all analysis in this chapter, *M* is accepted as 1. There is no doubt that, it is not the real case.

4.2. Fluid Flow Analysis

The flow in the channel is hydrodynamically fully developed and it is unidirectional in x-direction. Then, it can be hydrodynamically analysed by using Brinkman-extended Darcy equation as written below.

$$\mu_{eff} \frac{d^2u}{dy^2} - \frac{\mu}{K}u = \frac{dP}{dx} \tag{4.3}$$

As in the previous chapter, in which the heat and fluid flow in a clear channel was investigated, the governing equation for the velocity field can be made dimensionless by using the following dimensionless parameters.

$$Y = \frac{y}{H}, \qquad G = -\frac{\partial P}{\partial x}, \qquad S = \frac{1}{\sqrt{M\ Da}}, \qquad U = \frac{\mu u}{GH^2} \tag{4.4}$$

In Equation (4.4), S is called as the porous media shape parameter. H is the half of the channel height. After applying the dimensionless parameters into the Brinkman extended Darcy equation, the dimensionless momentum equation for the porous channel is found as in Equation (4.5).

$$\frac{d^2U}{dY^2} - S^2U + \frac{1}{M} = 0 \tag{4.5}$$

At this stage, the boundary conditions must be defined. No-slip condition states that the velocity of the fluid is zero at the boundaries as indicated in Equation (4.6). This boundary condition can also be made dimensionless by using the dimensionless parameters stated in Equations (4.1), (4.2), and (4.4). The dimensionless form of the boundary condition is stated as in Equation (4.7).

$$u(\pm H) = 0 \tag{4.6}$$

$$U(\pm 1) = 0 \tag{4.7}$$

Applying the dimensionless boundary conditions, Equation (4.7), onto the dimensionless governing equation, Equation (4.5), the following result is obtained for the velocity profile.

$$U(Y) = \frac{1 - \cosh{(SY)}\operatorname{sech}{(S)}}{MS^2} \tag{4.8}$$

The mean velocity of the fluid in the channel can be obtained by using the definition of the mean velocity defined in Equation (4.9), and it can be formulated as in Equation (4.10).

$$U_m = \frac{\int_{-1}^{1} U dY}{\int_{-1}^{1} dY} \tag{4.9}$$

$$U_m = \frac{S - tanh\,(S)}{MS^3} \tag{4.10}$$

The dimensionless velocity, found as in Equation (4.8), can be normalized by dividing it to the mean velocity shown in Equation (4.10).

$$\hat{u} = \frac{u}{u_m} = \frac{U}{U_m} = \frac{S[1 - \cosh\,(SY)\mathrm{sech}\,(S)]}{S - \tanh\,(S)} \tag{4.11}$$

4.3. Heat Flow Analysis

As in the energy analysis performed in Chapter 3, to begin; an energy balance must be applied to the channel. Neglecting the viscous dissipation, the energy conservation equation for a flow in a porous channel fully filled with porous medium can be written as in Equation (4.12).

$$\left(\rho C_p\right)_f \left(u\frac{\partial T}{\partial x} + v\frac{\partial T}{\partial y}\right) = k_{eff}\left(\frac{\partial^2 T}{\partial x^2} + \frac{\partial^2 T}{\partial y^2}\right) \tag{4.12}$$

Reminding that the y-component of the flow velocity is zero, and assuming the temperature gradient in y-direction is much greater than it is in x-direction, Equation (4.12) turns into the form as written in Equation (4.13).

$$\left(\rho C_p\right)_f u\frac{\partial T}{\partial x} = k_{eff}\frac{\partial^2 T}{\partial y^2} \tag{4.13}$$

To continue our energy analysis, the dimensionless temperature must be defined.

$$\theta = \frac{T - T_w}{T_m - T_w} \tag{4.14}$$

At this point, the energy equation in the form of Equation (4.13) must be made dimensionless to reduce the number of parameters. For this purpose, the dimensionless parameters stated in Equations (4.4) and (4.14) are used to obtain further form of the energy equation as written in Equation (4.15).

$$\left(\rho C_p\right)_f u\left[\theta\left(\frac{\partial T_m}{\partial x}-\frac{\partial T_w}{\partial x}\right)+(T_m-T_w)\frac{\partial \theta}{\partial x}+\frac{\partial T_w}{\partial x}\right]=k_{eff}(T_m-T_w)\frac{\partial^2\theta}{\partial y^2} \quad (4.15)$$

Since the walls are subjected to constant heat fluxes that are equal to each other, the gradient of wall heat fluxes with respect to x-direction must be equated to zero.

$$\frac{dq"}{dx}=\frac{d[h(T_w-T_m)]}{dx}=0 \qquad => \frac{\partial T_w}{\partial x}=\frac{\partial T_m}{\partial x} \quad (4.16)$$

The flow is accepted to be thermally and hydrodynamically fully developed. This condition makes the dimensionless temperature gradient in x-direction be zero.Using the thermally fully developed condition and the equation found as in Equation (4.16), the energy equation forms as in Equation (4.17).

$$\left(\rho C_p\right)_f u\frac{\partial T_m}{\partial x}=k_{eff}(T_m-T_w)\frac{\partial^2\theta}{\partial y^2} \quad (4.17)$$

The mean fluid temperature is defined as in Equation (4.18). However, it cannot be used to solve the Equation (4.17), because the fluid temperature is not known. A new relation for the mean temperature gradient in x-direction should be found. An energy balance must be applied for a control volume shown in Figure 4.2.

$$T_m=\frac{\int_{-1}^{1}\rho C_p u T dy}{\int_{-1}^{1}\rho C_p u dy} \quad (4.18)$$

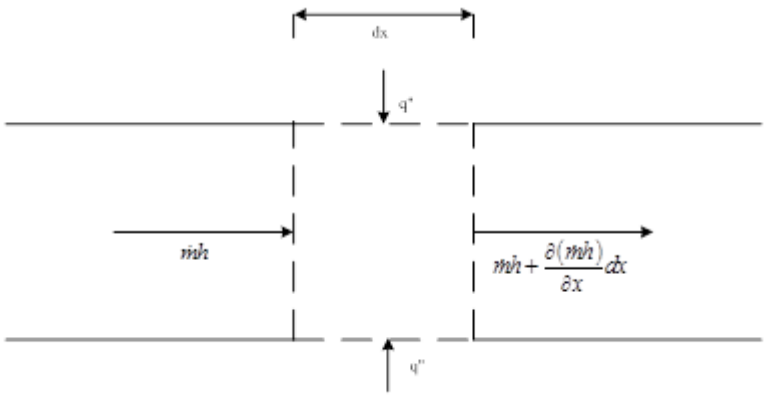

Figure 4.2. Total energy of the fluid is conserved. $h=C_pT_m$ is specific enthalpy and $\dot{m}=2H\rho u_m$ is the mass flow rate of the fluid

$$2H\rho u_m C_p T_m + 2q"dx = 2H\rho u_m C_p T_m + \frac{\partial\left(2H\rho u_m C_p T_m\right)}{\partial x}dx$$

After some manipulations, a formulation for the mean temperature gradient in x-direction is found as follows.

$$\frac{dT_m}{dx} = \frac{q"}{\rho C_p u_m H} \tag{4.19}$$

After inserting Equation (4.19) into Equation (4.17), the following equation is obtained for the energy balance.

$$\frac{u}{u_m}\frac{q"}{H} = k_{eff}(T_m - T_w)\frac{\partial^2\theta}{\partial y^2} \tag{4.20}$$

Introducing Equations (4.4) and (4.11) into Equation (4.20), and assuming the wall is thin enough to neglect the conduction resistance, the energy equation takes the form of Equation (4.22), remembering the convective heat flux is formulated as in Equation (4.21).

$$q" = h(T_w - T_m) \tag{4.21}$$

$$\frac{\partial^2\theta}{\partial Y^2} + \hat{u}\frac{hH}{k_f} = 0 \tag{4.22}$$

In this problem the conductivity term in the Nusselt equation should be taken as the effective conductivity of the fluid and the porous medium. Because, at the surface, the fluid flows in the porous media and the conductivity of the porous structures must

be considered. The definition of Nusselt number in this case and the final form of the energy equation are written in Equations (4.23) and (4.24), respectively.

$$Nu = \frac{h\,2H}{k_f} \tag{4.23}$$

$$\frac{\partial^2\theta}{\partial Y^2} + \frac{1}{2}\hat{u}Nu = 0 \tag{4.24}$$

At the boundaries, the wall temperatures are functions of x-direction. In the formulation of the normalized dimensionless temperature, Equation (4.14), it can be seen that the wall dimensionless temperatures are zero. The dimensionless forms of these boundary conditions are written in Equation (4.25).

$$\theta(\pm 1) = 0 \tag{4.25}$$

We have now sufficient information to solve the dimensionless energy equation, which is a second order ordinary differential equation. Using the boundary conditions stated above, the solution of Equation (4.24) is found as follows.

$$\theta(Y) = \frac{Nu[S^2(Y^2-1) + 2 - 2\cosh(SY)\operatorname{sech}(S)]}{4S[\tanh(S) - S]} \tag{4.26}$$

The compatibility condition, Equation (4.27), must be applied to find the dimensionless convective heat transfer coefficient.

$$\int_{-1}^{1} \theta\hat{u}dY = 2 \tag{4.27}$$

Using the compatibility condition, the Nusselt number equation is found as follows.

$$Nu = \frac{24S[S\cosh(S) - \sinh(S)]^2}{15\sinh(2S) + (4S^3 - 24S)cosh^2(S) - 6S} \tag{4.28}$$

4.4. Pressure Drop Calculations

The use of porous media in an internal flow may increase heat transfer through the channel, however it also increases pressure drop. As explained in Section 3.4, an increase in pressure drop in the channel makes fan power increase. That is why, both heat transfer and pressure drop should be analysed in this kind of problem. Friction factor for a channel in which fluid flows with u_m is defined as:

$$f = \frac{\left(-\frac{dP}{dx}\right) 2H}{\frac{1}{2}\rho u_m^2} \tag{4.29}$$

For a fully developed flow in a channel, the pressure gradient along the x-axis is constant and this negative gradient is denoted by *G*, as stated in Equation (4.4). Then the Equation (4.29) becomes as follows:

$$f = \frac{4GH}{\rho u_m^2} \tag{4.30}$$

Using the definition of the dimensionless velocity defined in Equation (4.4), the following equation is obtained for the friction factor.

$$f = \frac{4}{U_m} \frac{\mu}{\rho u_m H} \tag{4.31}$$

or

$$f\,Re = \frac{8}{U_m} \tag{4.32}$$

Equation (4.32) can be used for determination of pressure drop.

4.5. Analysis of Heat Transfer and Pressure Drop

To determine the heat transfer enhancement of full porous channel, dimensionless heat transfer coefficient of the system must be divided by the Nusselt

number of a flow in a clear channel, and the result is called **heat transfer increment ratio**.

$$\varepsilon_{th} = \frac{Nu}{Nu_c} \tag{4.33}$$

In this equation, Nu_c is the Nusselt number of the clear flow.

It is clear that $\varepsilon_{th} = 1$ for a clear fluid channel. Heat transfer enhancement is expected for the channel with $\varepsilon_{th} > 1$. The use of porous media will decrease heat transfer through a clear channel if $\varepsilon_{th} < 1$.

Similar definitions are valid for friction coefficient. The friction coefficient can be normalized by using friction coefficient of a clear channel.

$$\varepsilon_p = \frac{f\ Re}{(f\ Re)_c} \tag{4.34}$$

ε_p is called the **pressure drop increment ratio** in this thesis and for the values of ε_p greater than 1, the increase of pressure drop in the channel is expected, while for $\varepsilon_p < 1$, the use of porous medium decreases the pressure drop in the channel. The value of friction coefficient $(f\ Re)_c$ is determined as 24.

The ratio of ε_p and ε_{th} is shown by ε, and called the **overall performance**.

$$\varepsilon = \frac{\varepsilon_{th}}{\varepsilon_p} \tag{4.35}$$

For the values of ε greater than 1, heat transfer enhancement is greater than the increase of pressure drop. However, for the values of ε less than 1, the increase of pressure drop in the channel is greater than heat transfer enhancement.

All the results, which are obtained in this chapter will be discussed in Chapter 9.

CHAPTER 5

FULLY DEVELOPED HEAT AND FLUID FLOW IN A POROUS CHANNEL: ASYMMETRIC HEAT FLUX BOUNDARY CONDITIONS

5.1. Problem Definition

A two-dimensional parallel plate channel filled with a porous medium, and saturated with an incompressible fluid and also in local thermodynamic equilibrium is considered. The physical domain of interested problem is depicted in Figure 5.1. The channel has a rectangular cross-section with height of *2H*. The uniform heat fluxes of q''_l and q''_u are subjected to the channel walls. The heat flux of q''_l has positive direction while the direction of q''_u is negative. That is why the lower and upper heat fluxes are shown by q''_l (+) and q''_u (-), respectively. In the present study, the ratio of q''_l (+) and q''_u (-) is called as heat flux ratio ($q_r = q''_l$ (+) / q''_u(-)). The fluid that flows in the channel is Newtonian and its thermo-physical properties are assumed to be constant. The porous medium is isotropic with permeability of *K*. The flow in the channel is laminar, steady and hydrodynamically and thermally fully developed.

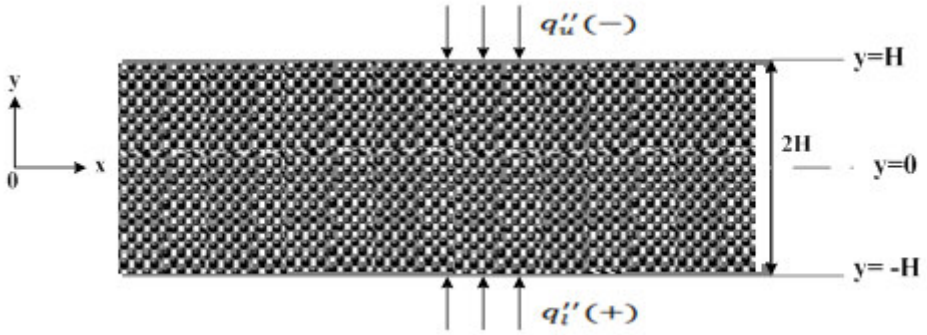

Figure 5.1.Schematic view of the channel that the fluid flows through.

5.2. Fluid Flow Analysis

For a hydrodynamically fully developed and unidirectional flow in a parallel plate channel, the following assumptions are valid;

$$v = 0, \qquad \frac{\partial u}{\partial x} = 0, \qquad \frac{\partial P}{\partial y} = 0 \tag{5.1}$$

where$v$ represents velocity in the y-direction and it vanishes for a unidirectional flow in a channel. The Darcy-Brinkman momentum equation for the considered fully-developed flow in the channel can be written as:

$$\mu_{eff}\frac{d^2u}{dy^2} - \frac{\mu}{K}u + \frac{\partial P}{\partial x} = 0 \tag{5.2}$$

whereμ and ρ represent fluid dynamic viscosity and density, and μ_{eff}shows effective viscosity whose value depends on the structure and geometry of the porous media, and the strength of the flow.Considering Figure 5.1, the boundary conditions for Equation (5.2) can be written as follows.

$$\left.\frac{\partial u}{\partial y}\right|_{y=0} = 0, \qquad u(\pm H) = 0 \tag{5.3}$$

and the mean velocity in the channel can be determined by following equation:

$$u_m = \frac{\int_{-H}^{H} u(y)dy}{\int_{-H}^{H} dy} \tag{5.4}$$

To obtain the dimensionless form of the Darcy-Brinkman momentum equation, the following dimensionless parameters can be used.

$$Y = \frac{y}{H}, \qquad M = \frac{\mu_{eff}}{\mu}, \qquad G = -\frac{\partial P}{\partial x}, \qquad Da = \frac{K}{H^2}, \qquad U = \frac{\mu u}{GH^2} \tag{5.5}$$

By using dimensionless parameters of Equation (5.5) and substituting them in Equation (5.2), the dimensionless form of Darcy-Brinkman momentum equation can be obtained as:

$$M\frac{d^2U}{dY^2}-\frac{1}{Da}U+1=0 \tag{5.6}$$

The dimensionless darcy-brinkman equation can be rewritten in the following form:

$$\frac{d^2U}{dY^2}-S^2U+\frac{1}{M}=0 \tag{5.7}$$

where the coefficient *S* is called as porous media shaping factor and it is defined as:

$$S=\frac{1}{\sqrt{M\ Da}}, \tag{5.8}$$

The dimensionless form of the boundary conditions for the problem can also be expressed in the following form.

$$\left.\frac{\partial U}{\partial Y}\right|_{Y=0}=0, \qquad U(\pm 1)=0 \tag{5.9}$$

The solution of dimensionless form of the Darcy-Brinkman momentum equation (5.7) with the given boundary conditions (5.9) can be found analytically.

$$U(Y)=Da\left[1-\frac{\cosh{(SY)}}{\cosh{(S)}}\right] \tag{5.10}$$

The definition of dimensionless mean velocity is:

$$U_m=\frac{1}{2}\int_{-1}^{1}U(Y)dY \tag{5.11}$$

The mean dimensionless velocity U_m can be found by using Equations (5.10) and (5.11) and is given by

$$U_m = Da\left[1 - \frac{\tanh(S)}{S}\right] \tag{5.12}$$

Furthermore, the dimensionless velocity profile can be normalized by the following relation,

$$\hat{u} = \frac{u}{u_m} = \frac{U}{U_m} \tag{5.13}$$

Based on the obtained dimensionless velocity given by Equation (5.10), the dimensionless normalized velocity can be obtained.

$$\hat{u} = \frac{S\,cosh(S) - S\,cosh(SY)}{S\,cosh(S) - sinh(S)} \tag{5.14}$$

5.3. Heat Flow Analysis

For a thermally and hydrodynamically fully developed laminar flow in a parallel plate channel, the heat transfer equation can be written as:

$$\left(\rho C_p\right)_f u\frac{\partial T}{\partial x} = k_{eff}\frac{\partial^2 T}{\partial y^2} \tag{5.15}$$

Introducing two new variables as the average wall heat flux, q''_{μ}, and the average wall temperature, $T_{w\mu}$, and defining the dimensionless temperature,

$$T_{w\mu} = \frac{T_{wl}+T_{wu}}{2}, \qquad q''_{\mu} = \frac{q''_{l}+q''_{u}}{2}, \qquad \theta = \frac{T-T_{w\mu}}{T_m-T_{w\mu}} \tag{5.16}$$

and applying the energy balance for a differential volume in the duct yields Equation (5.17) for the mean temperature gradient.

$$\frac{dT_{w\mu}}{dx} = \frac{dT_m}{dx} \tag{5.17}$$

Based on the relations expressed in Equation (5.16) on the average heat flux at boundaries and average temperature at boundaries, the overall Nusselt number can be defined as follows.

$$Nu = \frac{2Hq''_{\mu}}{k_{eff}(T_{w\mu} - T_m)} \tag{5.18}$$

Therefore, instead of two individual Nusselt numbers for the first and second plates, a unit Nusselt number can be defined.

The dimensionless form of the heat transfer equation can be found by substituting the dimensionless parameters defined by Equations (5.5) and (5.16) into Equation (5.15) and is given by

$$\frac{\partial^2\theta}{\partial Y^2} + \frac{1}{2}\hat{u}Nu = 0 \tag{5.19}$$

The related boundary conditions for the model problem shown in Figure 5.1 can be written as

$$\theta(1) = -\beta, \qquad \theta(-1) = \beta \tag{5.20}$$

where

$$\beta = \frac{T_{wl} - T_{wu}}{2(T_m - T_{w\mu})} \tag{5.21}$$

The solution of dimensionless heat transfer equation (5.19) under the boundary conditions (5.20) gives an equation for temperature distribution in the channel.

$$\theta(Y) = -\beta Y + \frac{Nu \cdot A}{2}\left(\frac{\cosh(S)}{2}(1 - Y^2) + \frac{\cosh(SY) - \cosh(S)}{S^2}\right) \tag{5.22}$$

where

$$A = \frac{S}{S\cosh(S) - \sinh(S)} \tag{5.23}$$

As can be seen from Equation (5.22), the dimensionless temperature distribution in Y direction is function of overall Nusselt number, shaping factor and β . According to Equation (5.21), the value of β depends on the surface and mean temperatures which are not known. In order to find another expression for βin terms of heat fluxes, the following manipulations can be done. Heat fluxes at the walls can be stated as follows:

$$\begin{aligned} q"_l &= -k_{eff}\left.\frac{\partial T}{\partial y}\right|_{y=-H} = -\frac{k_{eff}(T_m - T_{w\mu})}{H}\left.\frac{\partial \theta}{\partial Y}\right|_{Y=-1} \\ q"_u &= -k_{eff}\left.\frac{\partial T}{\partial y}\right|_{y=H} = -\frac{k_{eff}(T_m - T_{w\mu})}{H}\left.\frac{\partial \theta}{\partial Y}\right|_{Y=1} \end{aligned} \tag{5.24}$$

The derivative of dimensionless temperature at *Y = -1* and *1* can be calculated from the obtained dimensionless temperature equation (5.22). The ratio of equations in (5.24) yields a new definition forβin terms of heat flux ratio;

$$\beta = \frac{Nu}{2}\frac{(1+q_r)}{(1-q_r)} \tag{5.25}$$

Now, the compatibility condition

$$\int_{-1}^{1} \theta \hat{u} dY = 2 \tag{5.26}$$

can be used to obtain an expression for the overall Nusselt number. The overall Nusselt number can be obtained by substituting Equations (5.14) and (5.22) into Equation (5.26) and integration of the expression yields an expression for the overall Nusselt number;

$$Nu = \frac{24\,S\,[S\cosh(S) - \sinh(S)]^2}{15\sinh(2S) + (4\,S^3 - 24\,S)\cosh^2(S) - 6\,S} \tag{5.27}$$

As it was mentioned before, it is possible to obtain the individual Nusselt numbers by using the overall Nusselt number expression. The individual Nusselt numbers for the lower and upper plates are defined as:

$$Nu_l = -\frac{2Hq"_l}{k_{eff}(T_{wl} - T_m)}$$
$$Nu_u = -\frac{2Hq"_u}{k_{eff}(T_{wu} - T_m)} \tag{5.28}$$

The conservation of energy can be applied onto each wall and the following expressions can be obtained:

$$h(T_m - T_{wl}) = \frac{k_{eff}(T_m - T_{w\mu})}{H}\frac{\partial\theta}{\partial Y}\Big|_{Y=-1}$$
$$h(T_m - T_{wu}) = \frac{k_{eff}(T_m - T_{w\mu})}{H}\frac{\partial\theta}{\partial Y}\Big|_{Y=1} \tag{5.29}$$

After determination of dimensionless temperature gradient at the walls by using Equation (5.22) and performing some mathematical manipulations, the individual Nusselt numbers can be determined from Equations (5.29).

$$Nu_u = \frac{4\,Nu}{(Nu+2)+(Nu-2)/q_r}$$
$$Nu_u = \frac{-4\,Nu}{(Nu+2)+(Nu-2)q_r} \tag{5.30}$$

The overall Nusselt number can be calculated by Equation (5.27) for a given porous channel, and by substituting of *Nu* and heat flux ratio into Equations (5.30), the individual Nusselt numbers can be found. Figure 5.2 shows the sign of Nusselt number according to the direction of heat flux between walls and fluid. For instance, the positive value of lower plate Nusselt number indicates heat transfer from wall to the porous media, while negative value of Nusselt number at lower plate refers to heat transfer from fluid to the lower plate.

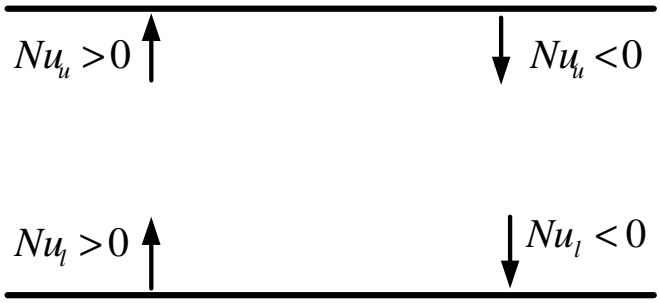

Figure 5.2. Signs of the individual Nusselt numbers

The denominators of Equations (5.30) take zero value for the specific values of heat flux ratio

$$q_{rl,cr} = \frac{2 - Nu}{2 + Nu}, \qquad q_{ru,cr} = \frac{2 + Nu}{2 - Nu} \tag{5.31}$$

where$q_{rl,cr}$ and $q_{ru,cr}$represent the critical heat flux ratios for lower and upper plates, respectively. Singularities in individual Nusselt numbers exist at critical heat flux ratios. The values of the lower and upper plate Nusselt numbers approach to infinity and heat transfer at the lower or upper plates changes direction at $q_{rl,cr}$ and $q_{ru,cr}$. The results will be discussed in Chapter 9.

CHAPTER 6

FULLY DEVELOPED HEAT AND FLUID FLOW IN A PARTIALLY POROUS CHANNEL: SYMMETRIC HEAT FLUX BOUNDARY CONDITIONS

6.1. Problem Definition

In this case; a partially porous channel with width of *2H* is heated from both walls. The heat fluxes at both walls are equal to each other. Porous material is located symmetrically as shown in Figure 6.1.Velocity and temperature distributions of flows with various Darcy numbers are analyzed. The Nusselt number variation with *Da* and heat flux ratio is also investigated.

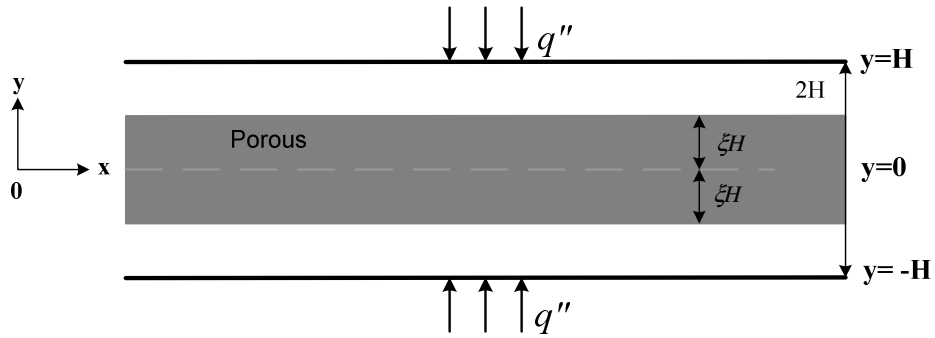

Figure 6.1. The schematic view of the channel which is wanted to be investigated

As seen in the figure, another variable, ξ, is introduced which have values between zero and one. When, ξ is equal to one, the channel becomes fully porous. Likewise, when it is zero, the channel is filled with fully clear.

6.2. Fluid Flow Analysis

For upper and lower clear regions, momentum equation can be written as follows.

$$u\frac{\partial u}{\partial x}+v\frac{\partial u}{\partial y}=-\frac{1}{\rho}\frac{\partial P}{\partial x}+\nu\left(\frac{\partial^2 u}{\partial x^2}+\frac{\partial^2 u}{\partial y^2}\right) \tag{6.1}$$

The flow in the channel is hydrodynamically fully developed and it is unidirectional in x direction. Hence, the left hand side of Equation (6.1) becomes zero. The gradient of *u* velocity in the direction of *x* is much greater than it is in the direction of *y*. Then, the momentum equation for the clear parts of the channel can be written as follows.

$$\nu\frac{\partial^2 u_c}{\partial y^2}-\frac{1}{\rho}\frac{\partial P}{\partial x}=0 \tag{6.2}$$

The subscript, *c*, stands for "clear fluid part of channel" and indicates the flow is in clear region.

Porous part of the channel can be analyzed by using Brinkman-extended Darcy equation as written below.

$$\mu_{eff}\frac{d^2 u_p}{dy^2}-\frac{\mu}{K}u_p=\frac{dP}{dx} \tag{6.3}$$

The subscript, *p,* stands for the word "porous" and it indicates the flow is in porous region. Boundary conditions for the problem can be written as follows.

$$\begin{aligned}\left.\frac{\partial u_p}{\partial y}\right|_{y=0}&=0, \qquad u_c(\pm H)=0\\ u_c(\pm\xi H)&=u_p(\pm\xi H), \qquad \tau_c(\pm\xi H)=\tau_p(\pm\xi H)\end{aligned} \tag{6.4}$$

To reduce the number of the variables of the governing equations and simplify the solution, the following dimensionless parameters are used.

$$\begin{aligned}Y&=\frac{y}{H}, \qquad M=\frac{\mu_{eff}}{\mu}, \qquad G=-\frac{\partial P}{\partial x}, \qquad Da=\frac{K}{H^2}\\ U&=\frac{\mu u}{GH^2}, \qquad S=\frac{1}{\sqrt{M\,Da}}, \qquad \theta=\frac{T-T_w}{T_m-T_w}\end{aligned} \tag{6.5}$$

After applying the boundary conditions stated in Equation (6.5), into the governing equations (Equation (6.2) and Equation (6.3)), dimensionless forms of the momentum equations for clear regions and for the porous region can be derived, respectively, as follows.

$$\frac{d^2U_c}{dY^2} + 1 = 0 \tag{6.6}$$

$$\frac{d^2U_p}{dY^2} - S^2U_p + \frac{1}{M} = 0 \tag{6.7}$$

Dimensionless forms of boundary conditions (Equation (6.4)) can also be derived by using the dimensionless parameters stated in Equation (6.5) and they can be obtained as in Equation (6.8).

$$\begin{aligned} \left.\frac{\partial U_p}{\partial Y}\right|_{Y=0} = 0, \qquad & U_c(\pm 1) = 0 \\ U_c(\pm\xi) = U_p(\pm\xi), \qquad & \tau_c(\pm\xi) = \tau_p(\pm\xi) \end{aligned} \tag{6.8}$$

Applying the dimensionless boundary conditions (Equation 6.8) to the dimensionless governing equations (Equations (6.6) and (6.7)), the following solutions for the three regions are obtained.

For the upper clear region that is shown with blue color in Figure 6.2, the velocity profile can be obtained as in Equation (6.9), whereas it can be written as (6.10) and (6.11) for lower clear region (Figure 6.3) and the porous region (Figure 6.4), respectively.

The equation for the velocity profile for upper region is:

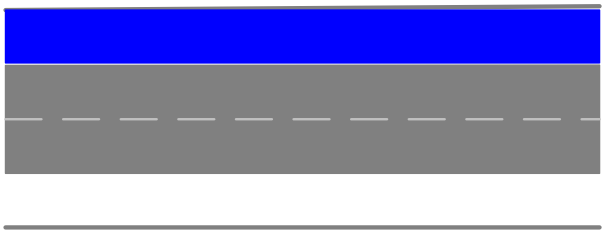

Figure 6.2. Upper clear region of the channel

$$U(Y) = A_1Y^2 + A_2Y + A_3 \tag{6.9}$$

$$A_1 = -\frac{1}{2}$$

$$A_2 = \frac{\xi^2 + 2V - 1}{2(\xi - 1)}$$

$$A_3 = \frac{\xi - \xi^2 - 2V}{2(\xi - 1)}$$

The equation for the velocity profile for lower region is:

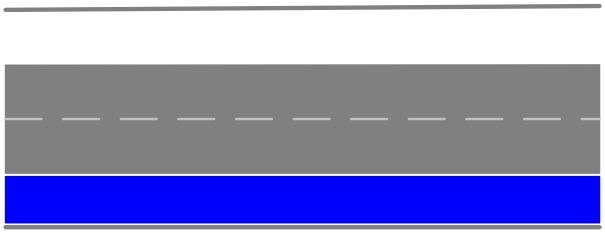

Figure 6.3. Lower clear part of the channel

$$U(Y) = A_1 Y^2 + A_4 Y + A_3 \tag{6.10}$$

$$A_4 = \frac{1 - \xi^2 - 2V}{2(\xi - 1)}$$

The equation for the velocity profile for the porous region can be expressed as:

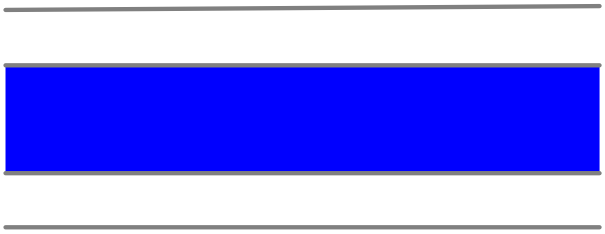

Figure 6.4. Porous part of the channel

$$U(Y) = P_1 \cosh(SY) + P_2 \tag{6.11}$$

$$P_1 = \frac{(VS^2M - 1)\operatorname{sech}(S\xi)}{MS^2}$$

$$P_2 = \frac{1}{MS^2}$$

V is the dimensionless velocity at the porous – clear region interfaces and can be calculated as follows.

$$V = \frac{(2\tanh(S\xi) - S\xi + S)(\xi - 1)}{2S\,[(\xi - 1)\,MS\tanh(S\xi) - 1]} \tag{6.12}$$

The mean velocity is defined as Equation (6.13), and can be calculated by Equation (6.14).

$$U_m = \frac{1}{2}\int_{-1}^{1} U(Y)dY \tag{6.13}$$

$$U_m = \frac{A_1}{3}(1 - \xi^3) + \frac{A_2 - A_4}{4}(\xi^2 - 1) + A_3(1 - \xi) + \frac{P_1}{S}\sinh(\mathrm{S}\xi) + \mathrm{P}_2\xi \tag{6.14}$$

Finally, the dimensionless normalized velocity must be introduced. It is defined as the ratio of fluid velocity at any point and the mean velocity. The analysis of this study is based on the dimensionless normalized velocity because of two reasons. First, it eases to demonstrate the velocity profiles of porous media with different Darcy numbers. Low Darcy number means the porous material has a large contribution in the channel and permits less fluid to flow. Then, its velocity is much lower than the fluid flowing in high-Darcy number media. The second reason is about the energy equation. As it is explained in the next section, the normalized velocity has a significant role in the analysis to find the temperature field.

$$\hat{u} = \frac{u}{u_m} = \frac{U}{U_m} \tag{6.15}$$

6.3. Heat Flow Analysis

Energy balance for a flow in a channel shown in Figure 6.1 can be written as follows:

$$(\rho C_p)_f\left(u\frac{\partial T}{\partial x} + v\frac{\partial T}{\partial y}\right) = \left(\lambda(k_{eff} - k) + k\right)\left(\frac{\partial^2 T}{\partial x^2} + \frac{\partial^2 T}{\partial y^2}\right) \tag{6.16}$$

where$k$ is the conductivity of the fluid, k_{eff} is the effective conductivity of the porous structures and the fluid, and λ is defined below.

$$\begin{aligned} -1 \le Y < -\xi \quad &=> \quad \lambda = 0 \\ -\xi \le Y \le \xi \quad &=> \quad \lambda = 1 \\ \xi < Y \le 1 \quad &=> \quad \lambda = 0 \end{aligned} \tag{6.17}$$

The velocity component in y-direction is accepted to be zero, for fully developed flow. Furthermore, the temperature gradient in y-direction is much greater than it is in x-direction. Therefore, the energy equation becomes into the form written below.

$$(\rho C_p)_f u \frac{\partial T}{\partial x} = \left(\lambda\left(k_{eff} - k\right) + k\right) \frac{\partial^2 T}{\partial y^2} \tag{6.18}$$

Energy equation can be written in dimensionless form by using the dimensionless parameters defined in Equation (6.5). Since the heat fluxes applied to both walls are held constant and equal to each other and the porous region is located into the channel symmetrically, the wall temperatures are equal to each other and it is designated as T_w. It must be stated that the wall temperature is not a constant; it is a function of x.

After further manipulations, the energy equation turns into the form as shown in Equation (6.19).

$$\begin{aligned} &(\rho C_p)_f u \left[\theta\left(\frac{\partial T_m}{\partial x} - \frac{\partial T_w}{\partial x}\right) + (T_m - T_w)\frac{\partial \theta}{\partial x} + \frac{\partial T_w}{\partial x}\right] \\ &= \left(\lambda\left(k_{eff} - k\right) + k\right)(T_m - T_w)\frac{\partial^2 \theta}{\partial y^2} \end{aligned} \tag{6.19}$$

As stated above, the applied heat fluxes at both walls are held constant. Therefore, the x-gradient of the heat fluxes are zero.

$$\frac{dq''}{dx} = \frac{d[h(T_w - T_m)]}{dx} = 0 \quad => \frac{\partial T_w}{\partial x} = \frac{\partial T_m}{\partial x} \tag{6.20}$$

Applying the condition stated in Equation (6.20), and using the thermally fully developed condition ($\partial\theta/\partial x=0$), the energy equation takes the form as follows.

$$(\rho C_p)_f u \frac{\partial T_m}{\partial x} = \left(\lambda\left(k_{eff} - k\right) + k\right)(T_m - T_w)\frac{\partial^2 \theta}{\partial y^2} \tag{6.21}$$

To find a definition for the mean temperature gradient in x-direction, an energy balance must be applied for a control volume shown in Figure 6.7.

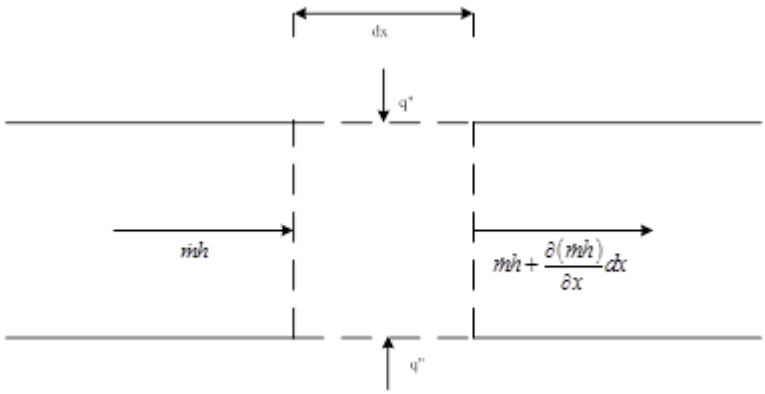

Figure 6.5. Total energy of the fluid is conserved. $h=C_pT_m$ is specific enthalpy and $\dot{m}=2H\rho u_m$ is the mass flow rate of the fluid

$$2H\rho u_m C_p T_m + 2q"dx = 2H\rho u_m C_p T_m + \frac{\partial\left(2H\rho u_m C_p T_m\right)}{\partial x}dx$$

Applying the energy balance shown in Figure 6.5, the following condition is obtained.

$$\frac{dT_m}{dx} = \frac{q"}{\rho C_p u_m H} \tag{6.22}$$

Inserting the Equation (6.22) into Equation (6.21), the following equation is obtained.

$$\frac{u}{u_m}\frac{q"}{H} = \left(\lambda\left(k_{eff} - k\right) + k\right)(T_m - T_w)\frac{\partial^2 \theta}{\partial y^2} \tag{6.23}$$

The applied heat fluxes at the walls will be convected to the fluid and will be equal to convective heat flux that is expressed as in Equation (6.24).

$$q" = h(T_w - T_m) \tag{6.24}$$

Inserting Equations (6.15) and (6.24) into Equation (6.23) and applying the dimensionless parameters stated in Eq, (6.5), the energy equation turns into the form stated below.

$$\frac{\partial^2\theta}{\partial Y^2} + \hat{u}\frac{hH}{\left(\lambda\left(k_{eff}-k\right)+k\right)} = 0 \tag{6.25}$$

The dimensionless temperature gradient at the surface, the Nusselt number, is defined as in Equation (6.26), and the final form of the dimensionless energy equation can be obtained by using this relation in Equation (6.25).

$$Nu = \frac{h\ 2H}{k_f} \tag{6.26}$$

$$\frac{\partial^2\theta}{\partial Y^2} + \frac{1}{2}\hat{u}Nu\frac{1}{(\lambda(k_r-1)+1)} = 0 \tag{6.27}$$

wherek_r is the ratio of the effective conductivity of porous medium and the fluid, and the conductivity of the fluid, and shown in Equation (6.28).

$$k_r = \frac{k_{eff}}{k} \tag{6.28}$$

In another words, the energy equations for the porous and clear regions can be written as follows, respectively.

$$\begin{aligned}\frac{\partial^2\theta}{\partial Y^2} + \frac{1}{2k_r}\hat{u}Nu = 0\\ \frac{\partial^2\theta}{\partial Y^2} + \frac{1}{2}\hat{u}Nu = 0\end{aligned} \tag{6.29}$$

Assuming the interface temperatures and conduction heat fluxes to be equal between the porous and clear media, the boundary conditions can be written as in Equation (6.30).

$$\begin{aligned}T_c(\pm H) = T_w\\ T_c(\pm\xi H) = T_p(\pm\xi H)\end{aligned} \tag{6.30}$$

$$k\frac{dT_c}{dy}\Big|_{y=\pm H\xi} = k_{eff}\frac{dT_p}{dy}\Big|_{y=\pm H\xi}$$

Using the dimensionless parameters stated in Equations (6.5) and (6.28), the following dimensionless forms of the boundary conditions are obtained.

$$\theta_c(\pm 1) = 0$$

$$\theta_c(\pm\xi) = \theta_p(\pm\xi) \tag{6.31}$$

$$\frac{d\theta_c}{dY}\Big|_{Y=\pm\xi} = k_r\frac{d\theta_p}{dY}\Big|_{Y=\pm\xi}$$

After solving the energy equation (6.29) by using boundary conditions (6.31), the following results are obtained.

In upper clear region, the dimensionless temperature profile is obtained as follows,

$$\theta = C_1 + C_2Y + C_3Y^2 + C_4Y^3 + C_5Y^4 \tag{6.32}$$

$$C_1 = \frac{24U_m\theta_i + Nu\xi(\xi-1)[2(A_2(\xi+1)+3A_3)+A_1(1+\xi+\xi^2)]}{24U_m(1-\xi)}$$

$$C_2 = \frac{24U_m\theta_i + Nu[6A_3(\xi^2-1)+2A_2(\xi^3-1)+A_1(\xi^4-1)]}{24U_m(\xi-1)}$$

$$C_3 = -\frac{A_3Nu}{4U_m}, \qquad C_4 = -\frac{A_2Nu}{12U_m}, \qquad C_4 = -\frac{A_1Nu}{24U_m}$$

In lower clear region, dimensionless temperature distribution is as written in Equation (6.33).

$$\theta = C_6 + C_7Y + C_3Y^2 + C_8Y^3 + C_5Y^4 \tag{6.33}$$

$$C_6 = \frac{-24U_m\theta_i + Nu\xi[A_1(1-\xi^3)-6A_3(\xi-1)+2A_4(\xi^2-1)]}{24U_m(\xi-1)}$$

$$C_7 = \frac{24U_m\theta_i + Nu[A_1(\xi^4-1)-2A_4(\xi^3-1)+6A_3(\xi^2-1)]}{24U_m(1-\xi)}$$

$$C_8 = -\frac{A_4 Nu}{12U_m}$$

For porous region, the results are shown below.

$$\theta = C_9 + C_{10}Y^2 + C_{11}\cosh(SY) \tag{6.34}$$

$$C_9 = \frac{4S^2 k_r U_m \theta_i + Nu[S^2 P_2 \xi^2 + 2P_1 \cosh(S\xi)]}{4S^2 k_r U_m}$$

$$C_{10} = -\frac{Nu\ P_2}{4k_r U_m}$$

$$C_{11} = -\frac{Nu\ P_1}{2k_r U_m S^2}$$

In temperature profiles for all regions, there is a term, θ_i, that designates the dimensionless interface temperature of porous and clear media and it can be calculated by the Equation (6.35). This equation was found by using the equal conductive heat transfer condition at the porous-clear media interfaces, as stated in Equation (6.31). After equating the heat fluxes, θ_i can be obtained.

$$\theta_i = \psi Nu \tag{6.35}$$

$$\psi = \sum_{k=1}^{3} \psi_k$$

$$\psi_1 = \frac{(\xi - 1)[P_2 S - P_1 \sinh(S\xi)]}{4U_m S}$$

$$\psi_2 = \frac{6A_3(1-\xi^2) + 2A_2(1-\xi^3) + A_1(1-\xi^4)}{24U_m}$$

$$\psi_3 = \frac{(1-\xi)}{2U_m}\left[A_3\xi + \frac{A_2\xi^2}{2} + \frac{A_1\xi^3}{3}\right]$$

To find the Nusselt number, the compatibility condition (Equation 6.36) must be applied.

$$\int_{-1}^{1} \theta \hat{u} dY = 2 \tag{6.36}$$

The derivation of the compatibility condition is explained in detail in Appendix A. After applying the compatibility condition; the following equation is obtained for Nusselt number:

$$Nu = \frac{2U_m}{\sum_{k=1}^{5} N_k} \tag{6.37}$$

$$N_1 = \frac{\psi(1-\xi)[8V + (\xi-1)^2]}{12}$$

$$N_2 = \frac{(1-\xi)^3[448V^2 + 168V(\xi-1)^2 + 17(\xi-1)^4]}{20160U_m}$$

$$N_3 = \frac{sech^2(S\xi)\xi\left[[\xi^2 - 3MV(MS^2V-4)]S^2 - 9 + 6k_rM\psi S^4U_m\right]}{6k_rM^2S^6U_m}$$

$$N_4 = \frac{sech^2(S\xi)\cosh(2S\xi)\xi^2[S^2[6M(k_r\psi S^2U_m + V) + \xi^2] - 6]}{3k_rM^2S^5U_m}$$

$$N_5 = \frac{sech^2(S\xi)\sinh(2S\xi)\xi(MS^2V-1)(MS^2V - 5 + 4k_rM\psi S^4U_m)}{2k_rM^2S^6U_m}$$

6.4. Pressure Drop Calculations

To find an expression that gives information about the pressure drop along the channel, friction factor is used. Friction factor for a channel in which fluid flows with u_m is defined as:

$$f = \frac{\left(-\frac{dP}{dx}\right)2H}{\frac{1}{2}\rho u_m^2} \tag{6.38}$$

For a fully developed flow in a channel, the pressure gradient along the x-axis is constant and this negative gradient is denoted by *G*, as stated in Equation (6.5). Then the Equation (6.38) becomes as follows:

$$f = \frac{4GH}{\rho u_m^2} \tag{6.39}$$

Using the definition of the dimensionless velocity defined in Equation (6.5), the following equation is obtained for the friction factor.

$$f = \frac{4}{U_m} \frac{\mu}{\rho u_m H} \tag{6.40}$$

or

$$f\,Re = \frac{8}{U_m} \tag{6.41}$$

Equation (6.41) can be used for determination of pressure drop.

6.5. Analysis of Heat Transfer and Pressure Drop

As explained in Chapter 4, to determine the heat transfer enhancement of full porous channel, the Nusselt number of the porous system must be divided by the Nusselt number of a flow in a clear channel, and the result is called **heat transfer increment ratio**.

$$\varepsilon_{th} = \frac{Nu}{Nu_c} \tag{6.42}$$

Thermal efficiency is equal to 1 for a clear channel. Heat transfer enhancement is expected for the channel with $\varepsilon_{th} > 1$. The use of porous media will decrease heat transfer through a clear channel if $\varepsilon_{th} < 1$.

Similar definitions are valid for friction coefficient. The friction coefficient can be normalized by using friction coefficient of a clear channel.

$$\varepsilon_p = \frac{f\,Re}{(f\,Re)_c} \tag{6.43}$$

ε_p is called the **pressure drop increment ratio** in this thesis and for the values of $\varepsilon_p$greater than *1*, the increase of pressure drop in the channel is expected, while for $\varepsilon_p < 1$, the use of porous layer decreases the pressure drop in the channel. The value of friction coefficient $(f\,Re)_c$ is determined as *24*.

The ratio of ε_p and $\varepsilon_{th}$is shown by ε, and called the **overall performance**.

$$\varepsilon = \frac{\varepsilon_{th}}{\varepsilon_p} \tag{6.44}$$

For the values of ε greater than *1*, heat transfer enhancement is greater than the increase of pressure drop if a porous layer is used at the core of the channel. However, for the values of ε less than *1*, the increase of pressure drop in the channel is greater than heat transfer enhancement.

All the results, which are obtained in this chapter, will be discussed in Chapter 9.

CHAPTER 7

FULLY DEVELOPED HEAT AND FLUID FLOW IN AN ASYMMETRIC PARTIALLY POROUS CHANNEL: SYMMETRIC CONSTANT HEAT FLUX BOUNDARY CONDITIONS

7.1. Problem Definition

In this case; a partially porous channel with width of *2H* is heated from both walls. The heat fluxes at both walls are equal to each other as in the case explained in Chapter 6. However, porous material is located asymmetrically as shown in Figure 7.1. The velocity and temperature distributions of flows with various Darcy numbers are analyzed. The Nusselt number variation with Da and heat flux ratio is also investigated.

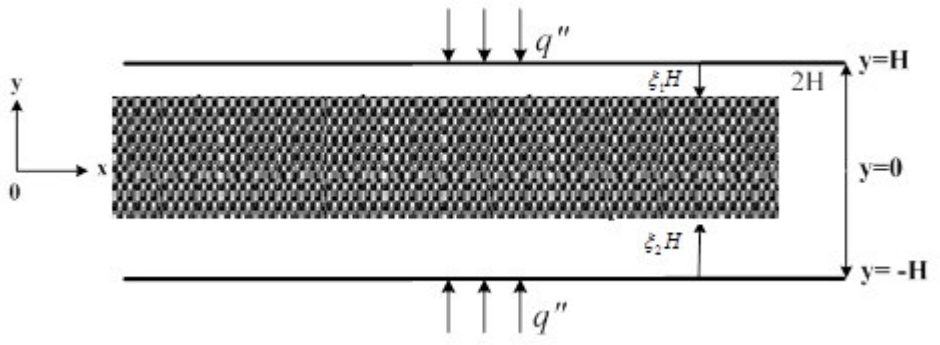

Figure 7.1. The schematic view of the channel which is wanted to be investigated ($\xi_1 \neq \xi_2$)

As seen in the figure, two new variables, ξ_1 and ξ_2, are introduced and they can have values between zero and one. Their values are different from each other. The arrangement of the channel structure can be made by playing with these two variables.

7.2. First Approach: Brinkman-Extended Darcy Law

7.2.1. Fluid Flow Analysis

For upper and lower clear regions, the momentum equation can be written as follows.

$$u\frac{\partial u}{\partial x}+v\frac{\partial u}{\partial y}=-\frac{1}{\rho}\frac{\partial P}{\partial x}+\nu\left(\frac{\partial^2 u}{\partial x^2}+\frac{\partial^2 u}{\partial y^2}\right) \tag{7.1}$$

The flow in the channel is hydrodynamically fully developed and it is unidirectional in x-direction. Hence, the left hand side of Equation (7.1) becomes zero. The gradient of *u* velocity in the direction of *x* is much greater than it is in the direction of *y*. Then, the momentum equation for the clear parts of the channel can be written as follows.

$$\nu\frac{\partial^2 u_c}{\partial y^2}-\frac{1}{\rho}\frac{\partial P}{\partial x}=0 \tag{7.2}$$

The subscript, *c*, stands for "clear" and indicates the flow is in clear region. The porous part of the channel can be analysed hydrodynamically by using Brinkman-extended Darcy equation as written below.

$$\mu_{eff}\frac{d^2 u_p}{dy^2}-\frac{\mu}{K}u_p=\frac{dP}{dx} \tag{7.3}$$

The subscript, *p,* stands for the word "porous" and it indicates the flow is in porous region. Boundary conditions for the problem can be written as follows. In these equations; the subscripts *cu* and *cl* stand for the upper and lower clear regions, respectively.

$$
\begin{aligned}
u_{cu}(H) = 0, \qquad & u_{cl}(-H) = 0 \\
u_{cl}[H(\xi_2 - 1)] &= u_p[H(\xi_2 - 1)] \\
u_{cu}[H(1 - \xi_1)] &= u_p[H(1 - \xi_1)] \\
\tau_{cl}[H(\xi_2 - 1)] &= \tau_p[H(\xi_2 - 1)] \\
\tau_{cu}[H(1 - \xi_1)] &= \tau_p[H(1 - \xi_1)]
\end{aligned}
\tag{7.4}
$$

To reduce the number of the variables of the governing equations and simplify the solution, the following dimensionless parameters are used.

$$
\begin{aligned}
Y = \frac{y}{H}, \qquad & M = \frac{\mu_{eff}}{\mu}, \qquad G = -\frac{\partial P}{\partial x}, \\
Da = \frac{K}{H^2}, \qquad & U = \frac{\mu u}{GH^2}, \qquad S = \frac{1}{\sqrt{M\,Da}}
\end{aligned}
\tag{7.5}
$$

After applying the non-dimensional parameters stated in Equation (7.5), into the governing equations (7.2 and 7.3), the dimensionless forms of the momentum equations for clear regions and for the porous region can be derived, respectively, as follows.

$$
\frac{d^2U_c}{dY^2} + 1 = 0 \tag{7.6}
$$

$$
\frac{d^2U_p}{dY^2} - S^2U_p + \frac{1}{M} = 0 \tag{7.7}
$$

In Equation (7.7), *S* represents the porous media shape parameter and it is formulized as in Equation (7.5). Dimensionless forms of boundary conditions (Equation 7.4) can also be derived by using the dimensionless parameters stated in Equation (7.5) and they can be obtained as in Equation (7.8).

$$
\begin{aligned}
U_{cu}(1) &= 0, \\
U_{cl}(-1) &= 0 \\
U_{cl}(\xi_2 - 1) &= U_p(\xi_2 - 1) \\
U_{cu}(1 - \xi_1) &= U_p(1 - \xi_1) \\
\tau_{cl}{}^*(\xi_2 - 1) &= \tau_p{}^*(\xi_2 - 1) \\
\tau_{cu}{}^*(1 - \xi_1) &= \tau_p{}^*(1 - \xi_1)
\end{aligned}
\tag{7.8}
$$

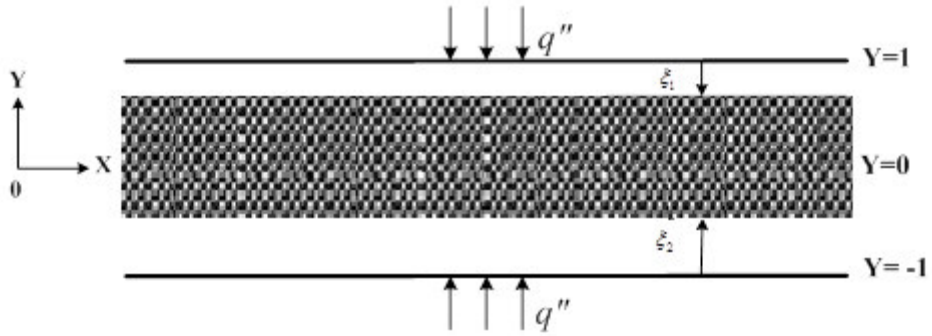

Figure 7.2. The schematic view of the dimensionless channel wanted to be investigated ($\xi_1 \neq \xi_2$)

Applying the dimensionless boundary conditions (Equation 7.8) to the dimensionless governing equations (Equations 7.6 and 7.7), the following velocity profiles of three regions shown in Figures (7.3), (7.4), and (7.5) are obtained and shown in Equations (7.9), (7.10), and (7.11), respectively.

For upper clear region:

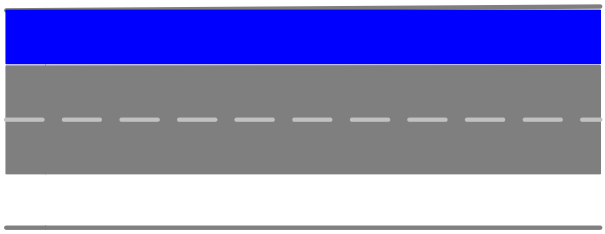

Figure 7.3. Upper clear region of the channel

$$U_{cu}(Y) = \frac{(1-Y)[2U_u + \xi_1(Y+\xi_1-1)]}{2\xi_1}$$

or

$$U_{cu}(Y) = -\frac{1}{2}Y^2 + \left(1 - \frac{\xi_1}{2} - \frac{U_u}{\xi_1}\right)Y + \left(\frac{U_u}{\xi_1} + \frac{\xi_1 - 1}{2}\right) \tag{7.9}$$

For lower clear region:

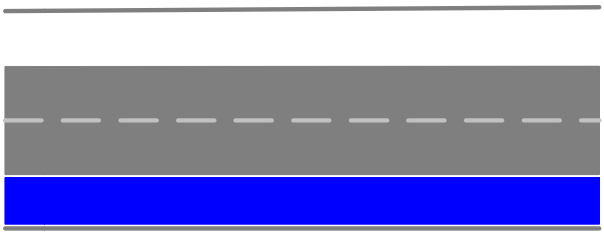

Figure 7.4. Lower clear part of the channel

$$U_{cl}(Y) = \frac{(1+Y)\,[2U_l + \xi_2(\xi_2 - Y - 1)]}{2\xi_2}$$

or

$$U_{cl}(Y) = -\frac{1}{2}Y^2 + \left(\frac{U_l}{\xi_2} - 1 + \frac{\xi_2}{2}\right)Y + \left(\frac{U_l}{\xi_2} + \frac{\xi_2 - 1}{2}\right) \tag{7.10}$$

For porous region:

Figure 7.5. Porous part of the channel

$$U_p(Y) = P_1 + P_2 e^{SY} + P_3 e^{-SY} \tag{7.11}$$

where

$$P_1 = \frac{1}{MS^2}$$

$$P_2 = \frac{e^{-S(\xi_2 - 1)}(1 - MS^2 U_u) - e^{S(\xi_1 - 1)}(1 - MS^2 U_l)}{2MS^2 sinh[S(\xi_1 + \xi_2 - 2)]} \tag{7.12}$$

$$P_3 = \frac{e^{-S(\xi_1 - 1)}(1 - MS^2 U_l) - e^{S(\xi_2 - 1)}(1 - MS^2 U_u)}{2MS^2 sinh[S(\xi_1 + \xi_2 - 2)]}$$

In equations from (7.9) to (7.12), U_l and U_u indicate the dimensionless velocities at porous and clear region interfaces at lower and upper parts, respectively, and formulated as below.

$$U_l = \frac{\xi_2\left(e^{S(\xi_1+\xi_2-2)}\left(4-2MS^2\xi_1^{\,2}\right)-e^{2S(\xi_1+\xi_2-2)}(MS\xi_1-1)(S\xi_2-2)-(1+MS\xi_1)(2+S\xi_2)\right)}{2e^{2S(\xi_1+\xi_2-2)}S(MS\xi_1-1)(MS\xi_2-1)-2S(1+MS\xi_1)(1+MS\xi_2)}$$

$$U_u = \frac{\xi_1\left(-e^{2S(\xi_1+\xi_2-2)}(S\xi_1-2)(MS\xi_2-1)-(S\xi_1+2)(1+MS\xi_2)+e^{S(\xi_1+\xi_2-2)}\left(4-2MS^2\xi_2^{\,2}\right)\right)}{2e^{2S(\xi_1+\xi_2-2)}S(MS\xi_1-1)(MS\xi_2-1)-2S(1+MS\xi_1)(1+MS\xi_2)}$$

The mean velocity in the channel can be defined as in Equation 7.13 and found as in Equation 7.14.

$$U_m = \frac{\int_{-1}^{1} U(Y)dY}{\int_{-1}^{1} dY} = \frac{\int_{-1}^{\xi_2-1} U_{cl}(Y)dY + \int_{\xi_2-1}^{1-\xi_1} U_p(Y)dY + \int_{1-\xi_1}^{1} U_{cu}(Y)dY}{2} \tag{7.13}$$

where

$$U_m = \frac{0.0416667}{MS^3}(R_1+R_2) \tag{7.14}$$

$$R_1 = MS^3\left(6U_u\xi_1+6U_l\xi_2+\xi_1^{\,3}+\xi_2^{\,3}\right)-12S(\xi_1+\xi_2-2)$$

$$R_2 = 12\tanh(0.5S(\xi_1+\xi_2-2))(2-MS^2(U_l+U_u))$$

A new variable named dimensionless normalized velocity is just the ratio of the dimensionless velocity and the mean velocity, as shown in Equation 7.15.

$$\hat{u} = \frac{u}{u_m} = \frac{U}{U_m} \tag{7.15}$$

7.2.2. Heat Flow Analysis

In the light of the first law of thermodynamics, energy equation for a flow in a channel can be written as follows,

$$\rho C_p\left(u\frac{\partial T}{\partial x}+v\frac{\partial T}{\partial y}\right)=\left(\lambda(k_{eff}-k)+k\right)\left(\frac{\partial^2 T}{\partial x^2}+\frac{\partial^2 T}{\partial y^2}\right) \tag{7.16}$$

where$k$ is the conductivity of the fluid, k_{eff} is the effective conductivity of the porous structures and the fluid, and λ is defined below.

$$\begin{aligned} -1\le Y<\xi_2-1 \quad &=> \quad \lambda=0 \\ \xi_2-1\le Y\le 1-\xi_1 \quad &=> \quad \lambda=1 \\ 1-\xi_1<Y\le 1 \quad &=> \quad \lambda=0 \end{aligned} \tag{7.17}$$

Since, $v=0$ in our case, neglecting the viscous dissipation term, and assuming that the temperature gradient in y-direction is much greater than it is in x-direction, the energy equation can be written as in Equation (7.18).

$$\rho C_p u\frac{\partial T}{\partial x}=\left(\lambda(k_{eff}-k)+k\right)\frac{\partial^2 T}{\partial y^2} \tag{7.18}$$

Introducing the dimensionless parameters defined below (Equation 7.19), into the energy equation (Equation 7.18), Equations (7.20) and (7.21) are obtained.

$$Y=\frac{y}{H},\quad G=-\frac{\partial P}{\partial x},\quad \theta=\frac{T-T_{w\mu}}{T_m-T_{w\mu}},\quad T_{w\mu}=\frac{T_{wu}+T_{wl}}{2} \tag{7.19}$$

$$\rho C_p u\frac{\partial}{\partial x}\left[\left(T_m-T_{w\mu}\right)\theta+T_{w\mu}\right]=\left(\lambda(k_{eff}-k)+k\right)\frac{\partial^2}{\partial y^2}\left[\left(T_m-T_{w\mu}\right)\theta+T_{w\mu}\right] \tag{7.20}$$

or

$$\rho C_p u\left[\theta\left(\frac{\partial T_m}{\partial x}-\frac{\partial T_{w\mu}}{\partial x}\right)+\left(T_m-T_{w\mu}\right)\frac{\partial\theta}{\partial x}+\frac{\partial T_{w\mu}}{\partial x}\right]=\left(\lambda(k_{eff}-k)+k\right)\left(T_m-T_{w\mu}\right)\frac{\partial^2\theta}{\partial y^2} \tag{7.21}$$

The applied heat fluxes at both walls are held constant. Hence, the gradient of wall heat flux with respect to x-direction should be taken zero.

$$For\ upper\ wall \quad => \quad \frac{dq''}{dx} = \frac{d\left(h_u\left(T_{wu} - T_m\right)\right)}{dx} = 0 \quad => \quad \frac{dT_{wu}}{dx} = \frac{dT_m}{dx}$$

$$For\ lower\ wall \quad => \quad \frac{dq''}{dx} = \frac{d\left(h_l\left(T_{wl} - T_m\right)\right)}{dx} = 0 \quad => \quad \frac{dT_{wl}}{dx} = \frac{dT_m}{dx}$$

$$\frac{dT_{wu}}{dx} + \frac{dT_{wl}}{dx} = 2\frac{dT_m}{dx} \quad => \quad \frac{d}{dx}\left[T_{wu} + T_{wl}\right] = 2\frac{dT_{w\mu}}{dx} = 2\frac{dT_m}{dx}$$

$$\frac{dT_{w\mu}}{dx} = \frac{dT_m}{dx} \tag{7.22}$$

Remembering the flow in the channel is thermally fully developed *(∂θ/∂x=0),* and using the condition of Equation 7.22, our last form of energy equation (Equation 7.21) becomes into the following form.

$$\rho C_p u \frac{dT_m}{dx} = \left(\lambda(k_{eff} - k) + k\right)\left(T_m - T_{w\mu}\right)\frac{d^2\theta}{dy^2} \tag{7.23}$$

To find a definition for the mean temperature gradient in x-direction, an energy balance must be applied for a control volume shown in Figure 7.6.

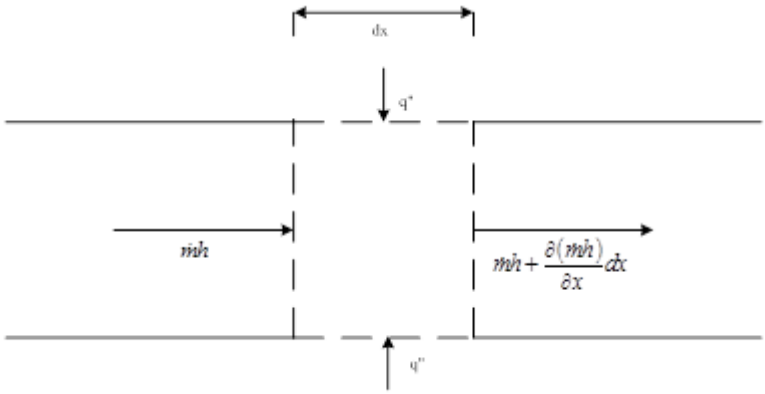

Figure 7.6. Total energy of the fluid is conserved. h=CpTm is specific enthalpy and □=2Hρum is the mass flow rate of the fluid

$$2H\rho u_m C_p T_m + 2q''dx = 2H\rho u_m C_p T_m + \frac{\partial\left(2H\rho u_m C_p T_m\right)}{\partial x}dx \tag{7.24}$$

After some manipulation, Equation 7.25 is obtained for mean temperature gradient.

$$\frac{dT_m}{dx} = \frac{q''}{\rho C_p u_m H} \tag{7.25}$$

Inserting the Equation 7.25 into Equation 7.23, the following equation is obtained.

$$\frac{u}{u_m}\frac{q''}{H} = \left(\lambda(k_{eff} - k) + k\right)\left(T_m - T_{w\mu}\right)\frac{d^2\theta}{dy^2} \tag{7.26}$$

The ratio of the velocity over the mean velocity is defined as dimensionless normalized velocity and expressed in Equation 7.15. The wall heat flux will be convected to the fluid and it will be equal to convective heat flux that is expressed as in Equation 7.27. Inserting Equation 7.27 into Equation 7.26 and applying the dimensionless parameters, Equation 7.19, into this equation, the energy equation takes the following form (Equation 7.28).

$$q'' = h\left(T_{w\mu} - T_m\right) \tag{7.27}$$

$$\frac{d^2\theta}{dY^2} + \hat{u}\frac{hH}{\left(\lambda(k_{eff} - k) + k\right)} = 0 \tag{7.28}$$

The dimensionless convective heat transfer coefficient, the Nusselt number, is defined as in Equation 7.29, and the final form of the dimensionless energy equation is obtained as in Equation 7.30,

$$Nu = \frac{h \cdot 2H}{k} \tag{7.29}$$

$$\frac{d^2\theta}{dY^2} + \frac{1}{2}\hat{u}Nu\frac{1}{\left(\lambda(k_r - 1) + 1\right)} = 0 \tag{7.30}$$

wherek_r is the ratio of the effective conductivity and the conductivity of the fluid, and shown in Equation 7.31.

$$k_r = \frac{k_{eff}}{k} \tag{7.31}$$

As in another words, the energy equation for the porous region and for the clear regions can be written as follows.

$$\frac{d^2\theta}{dY^2} + \frac{1}{2k_r}\hat{u}Nu = 0 \qquad \textit{in porous region}$$
$$\frac{d^2\theta}{dY^2} + \frac{1}{2}\hat{u}Nu = 0 \qquad \textit{in clear regions} \tag{7.32}$$

Boundary conditions can be written as in Equation 7.33. It is assumed that, at the interfaces of the clear and the porous regions, the temperatures and the conductive heat fluxes are the same.

$$T_{cu}(H) = T_{wu}$$
$$T_{cl}(-H) = T_{wl} \tag{7.33}$$
$$T_{cu}(H(1-\xi_1)) = T_p(H(1-\xi_1))$$
$$T_{cl}(H(\xi_2 - 1)) = T_p(H(\xi_2 - 1))$$
$$k\frac{dT_{cu}}{dy}\bigg|_{y=H(1-\xi_1)} = k_{eff}\frac{dT_p}{dy}\bigg|_{y=H(1-\xi_1)}$$
$$k\frac{dT_{cl}}{dy}\bigg|_{y=H(\xi_2-1)} = k_{eff}\frac{dT_p}{dy}\bigg|_{y=H(\xi_2-1)}$$

Another dimensionless parameter is introduced in Equation 7.34 for helping to derive the dimensionless boundary conditions stated as in Equation 7.35.

$$\beta = \frac{T_{wl} - T_{wu}}{2(T_m - T_{w\mu})} \tag{7.34}$$

$$\theta_{cu}(1) = -\beta$$
$$\theta_{cl}(-1) = \beta$$
$$\theta_{cu}(1-\xi_1) = \theta_p(1-\xi_1) \tag{7.35}$$

$$\theta_{cl}(\xi_2 - 1) = \theta_p(\xi_2 - 1)$$

$$\left.\frac{d\theta_{cu}}{dY}\right|_{Y=1-\xi_1} = k_r \left.\frac{d\theta_p}{dY}\right|_{Y=1-\xi_1}$$

$$\left.\frac{d\theta_{cl}}{dY}\right|_{Y=\xi_2-1} = k_r \left.\frac{d\theta_p}{dY}\right|_{Y=\xi_2-1}$$

After solving the energy equation (Equation 7.32) by using boundary conditions (Equation 7.35), the following results are obtained.

For upper clear region, the dimensionless temperature profile is found as follows,

$$\theta = CU_1 + CU_2 Y + CU_3 Y^2 + CU_4 Y^3 + CU_5 Y^4 \tag{7.36}$$

where

$$\begin{aligned}
CU_1 &= \frac{48\theta_u U_m + (\xi_1 - 1)\left[Nu\left[\xi_1\left(\xi_1 + \xi_1^{\,2} - 1\right) - 4U_u(\xi_1 - 1)\right] - 48\beta U_m\right]}{48U_m\,\xi_1} \\
CU_2 &= \frac{-48\theta_u U_m - 48\beta U_m + Nu\left[4U_u(\xi_1 - 3)(\xi_1 - 1) - \xi_1\left(4 - 6\xi_1 + \xi_1^{\,3}\right)\right]}{48U_m\,\xi_1} \\
CU_3 &= \frac{Nu\left[U_u(4\xi_1 - 6) - 3\xi_1(\xi_1 - 1)\right]}{24U_m\,\xi_1}
\end{aligned} \tag{7.37}$$

$$CU_4 = \frac{Nu\left[2U_u + \xi_1(\xi_1 - 2)\right]}{24U_m\,\xi_1}$$

$$CU_5 = \frac{Nu}{48U_m}$$

For lower clear region, dimensionless temperature distribution is as written in Equation 7.38,

$$\theta = CL_1 + CL_2 Y + CL_3 Y^2 + CL_4 Y^3 + CL_5 Y^4 \tag{7.38}$$

Where

$$CL_1 = \frac{48U_m[\theta_l + \beta(\xi_2 - 1)] + Nu\left[\xi_2 + (\xi_2 - 2)\xi_2{}^3 + 4U_l\left(\xi_2{}^2 - 1\right)\right]}{48U_m\,\xi_2}$$

$$CL_2 = \frac{48U_m(\theta_l - \beta) + Nu\left[4U_l\left(\xi_2{}^2 - 3\right) + \xi_2(\xi_2 - 2)\left(\xi_2{}^2 - 2\right)\right]}{48U_m\xi_2}$$

$$CL_3 = \frac{Nu[\xi_2(3 - 2\xi_2) - 6U_l]}{24U_m\,\xi_2} \tag{7.39}$$

$$CL_4 = -\frac{Nu[2U_l + \xi_2(\xi_2 - 2)]}{24U_m\,\xi_2}$$

$$CL_5 = \frac{Nu}{48U_m}$$

For the porous region; the results for the dimensionless temperature are shown below.

$$\theta(Y) = J_1 + J_2Y + J_3Y^2 + J_4e^{SY} + J_5e^{-SY} \tag{7.40}$$

$$J_1 = J_{1a} + J_{1b}$$

where

$$J_{1a} = \frac{NuP_4}{s^2\left(\xi_1 + \xi_2 - 2\right)}\left[(\xi_2 - 1)\left(P_2e^{S(1-\xi_1)} + P_3e^{-S(1-\xi_1)}\right) + (\xi_1 - 1)\left(P_2e^{-S(1-\xi_2)} + P_3e^{S(1-\xi_2)}\right)\right]$$

$$J_{1b} = \frac{NuP_1P_4}{2}(\xi_1 - 1)(\xi_2 - 1) + \frac{\theta_u(\xi_2 - 1) + \theta_l(\xi_1 - 1)}{\xi_1 + \xi_2 - 2} \tag{7.41}$$

$$J_2 = J_{2a} + J_{2b}$$

where

$$J_{2a} = \frac{NuP_4}{S^2\left(\xi_1 + \xi_2 - 2\right)}\left[P_2\left(e^{S(\xi_2-1)} + e^{S(1-\xi_1)}\right) + P_3\left(e^{S(1-\xi_2)} + e^{S(\xi_1-1)}\right)\right]$$

$$J_{2b} = \frac{NuP_1P_4}{2}\left(\xi_2 - \xi_1\right) + \frac{\theta_l - \theta_u}{\xi_1 + \xi_2 - 2}$$

$$J_3 = -\frac{NuP_1P_4}{2} \qquad J_4 = -\frac{NuP_2P_4}{S^2} \qquad J_5 = -\frac{NuP_3P_4}{S^2}$$

$$P_4 = \frac{1}{2k_r U_m}$$

The dimensionless temperatures at the lower and upper interfaces are:

$$\theta_l = \frac{\xi_2\left[k_r\psi_u\,\xi_1 + \psi_l\left(\xi_1 + \xi_2 - k_r\xi_1 - 2\right)\right]}{2 + \left(k_r - 1\right)\left(\xi_1 + \xi_2\right)}$$
$$\theta_u = \frac{\xi_1\left[k_r\psi_l\,\xi_2 + \psi_u\left(\xi_1 + \xi_2 - k_r\xi_2 - 2\right)\right]}{2 + \left(k_r - 1\right)\left(\xi_1 + \xi_2\right)} \tag{7.42}$$

Ψ_l and $\Psi_u$are two constants which can be calculated as follows.

$$\psi_l = \psi_{la} + \psi_{lb}$$
$$\psi_u = \psi_{ua} + \psi_{ub} \tag{7.43}$$

where

$$\psi_{la} = 2k_r J_3\left(\xi_2 - 1\right) + Sk_r J_4 e^{S(\xi_2 - 1)} - Sk_r J_5 e^{-S(\xi_2 - 1)} - 2CL_3\left(\xi_2 - 1\right) - 3CL_4\left(\xi_2 - 1\right)^2$$

$$\psi_{lb} = k_r\left(J_{2a} + Nu\frac{P_1 P_4}{2}\left(\xi_2 - \xi_1\right)\right) - 4CL_5\left(\xi_2 - 1\right)^3 - CL_{2R}$$

$$\psi_{ua} = 2k_r J_3\left(1 - \xi_1\right) + Sk_r\left[J_4 e^{S(1-\xi_1)} - J_5 e^{-S(1-\xi_1)}\right] - 2CU_3\left(1 - \xi_1\right) - 3CU_4\left(1 - \xi_1\right)^2$$

$$\psi_{ub} = k_r\left(J_{2a} + Nu\frac{P_1 P_4}{2}\left(\xi_2 - \xi_1\right)\right) - 4CU_5\left(1 - \xi_1\right)^3 - CU_{2R}$$

$$CU_{2R} = \frac{-48\beta U_m + Nu\left[4U_u\left(\xi_1 - 3\right)\left(\xi_1 - 1\right) - \xi_1\left(4 - 6\xi_1 + \xi_1^{\,3}\right)\right]}{48U_m\,\xi_1}$$

$$CL_{2R} = \frac{-48\beta U_m + Nu\left[4U_l\left(\xi_2^{\,2} - 3\right) + \xi_2\left(\xi_2 - 2\right)\left(\xi_2^{\,2} - 2\right)\right]}{48U_m\xi_2}$$

P_1, P_2, P_3, U_l, and $U_u$were written in Equation 7.12.

To find the Nusselt number, the compatibility condition (Equation 7.44) must be applied.

$$\int_{-1}^{1}\theta\hat{u}dY = 2 \tag{7.44}$$

The derivation of the compatibility condition is explained in Appendix A.

7.3. Second Approach: Darcy Law

Since the analytical solution of the Nusselt number from the Equation 7.44 is too long and too complex, one extra assumption was made to simplify the governing equations without losing significant amount of accuracy. As known, for low Darcy numbers, Darcy Law can be applied to the porous region, instead of the Brinkman-Extended Darcy Law. With this approach, the shear stress effects are neglected.

7.3.1. Fluid Flow Analysis

In this case, the momentum equations in clear regions are as the same as in the section 7.2. However, the Brinkman-Extended Darcy Law will not be used in this case. The Darcy Law shown in the Equation 7.45 is used for the porous region.

$$-\frac{\mu}{K}u = \frac{dP}{dx} \tag{7.45}$$

The non-dimensional parameters written in Equation 7.5 are used and the Equation 7.46 is obtained as the fluid flow equation for the porous region.

$$U(Y) = Da \tag{7.46}$$

As a summary, the dimensionless governing equations for fluid flow, and the related dimensionless boundary conditions are stated below.

$$\begin{aligned}
&\frac{d^2U}{dY^2} + 1 = 0 \qquad => \qquad For\ clear\ regions \\
&U(Y) = Da \qquad => \qquad For\ porous\ region \\
&U(1) = 0 \\
&U(-1) = 0 \\
&\left.\frac{dU}{dY}\right|_{Y=1-\xi_1} = \gamma(U - Da) \\
&-\left.\frac{dU}{dY}\right|_{Y=\xi_2-1} = \gamma(U - Da) \quad where\ \gamma = \sqrt{\frac{M}{Da}}
\end{aligned} \tag{7.47}$$

The last equation in Eqs 7.47 is dimensionless form of Beaver-Joseph boundary condition and it is compatible to the equal shear stress approximation with low Darcy numbers.

After solving the governing equations with boundary conditions (both are stated in Equation 7.47) the following velocity profiles are obtained.

For upper clear region:

$$U_{cu}(Y) = A_1 + A_2 Y + A_3 Y^2 \tag{7.48}$$

For porous region:

$$U_p(Y) = Da \tag{7.49}$$

For lower clear region:

$$U_{cl}(Y) = B_1 + B_2 Y + B_3 Y^2 \tag{7.50}$$

where:

$$A_1 = \frac{2\gamma Da - 1 + \xi_1[2 + \gamma(\xi_1 - 1)]}{2(\gamma\xi_1 + 1)}$$

$$A_2 = \frac{2 - 2\gamma Da - \xi_1[2 + \gamma(\xi_1 - 2)]}{2(\gamma\xi_1 + 1)} \tag{7.51}$$

$$A_3 = -\frac{1}{2}$$

$$B_1 = \frac{2\gamma Da - 1 + \xi_2[2 + \gamma(\xi_2 - 1)]}{2(\gamma\xi_2 + 1)}$$

$$B_2 = \frac{2\gamma Da - 2 + \xi_2[2 + \gamma(\xi_2 - 2)]}{2(\gamma\xi_2 + 1)}$$

$$B_3 = -\frac{1}{2}$$

As in Section 7.2, the mean velocity can be defined as Equation 7.13 and found as in Equation 7.52.

$$U_m = \frac{\int_{-1}^{1} U(Y)dY}{\int_{-1}^{1} dY} = \frac{\int_{-1}^{\xi_2 - 1} U_{cl}(Y)dY + \int_{\xi_2 - 1}^{1 - \xi_1} U_p(Y)dY + \int_{1-\xi_1}^{1} U_{cu}(Y)dY}{2} \tag{7.13}$$

$$U_m = R_U + R_L + R_P$$

where (7.52)

$$R_U = \frac{\xi_1^{\,2}\left[6\gamma Da + \xi_1(4+\gamma\xi_1)\right]}{24(1+\gamma\xi_1)}$$

$$R_L = \frac{\xi_2^{\,2}\left[6\gamma Da + \xi_2(4+\gamma\xi_2)\right]}{24(1+\gamma\xi_2)}$$

$$R_p = \frac{1}{2}Da(2-\xi_1-\xi_2)$$

7.3.2. Heat Flow Analysis

Same procedures as in Section 7.2.2 are performed to obtain the following dimensionless energy equations and the boundary conditions for all regions.

$$\frac{d^2\theta}{dY^2} + \frac{1}{2k_r}\hat{u}Nu = 0 \qquad \textit{in porous region}$$

$$\frac{d^2\theta}{dY^2} + \frac{1}{2}\hat{u}Nu = 0 \qquad \textit{in clear regions} \tag{7.32}$$

$$\theta_{cu}(1) = -\beta$$

$$\theta_{cl}(-1) = \beta$$

$$\theta_{cu}(1-\xi_1) = \theta_p(1-\xi_1)$$

$$\theta_{cl}(\xi_2 - 1) = \theta_p(\xi_2 - 1) \tag{7.35}$$

$$\left.\frac{d\theta_{cu}}{dY}\right|_{Y=1-\xi_1} = k_r \left.\frac{d\theta_p}{dY}\right|_{Y=1-\xi_1}$$

$$\left.\frac{d\theta_{cl}}{dY}\right|_{Y=\xi_2-1} = k_r \left.\frac{d\theta_p}{dY}\right|_{Y=\xi_2-1}$$

After solving the dimensionless energy equation, Equation 7.32, by using the dimensionless boundary conditions, Equation 7.35, the following dimensionless

temperature profiles are obtained for the upper clear region, Equation 7.53, the porous region, Equation 7.54, and the lower clear region, Equation 7.55, respectively.

$$\theta_{cu} = CU_1 + CU_2 Y + CU_3 Y^2 + CU_4 Y^3 + CU_5 Y^4 \tag{7.53}$$

where

$$CU_1 = \frac{24\theta_u U_m - 24\beta U_m(\xi_1 - 1) + Nu\,\xi_1(\xi_1 - 1)[6A_1 - 2A_2(\xi_1 - 2) + A_3[3 + \xi_1(\xi_1 - 3)]]}{24U_m\xi_1}$$

$$CU_2 = \frac{-24U_m(\beta + \theta_u) + Nu\,\xi_1[-6A_1(\xi_1 - 2) + 2A_2[3 + \xi_1(\xi_1 - 3)] - A_3(\xi_1 - 2)[2 + \xi_1(\xi_1 - 2)]]}{24U_m\xi_1}$$

$$CU_3 = -\frac{A_1 Nu}{4U_m}$$

$$CU_4 = -\frac{A_2 Nu}{12U_m}$$

$$CU_5 = -\frac{A_3 Nu}{24U_m}$$

$$\theta_p = CP_1 + CP_2 Y + CP_3 Y^2 \tag{7.54}$$

where

$$CP_1 = \frac{4k_r U_m[\theta_l(\xi_1 - 1) + \theta_u(\xi_2 - 1)] + Da\,Nu\,(\xi_1 - 1)(\xi_2 - 1)(\xi_1 + \xi_2 - 2)}{4k_r U_m(\xi_1 + \xi_2 - 2)}$$

$$CP_2 = \frac{4k_r U_m[\theta_l - \theta_u] - Da\,Nu\,(\xi_1 - \xi_2)(\xi_1 + \xi_2 - 2)}{4k_r U_m(\xi_1 + \xi_2 - 2)}$$

$$CP_3 = -\frac{Da\,Nu}{4k_r U_m}$$

$$\theta_{cl} = CL_1 + CL_2 Y + CL_3 Y^2 + CL_4 Y^3 + CL_5 Y^4 \tag{7.55}$$

where

$$CL_1 = \frac{24\theta_l U_m + 24\beta U_m(\xi_2 - 1) + Nu\xi_2(\xi_2 - 1)[6B_1 + 2B_2(\xi_2 - 2) + B_3[3 + \xi_2(\xi_2 - 3)]]}{24U_m\xi_2}$$

$$CL_2 = \frac{24U_m(\beta - \theta_l) - Nu\xi_2[6B_1(\xi_2 - 2) + 2B_2[3 + \xi_2(\xi_2 - 3)] + B_3(\xi_2 - 2)[2 + \xi_2(\xi_2 - 2)]]}{-24U_m\xi_2}$$

$$CL_3 = -\frac{B_1 Nu}{4U_m}$$

$$CL_4 = -\frac{B_2 Nu}{12U_m}$$

$$CL_5 = -\frac{B_3 Nu}{24U_m}$$

Dimensionless temperatures at the upper and lower interfaces of the porous – clear media can be calculated by the formulas stated below in Equations 7.56 and 7.57, respectively.

$$\theta_u = \psi_{U1}\beta + \psi_{U2} Nu \tag{7.56}$$

where

$$\psi_{U1} = \frac{\xi_1 + \xi_2 - 2 + k_r(\xi_1 - \xi_2)}{2 - \xi_1 - \xi_2 + k_r(\xi_1 + \xi_2)}$$

$$\psi_{U2} = \psi_{u2a} + \psi_{u2b} + \psi_{u2c}$$

$$\psi_{U2a} = \frac{\xi_1^2\left[6(A_1 + A_2 + A_3) - 4\xi_1(A_2 + 2A_3) + 3A_3\xi_1^2\right](2 - \xi_1 + k_r\xi_2 - \xi_2)}{24U_m[2 - \xi_1 - \xi_2 + k_r(\xi_1 + \xi_2)]}$$

$$\psi_{U2b} = \frac{\xi_1\xi_2^2\left[6k_r(B_1 - B_2 + B_3) + 4k_r\xi_2(B_2 - 2B_3) + 3k_r\xi_2^2 B_3\right]}{24U_m[2 - \xi_1 - \xi_2 + k_r(\xi_1 + \xi_2)]}$$

$$\psi_{U2c} = \frac{6Da\xi_1(2 - \xi_1 + 2k_r\xi_2 - \xi_2)(2 - \xi_1 - \xi_2)}{24U_m[2 - \xi_1 - \xi_2 + k_r(\xi_1 + \xi_2)]}$$

$$\theta_l = \psi_{L1}\beta + \psi_{L2}Nu \tag{7.57}$$

where

$$\psi_{L1} = \frac{\xi_1 + \xi_2 - 2 + k_r(\xi_1 - \xi_2)}{2 - \xi_1 - \xi_2 + k_r(\xi_1 + \xi_2)}$$

$$\psi_{L2} = \psi_{l2a} + \psi_{l2b} + \psi_{l2c} + \psi_{l2d} + \psi_{l2e}$$

$$\psi_{l2a} = \frac{\xi_2 \xi_1^{\,2} k_r \left[6(A_1 + A_2 + A_3) - 4\xi_1(A_2 + 2A_3) + 3A_3\xi_1^{\,2}\right]}{24U_m\left[2 + (k_r - 1)\xi_1 + (k_r - 1)\xi_2\right]}$$

$$\psi_{l2b} = \frac{\xi_2^{\,2}\left[6(B_1 - B_2 + B_3)[2 + (k_r - 1)\xi_1]\right]}{24U_m\left[2 + (k_r - 1)\xi_1 + (k_r - 1)\xi_2\right]}$$

$$\psi_{l2c} = \frac{-2\xi_2^{\,3}\left[3B_1 - 7B_2 + 11B_3 - 2\xi_1(B_2 - 2B_3)(kr - 1)\right]}{24U_m\left[2 + (k_r - 1)\xi_1 + (k_r - 1)\xi_2\right]}$$

$$\psi_{l2d} = \frac{-\xi_2^{\,3}\left[4B_2 + B_3(-14 + 3\xi_1 - 3k_r\xi_1) + 3B_3\xi_2\right]}{24U_m\left[2 + (k_r - 1)\xi_1 + (k_r - 1)\xi_2\right]}$$

$$\psi_{l2e} = \frac{-\xi_2\left[6Da(2 - \xi_1 + 2k_r\xi_1 - \xi_2)(\xi_1 + \xi_2 - 2)\right]}{24U_m\left[2 + (k_r - 1)\xi_1 + (k_r - 1)\xi_2\right]}$$

At this point, the term β, defined in Equation 7.34, can be redefined in terms of Nusselt number. To do this, the heat fluxes at the walls which are constants and equal to each other, are used. Firstly, the dimensional forms of the heat fluxes are written. Then, they are turned into non-dimensional forms by using the parameters shown in Equation 7.5. Finally, taking the first derivative of the dimensionless temperatures of the upper and the lower clear regions, and equating two heat fluxes, β can be formulated as in Equation 7.58.

$$q_u'' = -k\left(\frac{dT}{dy}\right)_{y=H} = -\frac{k}{H}\left(T_m - T_{w\mu}\right)\left(\frac{d\theta}{dY}\right)_{Y=1}$$

$$q_l'' = -k\left(\frac{dT}{dy}\right)_{y=-H} = -\frac{k}{H}\left(T_m - T_{w\mu}\right)\left(\frac{d\theta}{dY}\right)_{Y=-1}$$

$$\beta = \psi_B Nu \tag{7.58}$$

where

$$\psi_B = \psi_{B1} + \psi_{B2} + \psi_{B3}$$

$$\psi_{B1} = \frac{\psi_{U2}\xi_2 - \psi_{L2}\xi_1}{(\psi_{L1} - 1)\xi_1 - (\psi_{U1} + 1)\xi_2}$$

$$\psi_{B2} = \frac{\xi_1^{\,2}\xi_2\left[6(A_1 + A_2 + A_3) - 2\xi_1(A_2 + 2A_3) + A_3\xi_1^{\,2}\right]}{24U_m\left[(\psi_{L1} - 1)\xi_1 - (\psi_{U1} + 1)\xi_2\right]}$$

$$\psi_{B3} = \frac{-\xi_1\xi_2^{\,2}\left[6B_1 + 2B_2(\xi_2 - 3) + B_2\left[6 + \xi_2(\xi_2 - 4)\right]\right]}{24U_m\left[(\psi_{L1} - 1)\xi_1 - (\psi_{U1} + 1)\xi_2\right]}$$

After forming β in terms of Nu, the compatibility condition stated below is used to find an expression for overall Nusselt number.

$$\int_{-1}^{1} \theta \hat{u} dY = 2 \tag{7.44}$$

The detailed derivation of the compatibility condition is explained in Appendix A. Using the compatibility condition, the analytical expression of the Nusselt number can be written as follows.

$$Nu = \frac{2U_m}{\sum_{k=1}^{13} J_k} \tag{7.59}$$

where

$$J_1 = \frac{1}{2}\xi_1(A_1 + A_2 + A_3)\left[\psi_B(\psi_{U1} - 1) + \psi_{U2}\right]$$

$$J_2 = -\frac{1}{6}\xi_1^{\,2}(A_2 + 2A_3)\left[\psi_B(2\psi_{U1} - 1) + 2\psi_{U2}\right]$$

$$J_3 = \frac{1}{24}\xi_1^{\,3}\left[\frac{(A_1 + A_2 + A_3)^2}{U_m} + 2A_3\left[\psi_B(3\psi_{U1} - 1) + 3\psi_{U2}\right]\right]$$

$$J_4 = -\frac{1}{24}\xi_1^{\,4}\,\frac{(A_1 + A_2 + A_3)(A_2 + 2A_3)}{U_m}$$

$$J_5 = \frac{1}{360}\frac{\xi_1^{\,5}}{U_m}\,\frac{[9A_1A_3 + (A_2 + 5A_3)(4A_2 + 5A_3)]}{U_m}$$

$$J_6 = -\frac{1}{72}\xi_1^{\,6}\,\frac{A_3(A_2 + 2A_3)}{U_m} + \frac{1}{224}\frac{A_3^{\,2}\xi_1^{\,7}}{U_m}$$

$$J_7 = \frac{Da(2 - \xi_1 - \xi_2)\left[12k_r(\psi_{L2} + \psi_B(\psi_{L1} + \psi_{U1}) + \psi_{U2})U_m + Da(\xi_1 + \xi_2 - 2)^2\right]}{24k_rU_m}$$

$$J_8 = \frac{1}{2}\xi_2(B_1 - B_2 + B_3)[\psi_B + \psi_B\psi_{L1} + \psi_{L2}]$$

$$J_9 = \frac{1}{6}\xi_2^{\,2}(B_2 - 2B_3)[\psi_B + 2\psi_B\psi_{L1} + 2\psi_{L2}]$$

$$J_{10} = \frac{1}{24}\xi_2^{\,3}\left[\frac{(B_1 - B_2 + B_3)^2}{U_m} + 2B_3(\psi_B + 3\psi_B\psi_{L1} + 3\psi_{L2})\right]$$

$$J_{11} = \frac{1}{24}\xi_2^{\,4}\,\frac{(B_1 - B_2 + B_3)(B_2 - 2B_3)}{U_m}$$

$$J_{12} = \frac{1}{360}\frac{\xi_2^{\,5}}{U_m}[(B_2 - 5B_3)(4B_2 - 5B_3) + 9B_1B_3]$$

$$J_{13} = \frac{1}{72}\xi_2^{\,6}\,\frac{B_3(B_2 - 2B_3)}{U_m} + \frac{1}{224}\frac{B_3^{\,2}\xi_2^{\,7}}{U_m}$$

Finally, the individual Nusselt numbers at the lower and upper walls are needed to be investigated. To do this, the heat fluxes at both walls are used. The walls are assumed to be so thin that the conduction resistance can be neglected. Hence, the wall heat fluxes directly convected to the fluid and the following equations for the upper and lower walls can be written.

$$q_u'' = -k\left.\frac{dT}{dy}\right|_{y=H} = h(T_{wu} - T_m) \qquad (7.60)$$

$$q_l'' = -k\left.\frac{dT}{dy}\right|_{y=-H} = h(T_{wl} - T_m)$$

The dimensionless parameters, defined in Equation 7.19, are used to continue our analysis of individual Nusselt numbers. Let's go on with upper wall first.

$$-\frac{k}{H}\left(T_m - T_{w\mu}\right)\left.\frac{d\theta}{dY}\right|_{Y=1} = h\left(T_{wu} - T_m\right) \quad => \quad \left.\frac{d\theta}{dY}\right|_{Y=1} = \frac{hH\left(T_m - T_{wu}\right)}{k\left(T_m - T_{w\mu}\right)} = \frac{h\,2H\left(T_m - T_{wu}\right)}{2k\left(T_m - T_{w\mu}\right)}$$

$$\left.\frac{d\theta}{dY}\right|_{Y=1} = \frac{1}{2}Nu_u\frac{\left(T_m - T_{wu}\right)}{\left(T_m - T_{w\mu}\right)} = \frac{1}{2}Nu_u\frac{\left(T_m - \frac{T_{wu}}{2} - \frac{T_{wu}}{2} + \frac{T_{wl}}{2} - \frac{T_{wl}}{2}\right)}{\left(T_m - T_{w\mu}\right)}$$

$$\left.\frac{d\theta}{dY}\right|_{Y=1} = \frac{1}{2}Nu_u\left(1+\beta\right)$$

After further manipulations, the dimensionless temperature gradient at the lower and upper wall can be written as in Equation 7.61 and Equation 7.62.

$$Nu_u = \frac{2\left(CU_2 + 2CU_3 + 3CU_4 + 4CU_5\right)}{\left(1+\beta\right)} \tag{7.61}$$

$$Nu_l = \frac{2\left(CL_2 - 2CL_3 + 3CL_4 - 4CL_5\right)}{\left(1-\beta\right)} \tag{7.62}$$

7.4. Pressure Drop Calculations

To take the pressure drop into consideration, friction factor is used. Friction factor for a channel in which fluid flows with a mean velocity of u_m is defined as:

$$f = \frac{\left(-\frac{dP}{dx}\right)2H}{\frac{1}{2}\rho u_m^2} \tag{7.63}$$

For a fully developed flow in a channel, the pressure gradient along the x-axis is constant and this negative gradient is denoted by *G*, as stated in Equation (7.5). Then the Equation (7.63) becomes as follows:

$$f = \frac{4GH}{\rho u_m^2} \tag{7.64}$$

Using the definition of the dimensionless velocity defined in Equation (7.5), the following equation is obtained for the friction factor.

$$f = \frac{4}{U_m} \frac{\mu}{\rho u_m H} \tag{7.65}$$

or

$$f\,Re = \frac{8}{U_m} \tag{7.66}$$

Equation (7.66) can be used for determination of pressure drop.

7.5. Analysis of Heat Transfer and Pressure Drop

In Chapter 3, the individual Nusselt numbers of both walls are found as *4.1176* when the subjected heat fluxes are equal to each other and the channel is clear. In this chapter, to determine the heat transfer enhancement at both walls, the individual Nusselt numbers of both walls must be divided by the Nusselt number of a flow in a clear channel (Nu_c=*4.1176*). This division is called **heat transfer increment ratio** in this study.

$$\varepsilon_{th,u} = \frac{Nu_u}{4.1176} \tag{7.67}$$

$$\varepsilon_{th,l} = \frac{Nu_l}{4.1176} \tag{7.68}$$

Thermal efficiency is equal to *1* for a clear channel. Heat transfer enhancement is expected for the channel withε_{th}> *1*. The use of porous media will decrease heat transfer through a channel ifε_{th}< *1*.

Similar definitions are valid for friction coefficient. The friction coefficient can be normalized by using friction coefficient of a clear channel.

$$\varepsilon_p = \frac{f\,Re}{(f\,Re)_c} \tag{7.69}$$

ε_p is called the **pressure drop increment ratio** in this thesis and for the values of $\varepsilon_p$greater than *1*, the increase of pressure drop in the channel is expected, while for $\varepsilon_p < 1$, the use of porous layer decreases the pressure drop in the channel. The value of friction coefficient $(f\,Re)_c$ is determined as *24*.

The ratio of ε_p and $\varepsilon_{th}$is shown by ε, and called the **overall performance**.

$$\varepsilon_u = \frac{\varepsilon_{th,u}}{\varepsilon_p} \tag{7.70}$$

$$\varepsilon_l = \frac{\varepsilon_{th,l}}{\varepsilon_p} \tag{7.71}$$

For the values of ε greater than *1*, heat transfer enhancement is greater than the increase of pressure drop. However, for the values of ε less than *1*, the increase of pressure drop in the channel is greater than heat transfer enhancement.

All these results except the pressure drop analysis will be discussed in Chapter 9.

CHAPTER 8

HEAT AND FLUID FLOW IN A SOLAR AIR HEATER COLLECTOR PARTIALLY FILLED WITH POROUS MEDIA

8.1. Problem Definition

Heat transfer enhancement by using porous media approach was investigated for a solar air heater, in this case. The physical demonstration of the system is shown in Figure 8.1.

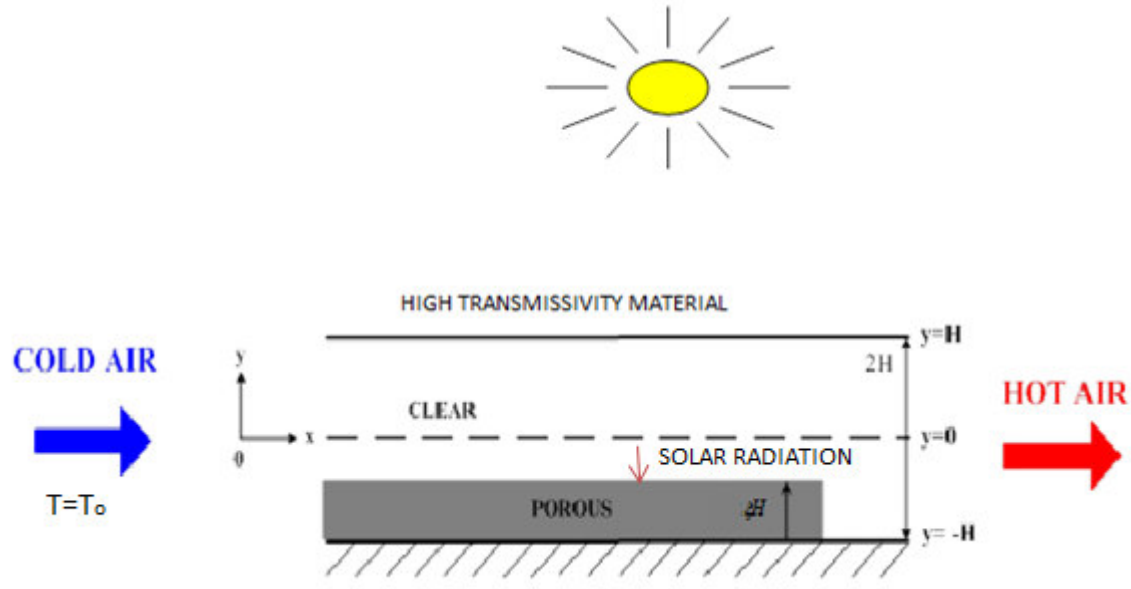

Figure 8.1. Physical demonstration of the solar air heater collector, which is wanted to be investigated

The upper wall has to be made up with a high-transmissivity material to permit the maximum amount of radiation heat transfer enter into the channel. Hence, the porous medium absorbs all the radiation heat flux. It is assumed that all the radiation was absorbed homogeneously by the porous structures. Bottom wall of the channel is well-insulated. Air enters into the channel with the temperature of T_0. The air flow is assumed to be incompressible, laminar and hydrodynamically fully developed.

Thermal-hydraulic analyses were performed to investigate the effects of using porous media on heat flow in a solar air heater collector.

8.2. Fluid Flow Analysis

For an incompressible flow of a Newtonian fluid; the Navier-Stokes equations are used for the hydrodynamic analyses of the fluid flow in the clear part of the channel. The governing equations are written below.

$$\frac{\partial u}{\partial x}+\frac{\partial v}{\partial y}=0 \tag{8.1}$$

$$u\frac{\partial u}{\partial x}+v\frac{\partial u}{\partial y}=-\frac{1}{\rho}\frac{\partial P}{\partial x}+\nu\left(\frac{\partial^2 u}{\partial x^2}+\frac{\partial^2 u}{\partial y^2}\right) \tag{8.2}$$

$$u\frac{\partial v}{\partial x}+v\frac{\partial v}{\partial y}=-\frac{1}{\rho}\frac{\partial P}{\partial y}+\nu\left(\frac{\partial^2 v}{\partial x^2}+\frac{\partial^2 v}{\partial y^2}\right) \tag{8.3}$$

Since the y-component of the velocity, *v*, is assumed to be zero, then the following equations are obtained.

$$\frac{\partial u}{\partial x}=0 \tag{8.4}$$

$$\mu\frac{\partial^2 u}{\partial y^2}-\frac{\partial P}{\partial x}=0 \tag{8.5}$$

$$\frac{\partial P}{\partial y}=0 \tag{8.6}$$

For the porous part, the Brinkman-extended Darcy equation is used.

$$\mu_{eff}\frac{d^2 u}{dy^2}-\frac{\mu}{K}u=\frac{dP}{dx} \tag{8.7}$$

The no-slip condition is used as the boundary conditions at the walls and at the clear-porous media interface; the continuous shear stresses are applied. These boundary conditions are shown below.

$$
\begin{aligned}
u(\pm H) &= 0 \\
u_c\big((\xi-1)H\big) &= u_p\big((\xi-1)H\big) \\
\tau_c\big((\xi-1)H\big) &= \tau_p\big((\xi-1)H\big)
\end{aligned}
\tag{8.8}
$$

To ease the solution by reducing the variables in the governing equations, the following dimensionless parameters are used.

$$
\begin{aligned}
Y &= \frac{y}{H}, \qquad M = \frac{\mu_{eff}}{\mu}, \qquad G = -\frac{\partial P}{\partial x} \\
Da &= \frac{K}{H^2}, \qquad U = \frac{\mu u}{GH^2}, \qquad S = \frac{1}{\sqrt{M\,Da}}
\end{aligned}
\tag{8.9}
$$

Applying the dimensionless parameters into the governing equations (8.5 and 8.7) and the boundary conditions (Equation 8.8), the following dimensionless forms of the momentum equations and the boundary conditions are obtained.

Momentum equation for clear region:

$$
\frac{d^2U_c}{dY^2} + 1 = 0 \tag{8.10}
$$

Momentum equation for porous region:

$$
\frac{d^2U_p}{dY^2} - S^2U_p + \frac{1}{M} = 0 \tag{8.11}
$$

Boundary conditions:

$$
\begin{aligned}
U(\pm 1) &= 0 \\
U_c(\xi-1) &= U_p(\xi-1) \\
\tau_c(\xi-1) &= \tau_p(\xi-1)
\end{aligned}
\tag{8.12}
$$

The numerical solution procedure is shown in Section 8.6 and the related results are discussed in Chapter 9.

8.3. Heat Flow Analysis

To start the heat flow analyses of the current problem; it should be reminded that all the radiation heat flux is absorbed homogeneously by the porous medium. Therefore, a heat generation term can be defined as follows.

$$q"L = \dot{q}2HL\xi$$

$$\dot{q} = \frac{q"}{2H\xi} \tag{8.13}$$

Then, energy balances should be performed to each differential control volume in clear and porous media, illustrated in Figures 8.2 and 8.3.

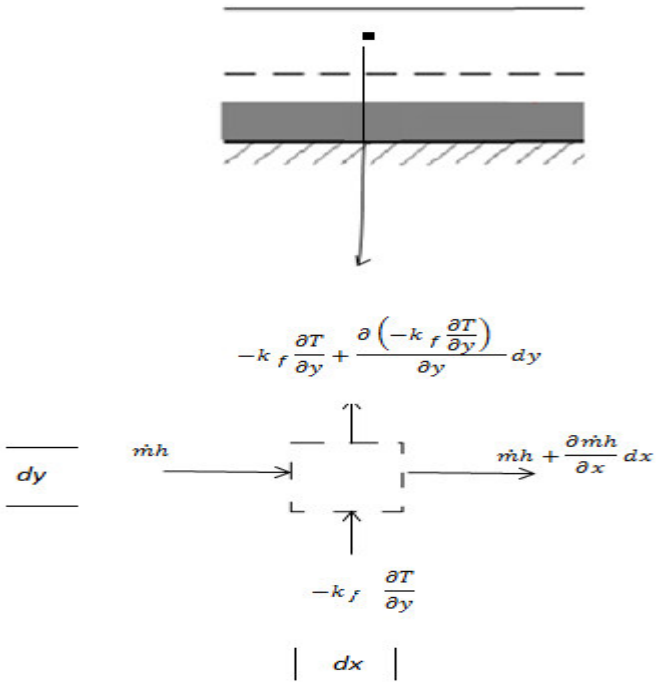

Figure 8.2. Energy balance for the clear fluid region

Energy balance for clear medium can be written as follows.

$$\left(\rho C_p\right)_f uTdy - k_f \frac{\partial T}{\partial y} dx$$

$$= \left(\rho C_p\right)_f uTdy + \frac{\partial\left(\left(\rho C_p\right)_f uTdy\right)}{\partial x} dx - k_f \frac{\partial T}{\partial y} dx - \frac{\partial\left(-k_f \frac{\partial T}{\partial y} dx\right)}{\partial x}$$

After further manipulations, the following energy equation is obtained.

$$u\frac{\partial T}{\partial x} = \alpha_f \frac{\partial^2 T}{\partial y^2} \tag{8.14}$$

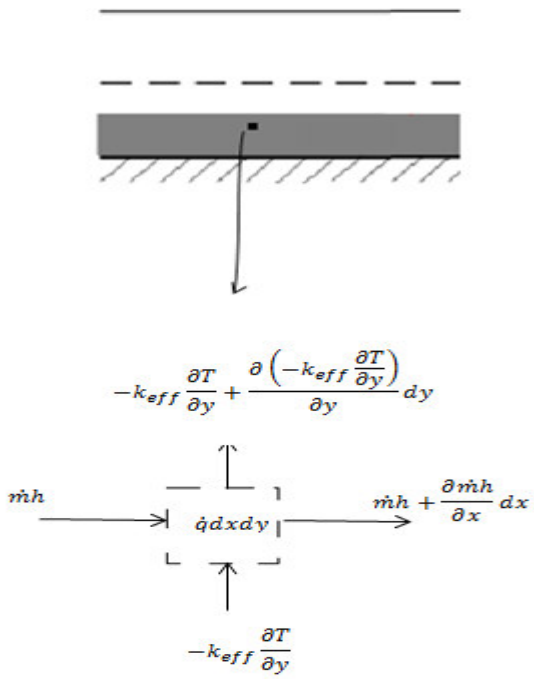

Figure 8. 3. Energy balance for the porous region

Energy balance for porous medium can be written as follows.

$$\left(\rho C_p\right)_f uTdy - k_{eff}\frac{\partial T}{\partial y}dx + \dot{q}dxdy$$
$$= \left(\rho C_p\right)_f uTdy + \frac{\partial\left(\left(\rho C_p\right)_f uTdy\right)}{\partial x}dx - k_f\frac{\partial T}{\partial y}dx - \frac{\partial\left(-k_f\frac{\partial T}{\partial y}dx\right)}{\partial x}$$

After further manipulations, the following energy equation is obtained.

$$\left(\rho C_p\right)_f u\frac{\partial T}{\partial x} = k_{eff}\frac{\partial^2 T}{\partial y^2} + \dot{q} \tag{8.15}$$

Beyond the dimensionless parameters written in Equation 8.9, the following parameters should also be introduced.

$$X = \frac{x}{Pe}, \qquad \theta = \frac{T - T_0}{\Delta T}, \qquad \Delta T = \frac{q"H}{k_f}, \qquad k_r = \frac{k_{eff}}{k_f}$$
$$\hat{u} = \frac{u}{u_m}, \qquad Pe = \frac{u_m H}{\alpha_f}, \qquad \alpha_r = \frac{\alpha_{eff}}{\alpha_f} \tag{8.16}$$
$$\alpha_{eff} = \varepsilon\alpha_f + (1-\varepsilon)\alpha_s$$

ε is called the **porosity**, and explained in Section 2.1.

Using the dimensionless parameters (Equations 8.9 and 8.16), the energy equations can be written as follows.

$$\hat{u}\frac{\partial\theta}{\partial X} = \frac{\partial^2\theta}{\partial Y^2} \Rightarrow \text{for clear region}$$
$$\hat{u}\frac{\partial\theta}{\partial X} = \alpha_r\frac{\partial^2\theta}{\partial Y^2} + \frac{1}{2\xi} \Rightarrow \text{for porous region} \tag{8.17}$$

To solve Equation (8.17); boundary conditions are needed. Since the lower wall is insulated, then the temperature gradient is zero. At the interface of clear – porous media, the temperatures and the conduction heat fluxes are equal.

$$\left.\frac{\partial\theta_p}{\partial Y}\right|_{Y=-1} = 0$$
$$k_r\left.\frac{\partial\theta_p}{\partial Y}\right|_{Y=\xi-1} = \left.\frac{\partial\theta_c}{\partial Y}\right|_{Y=\xi-1} \tag{8.18}$$

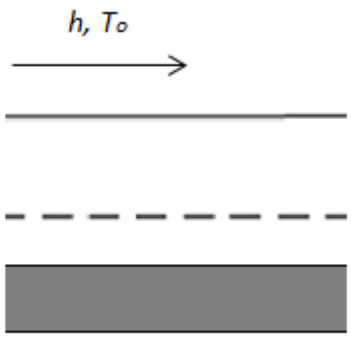

Figure 8.4. The energy balance for the upper wall

At the upper wall, the following energy balance should be performed to obtain the boundary condition.

$$-k_f \frac{\partial T}{\partial y} = U(T - T_0) \quad => \quad -\frac{k_f \Delta T}{H}\frac{\partial \theta}{\partial Y} = U\Delta T\theta$$

$$-\frac{\partial \theta}{\partial Y}\Big|_{Y=1} = Nu_o\theta \tag{8.18}$$

In Equation (8.19), Nu_o stands for the dimensionless temperature gradient at the upper surface, hence it shows the energy loss from the channel to outside. If Nu_o is zero, then the channel is well-insulated. The governing equations (8.17) can be solved numerically by using the boundary conditions (Equations 8.18 and 8.19). The numerical solution procedure is explained in Section 8.6.

8.4. Pressure Drop Calculations

To calculate the pressure drop, the friction factor should be introduced first. It can be defined as:

$$f = \frac{\left(-\frac{dP}{dx}\right)2H}{\frac{1}{2}\rho u_m^2} \tag{8.19}$$

In this case, fluid flow is hydrodynamically fully developed, hence the pressure gradient along the x-axis is constant and this negative gradient is denoted by *G*. Then Equation (8.19) becomes as follows:

$$f = \frac{4GH}{\rho u_m^2} \tag{8.20}$$

Using the definition of the dimensionless velocity defined in Equation (8.9), the following equation is obtained for the friction factor.

$$f = \frac{4}{U_m}\frac{\mu}{\rho u_m H} \tag{8.21}$$

or

$$f\,Re = \frac{8}{U_m} \tag{8.22}$$

Equation (8.22) can be used for determination of pressure drop.

8.5. Analysis of Heat Transfer and Pressure Drop

To compare the total heat transfers, which are subjected to the fluid in both clear and porous channels; heat transfer equations must be written as follows.

$$q" = \dot{m}C_p\left(T_{m,o} - T_{m,i}\right) \tag{8.23}$$

In this equation, *q"* is the total heat transfer subjected to fluid, □ is the mass flow rate and C_p is the heat capacity of the fluid at constant pressure, $T_{m,o}$ and $T_{m,i}$ are the mean temperatures at outlet and inlet of the channel, respectively.

In order to evaluate the heat transfer enhancement in the channel by using porous media, a new parameter named **thermal efficiency**, ε_{th}, is introduced as follows.

$$\varepsilon_{th} = \frac{q"}{q"_c} = \frac{\dot{m}C_p\left(T_{m,o} - T_{m,i}\right)}{\left[\dot{m}C_p\left(T_{m,o} - T_{m,i}\right)\right]_c} \tag{8.24}$$

In this formula, *c* stands for the full clear channel and the thermal efficiency is just the ratio of heat transfer in any media and heat transfer in full clear channel. Since all the equations are constructed dimensionless, then Equation (8.24) should also be made dimensionless by using Equation (8.16).

$$\varepsilon_{th} = \frac{\dot{m}C_p\theta_{m,o}q"Hk_f}{\left[\dot{m}C_p\theta_{m,o}q"Hk_f\right]_c} = \frac{\theta_{m,o}}{\left(\theta_{m,o}\right)_c} \tag{8.25}$$

It is clear that $\varepsilon_{th} = 1$ for a clear fluid channel. Heat transfer enhancement is expected for the channel with $\varepsilon_{th} > 1$. The use of porous media may decrease heat transfer through a clear channel if $\varepsilon_{th} < 1$.

Similar definitions are valid for friction coefficient. The friction coefficient can be normalized by using friction coefficient of a clear channel.

$$\varepsilon_p = \frac{f\,Re}{(f\,Re)_c} \tag{8.26}$$

For the values of ε_p greater than 1, the increase of pressure drop in the channel is expected, while for $\varepsilon_p < 1$, the use of porous layer decreases the pressure drop in the channel. The value of friction coefficient ($(f\,Re)_{cl}$ is determined as 24 (i.e. $(f\,Re)_{cl} = 24$).

The ratio of ε_p and ε_{th} is shown by ε, and called the **general efficiency**.

$$\varepsilon = \frac{\varepsilon_{th}}{\varepsilon_p} \tag{8.27}$$

For the values of ε greater than 1 (i.e., $\varepsilon > 1$), heat transfer enhancement is greater than the increase of pressure drop if a porous layer is used at the core of the channel. However, for the values of ε less than 1 (i.e., $\varepsilon < 1$), the increase of pressure drop in the channel is greater than heat transfer enhancement.

8.6. Numerical Solution Procedure

The governing equations for the momentum and energy balances are solved by using finite difference method. *101* nodes are used for each equation. The following nodal equations are found for the momentum equations, energy equations and for the boundary conditions.

Nodal equations for the velocity distribution:

In porous region:

$$u(j) = \frac{M\big(u(j+1) + u(j-1)\big) + dY^2}{M(2 + S^2 dY^2)}$$

In clear region:

$$u(j) = 0.5\big(u(j+1) + u(j-1)\big) + dY^2$$

At the interface:

$$u(j) = \frac{u(j+1) + Mu(j-1)}{1+M}$$

Nodal equations for the dimensionless temperature distribution:

In porous region:

$$T(j,i) = \frac{2dX\alpha_r\xi\big(T(j+1,i) + T(j-1,i)\big) + dXdY^2 + 2\hat{u}(j)\xi dY^2 T(j,i-1)}{2\xi(2dX\alpha_r + \hat{u}(j)\xi dY^2)}$$

In clear region:

$$T(j,i) = \frac{dX\big(T(j+1,i) + T(j-1,i)\big) + \hat{u}(j)dY^2 T(j,i-1)}{2dX + \hat{u}(j)dY^2}$$

At the interface:

$$T(j,i) = \frac{T(j+1,i) + k_r T(j-1,i)}{1+k_r}$$

At the lower boundary:

$$T(j,i) = T(j+1,i)$$

At the upper boundary:

$$T(j,i) = \frac{T(j-1,i)}{dY\ Nu_o + 1}$$

The directions of i and j, shown in Equations (8.28), are demonstrated in Figure 8.5 and all the results are discussed in Chapter 9.

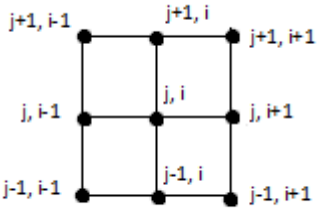

.

Figure 8.5. The nodes used in the numerical solution

CHAPTER 9

RESULTS AND DISCUSSION

In this thesis; six different cases are analysed. In all cases, the velocity profiles and the Nusselt numbers are derived and the pressure drop effects are investigated. First, the results for flows in a clear channel with two different boundary conditions, which are investigated in Chapter 3, are presented. The Nusselt number for this flow was found as 4.1176 and all the results are discussed in Section. 9.1. A fluid flow in a fully filled porous channel with symmetric heat flux boundary conditions was studied in Chapter 4, and it is observed that the Nusselt number decreases with increasing Darcy and at very large Darcy numbers the flow resembles to that in a clear channel. The results for his problem are presented in Section 9.2. In Chapter 5, the same case with the previous chapter except the boundary conditions was investigated. In this case, both walls were subjected to heat fluxes, which their values are different from each other. As in the asymmetric heating case in Chapter 2, the individual Nusselt numbers at the lower and upper walls were analyzed. The results are discussed in Section 9.3. A flow in a channel with partially and symmetrically located porous medium was investigated in Chapter 6. For the porous media with large range of Darcy numbers, the Nusselt numbers have peaks where the heat transfer can be maximum. Velocity profiles and further analyses are discussed in Section 9.4. In Section 9.5., the flow in a channel with partially and asymmetrically located porous medium with symmetric heat flux boundary conditions are investigated. The overall and individual Nusselt numbers found after the calculations are studied. Finally, a solar air heater is analyzed and all the results were discussed in Section 9.6.

9.1. Results for Flow in a Clear Channel

In Chapter 3, heat and fluid flow in a clear channel with two different boundary conditions are investigated. Figure 9.1 shows the dimensionless normalized velocity profile in the channel. The shear effects near the walls can be clearly seen in this figure. As mentioned in Section 3.1.1; the no-slip condition causes these effects. The closest fluid particle to the wall sticks to it and since the walls are stationary, the velocity of

this fluid particle is zero. The flow has its maximum velocity at the channel centre where *Y=0*. This flow is called as *poiseuille flow*.

Figure 9.2 demonstrates the dimensionless temperature profile of the Poiseuille flow. The maximum temperature is observed at the centre of the channel, and at the boundaries, no-temperature- jump condition is observed. The Nusselt number for the channel with the height of 2H is calculated as 4.1176.

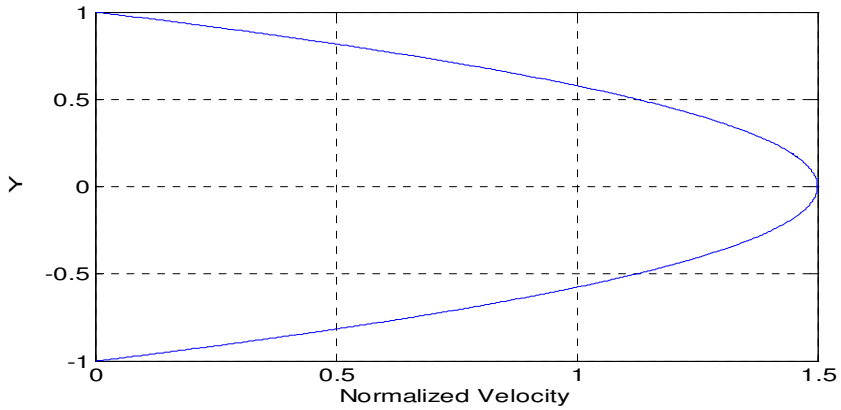

Figure 9. 1. Normalized velocity distribution of a fluid in a clear channel

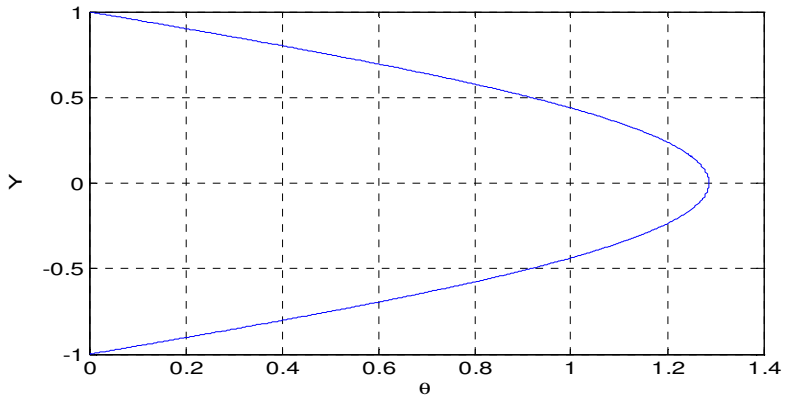

Figure 9. 2. Dimensionless temperature distribution of a fluid in a clear channel

For the asymmetric wall heat flux case, two individual Nusselt numbers are obtained for the lower and the upper walls. These Nusselt numbers have critical points on where heat transfer direction is changed. These discontinuities will be discussed in porous channel case (Chapter 5) in detail but at this stage, the following information will be sufficient. When the heat fluxes at both walls are equal to each other, then the

upper and lower wall Nusselt numbers are equal to each other and they are equal to *4.1176*.

Finally, it is explained in Section 3.4 that the multiplication of the friction factor and the Reynolds number is calculated as *24*. These results can be summarized as follows.

$$Nu_c = 4.1176 \tag{9.1}$$

$$Nu_{cu} = Nu_{cu} = Nu_c = 4.1176 \quad \text{if} \quad q''_l = q''_u \tag{9.2}$$

$$(f\ Re)_c = 24 \tag{9.3}$$

9.2. Results for Flow in a Porous Channel with Symmetrical Heating

A fluid flow in a fully filled porous channel with symmetric heat flux boundary condition is studied in Chapter 4. Dimensionless velocity profiles of flows through four different porous media with various Darcy numbers are plotted in Figure 9.3. As seen in this figure, analyzing the dimensionless velocity profile is extremely hard for flows through low Darcy number media. Therefore, normalized velocities are used. The most important point that we understand from this figure is that the velocity decreases by reducing Darcy number, because the fluid encounters more obstacles in the channels with low Darcy number.

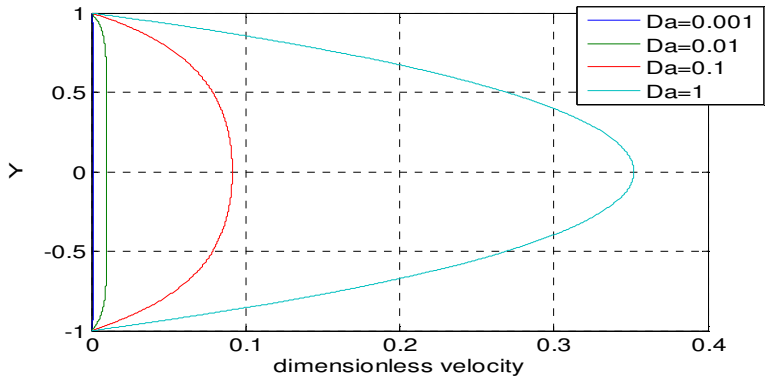

Figure 9.3. Dimensionless velocity distributions for the flows with four different darcy numbers

The normalized velocity distributions for the same flows (shown in Figure 9.3) are shown in Figure 9.4. As clearly seen, for the flow through a medium with *Da=1*, the

flow is similar to the flow in a clear channel. As Darcy number increases, porous media effects decreases. With low Darcy-number flows, the velocity profile looks like a turbulent flow and becomes flattened.

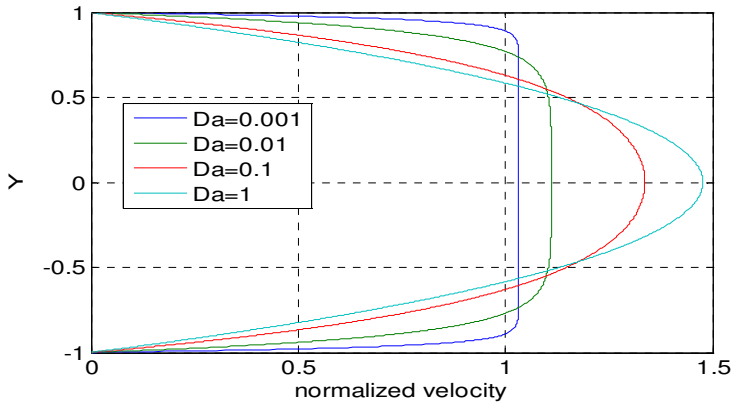

Figure 9.4. Normalized velocity distribution for fully porous channel for different Darcy number

As seen in Figure 9.5, the dimensionless temperature gradient at the surface for flows with low values of Darcy-number such as Da = 0.001 is larger than flows with higher values of Darcy-number. This result is caused by the porous media. Figures 9.6 and 9.7 are the other demonstrations of the same result. When Darcy number increases, the Nusselt number approaches to 4.1176, which indicates the flow through a clear channel. For flows with low Darcy numbers, the Nusselt number increases, that means, more heat transfer is observed. The Nusselt number for *Da=0.001* is *5.6591* which is greater than that of clear fluid.

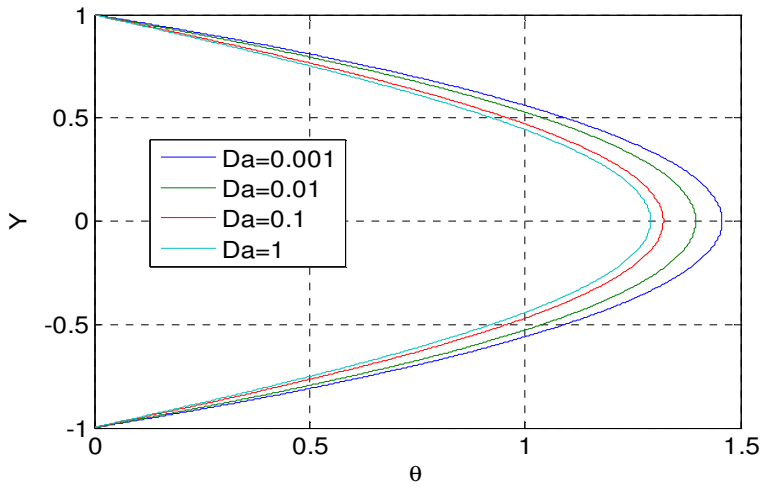

Figure 9.5. Dimensionless temperature vs. Y-axis for the flows with four different Darcy numbers

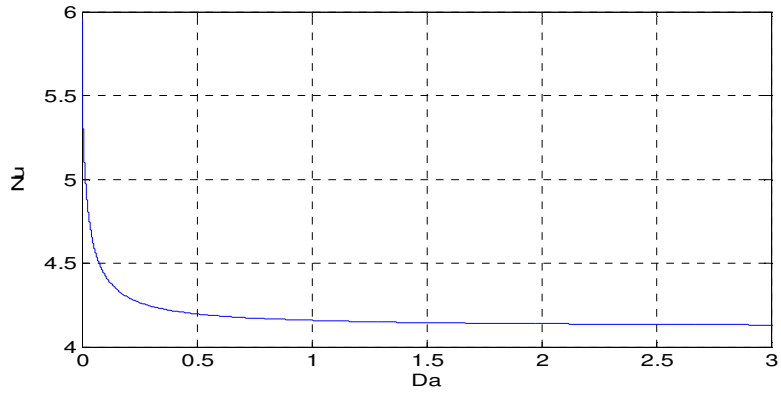

Figure 9.6. Nusselt number variation with darcy

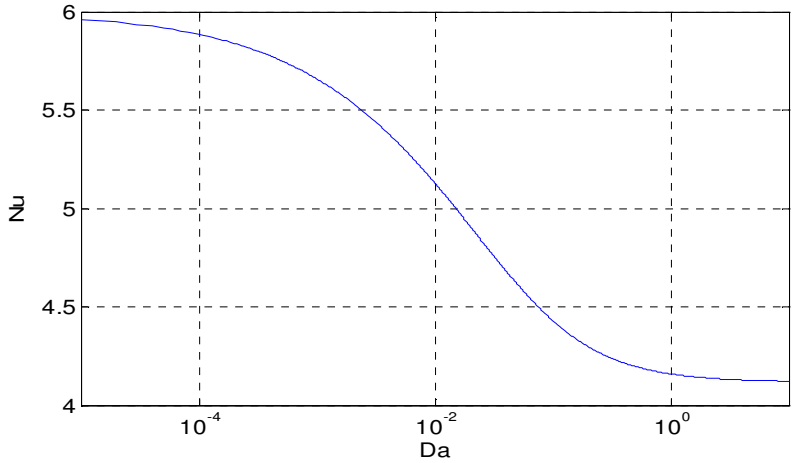

Figure 9.7. Logarithmic plot of Nu vs. Da

In Figure 9.8, heat transfer increment ratio (Equation 4.33) is plotted against the Darcy number. It is obvious that, decreasing the dimensionless permeability *(Da)* increases the heat transfer. When Darcy number increases, then the heat transfer increment ratio approaches to 1, which is its value for clear flow. However, the porous media with low Darcy number have a significant drawback on fluid flow in channel as clearly seen in Figure 9.9. For the flow with $Da=10^{-5}$, the pressure drop increment ratio (Equation 4.34) reaches about $3.2 \cdot 10^{4}$. That means the fan (or pump), which forces the fluid into the channel, needs *10000* times more energy input. With this Darcy number, filling the channel fully by porous medium increases the heat transfer by only *1.5* times. When Darcy number increases, the pressure drop increment ratio approaches to *1*, which is for clear flow. The overall performance of the system is plotted against the Darcy number in Figure 9.10. The flows with Darcy numbers lower than 10^{-3}, the overall performance (Equation 4.35) approaches to zero. For higher Darcy number flows it increases. However, it never becomes greater than *1*. Therefore, for fully filled

porous channels, the pressure drop increment ratios are always greater than the heat transfer enhancement ratios. It means that, it is not feasible to use such systems if a free energy source is not had.

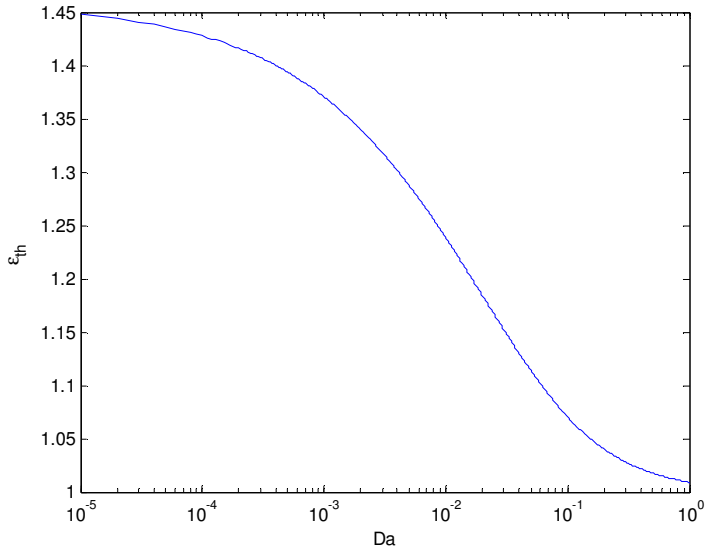

Figure 9.8.Logarithmic plot of heat transfer increment ratio vs. Da

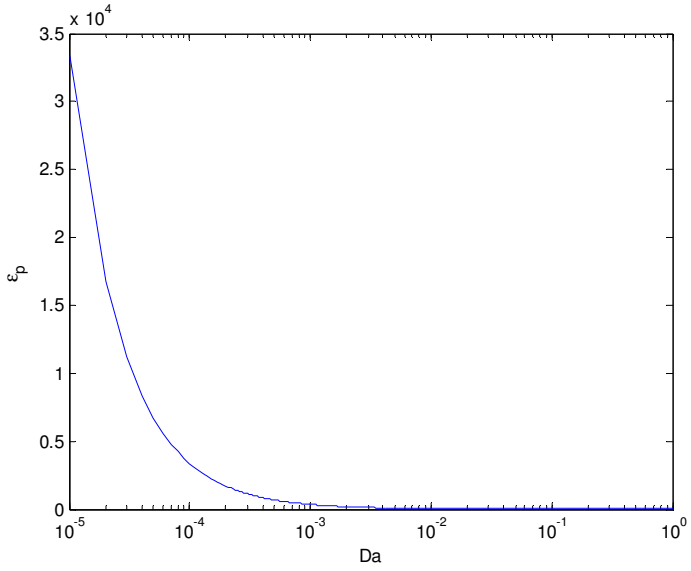

Figure 9.9. Logarithmic plot of pressure drop increment ratio vs. Da

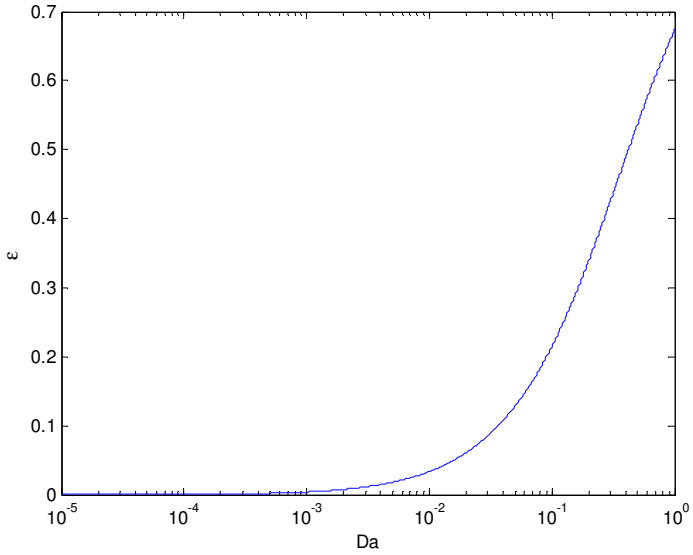

Figure 9.10. Logarithmic plot of overall performance

9.3. Results for Flow in a Porous Channel with Asymmetric Heating

In this case, a full porous channel was being heated by asymmetric heat fluxes at both walls. The flow is hydro-dynamically and thermally fully developed and laminar. The fluid is assumed to be incompressible and Newtonian.

The temperature profile, overall and individual Nusselt numbers are calculated and their changes with Darcy number and heat flux ratio are discussed via graphics and tables. In order to easily realize the physical meaning of the derived relations, discussions are performed based on Darcy number which means $M = 1$ in the following discussion. As it was mentioned before, the energy equation was solved both numerically and analytically to be ensure from the obtained results. Table 9.1 shows the overall and individual Nusselt numbers calculated both numerically and analytically for a channel with $Da = 0.01$ and for four different values of heat flux ratio as *1, 2, 10* and *100*. As seen, there is a good agreement between the numerical and analytical solutions. Table 9.2 was also prepared to indicate the accuracy of the obtained results. In this table, the overall and individual Nusselt numbers for two channel, one with $Da = 1000$ and another for a clear fluid flow are presented at different values of heat flux ratios. Table 9.2 shows that the overall and individual Nusselt numbers are almost identical for the channel of clear fluid and the $Da = 1000$ channel in which the flow behaves like clear fluid flow.

Table 9.1. Comparison of the analytical and numerical results for the Nusselt numbers of a flow in a porous medium when Da = 0.01

	Nusselt number from Analytical solution			**Nusselt number from numerical solution**		
	Nu_l	**Nu_u**	**Nu**	**Nu_l**	**Nu_u**	**Nu**
q1/q2=1	5.1293	-5.1293	5.1293	5.1281	-5.1281	5.1281
q1/q2=2	3.6871	-23.564	5.1293	3.6866	-23.524	5.1281
q1/q2=10	3.0100	0.8491	5.1293	3.0097	0.8493	5.1281
q1/q2=100	2.8906	0.0671	5.1293	2.8904	0.0671	5.1281

Table 9.2. Comparison of the Nu, Nu1 and Nu2 variation for a clear fluid and a porous medium for Da=1000

	Nusselt number for Da=1000			**Nusselt number for clear fluid**		
	Nu_l	**Nu_u**	**Nu**	**Nu_l**	**Nu_u**	**Nu**
q1/q2=1	4.1177	-4.1177	4.1177	4.1177	-4.1177	4.1177
q1/q2=2	3.2558	-8.7503	4.1177	3.2558	-8.7500	4.1177
q1/q2=10	2.7889	1.0937	4.1177	2.7888	1.0937	4.1177
q1/q2=100	2.7017	0.0801	4.1177	2.7017	0.0801	4.1177

Figure 9.11 shows the variation of overall Nusselt number with Darcy number for the analyzed channel. The overall Nusselt number does not depend on heat flux ratio. For a specified Darcy number, the value of overall Nusselt number is constant. No singularity is observed in the changes of overall Nusselt with Darcy number. Hence, heat transfer rate to/from parallel plates for the entire possible values of heat flux ratio and Darcy number can be calculated. The total heat transfer rate through different channels can be easily calculated and compared with each other by considering the definition of overall Nusselt number. As seen from Figure 9.11, the overall Nusselt number steeply drops with the increase of Darcy number in the region of $Da < 1$. The value of overall Nusselt number becomes almost constant for high values of Darcy number (i.e., $Da >> 1$). For high values of Darcy number, when flow behaves like a clear fluid flow, the overall Nusselt number takes value of *4.12* which is identical to the value of Nusselt number for a fully developed clear flow in a channel with *2H* height (Nield, 2004).

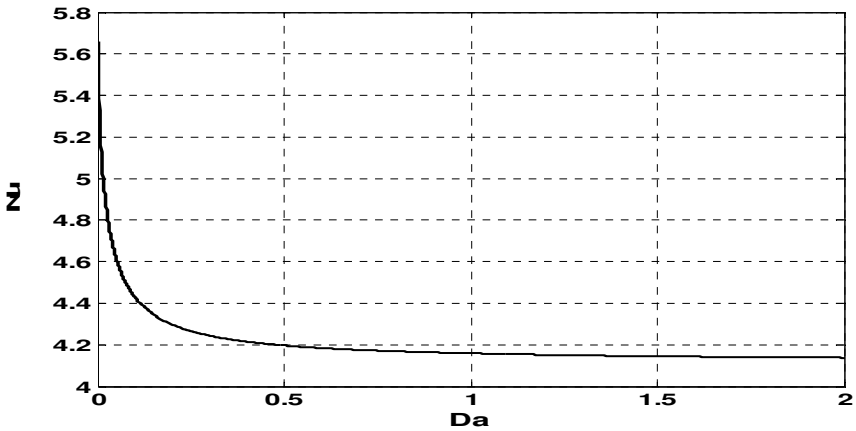

Figure 9. 11. Nusselt number variation with darcy

The changes in the upper and lower plates Nusselt numbers with heat flux ratio are shown in Figures 9.12(a) and 9.12(b), respectively. Figure 9.12 was prepared for a flow in a channel with Da = 100 to firstly discuss heat and fluid flow in an almost clear fluid flow channel. As seen from Figure 9.12, the value of lower plate Nusselt number is almost zero at the low values of heat flux ratio such as $q_r=0.1$. For the low values of q_r, the value of lower plate Nusselt number is negative which refers to the heat transfer from fluid to the lower plate. The lower plate Nusselt number decrease with further increase in q_r. This trend continues up to a heat flux ratio of q_r =0.346. The direction of Nusselt number at the lower plate is changed at q_r=0.346 and after it, the lower plate Nusselt number takes positive values. A singularity for the lower plate Nusselt number is observed at $q_r = 0.346$. As it was mentioned before, in this study, the heat flux ratio at which the heat flux between wall and fluid changes direction is called as critical heat flux ratio. In the channels with $Da = 100$, the lower plate Nusselt number takes positive value in the region of $q_r>q_{rl,cr}$. The value of Nu_l decreases with further increase in heat flux ratio in the region of $q_r>q_{rl,cr}$. The value of Nu_l approaches to 2.789 for high values of heat flux ratio such as $q_r=10$.

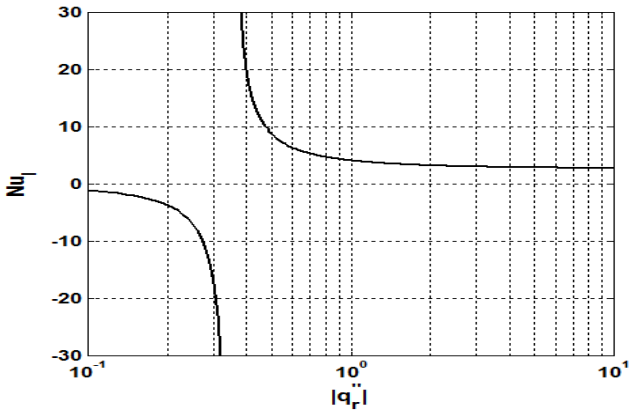

(a)

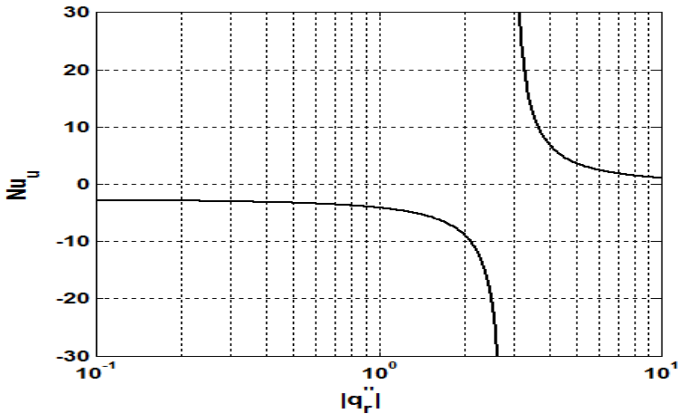

(b)

Figure 9. 12. Individual Nusselt number variations with darcy for Da=100

The variation of the upper plate Nusselt number with heat flux ratio is shown in Figure 9.12(b) when *Da = 100*. For the low values of heat flux ratio such as $q_r=0.1$, the value of upper plate Nusselt number is almost constant as $Nu_u=-2.789$. The value of upper plate Nusselt number is negative which shows heat transfer from upper plate to the fluid. The value of upper plate Nusselt number decreases with increase of heat flux ratio, and at a critical heat flux ratio (i.e.,$q_{ru,cr}=2.889$), Nu_u changes direction and the upper plate Nusselt number takes positive values. This change of heat flux direction refers to the heat transfer from saturated porous media to the upper plate. For the regions with $q_{ru,cr}>2.889$, further increase in heat flux ratio causes Nu_u approaches to zero and the upper plate behaves like an insulated wall.

Figure 9.12 shows that three different heat flux regions should be considered in analyzing of heat transfer in a channel with asymmetric boundary conditions. The first region is the region with $q_r>q_{rl,cr}$, for which the lower plate Nusselt number is negative and heat is transferred from fluid to the lower plate. In this region, the value of upper

plate Nusselt number is also negative and it refers to the heat transfer from the upper plate to the porous media. The second region is the region in which $q_{rl,cr}<q_r<q_{ru,cr}$. In this region, the lower plate Nusselt number is positive while the upper plate Nusselt number takes negative values. In this region, heat is transferred from both upper and lower plates to the porous media. The third region is $q_r>q_{ru,cr}$, for which the values of lower and upper plate Nusselt numbers are positive. This shows that heat is transferred from the lower plate to the fluid while the upper plate receives heat from the fluid flowing through the channel.

Figure 9.13 shows the changes in individual Nusselt numbers with heat flux ratio for *Da = 0.1, 0.01* and *0.001*. As seen, the changes in upper and lower plate Nusselt numbers of different Darcy numbers are very similar to the channel with *Da = 100*. Figure 9.13 reveals that the value of critical heat flux ratio is not constant and it varies with Darcy number. By decrease of Darcy number, the lower plate critical heat flux ratio slightly increases while a little decrease in upper plate critical heat flux ratio is observed.

Figure 9.14 indicates the variation of critical heat flux ratio of lower and upper plates with Darcy numbers between *0.1* and *10*. The values of lower plate critical heat flux are around *0.4* while the values of upper plate critical heat flux are around *2.5*. As seen from Figure 9.14, the heat transfer between the upper and lower plates with porous media can be divided into three regions. Once the value of Darcy number is known for a channel filled with porous media, the critical heat flux of lower and upper plates can be easily calculated. By comparing the calculated critical heat flux ratio of upper and lower plates based on the subjected heat flux ratio to the channel, the direction of heat transfer between the plates and porous media can be easily predicted. It should be mentioned that critical heat flux ratio is almost constant for very small Darcy number ($Da < 0.1$) or large Darcy number ($Da > 10$) as seen from Figure 9.14.

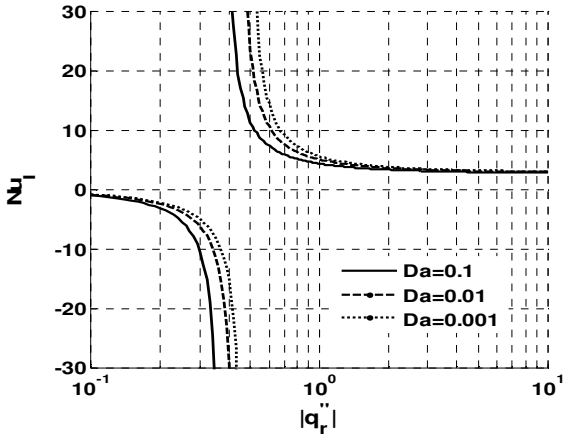

(a)

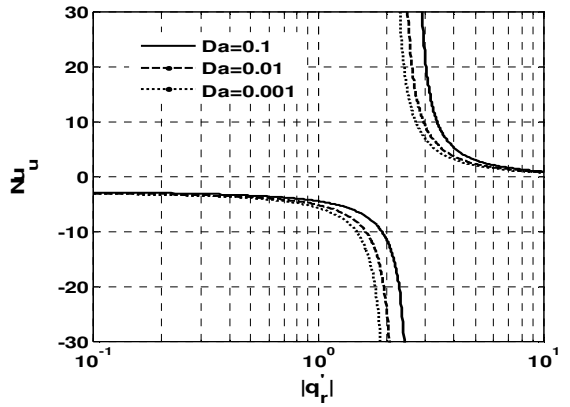

(b)

Figure 9.13. Variation of individual Nusselt number with absolute value of heat flux ratio when Da = 0.1, 0.01 and 0.001 a) lower plate, b) upper plate

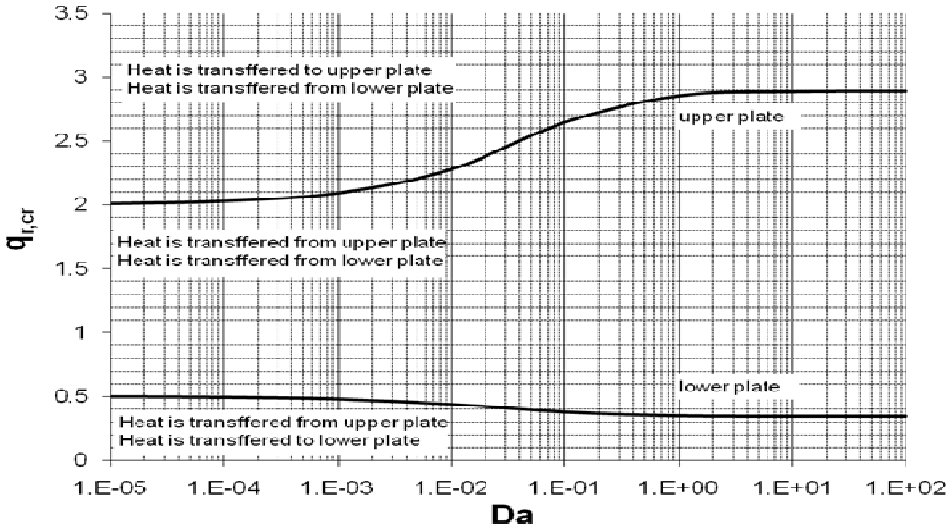

Figure 9.14. Critical heat flux ratio variation with darcy number

9.4. Results for Chapter 6: Flow in a Symmetrically Filled Partial Porous Channel

In this study, the channel is partially filled with porous medium and the location of the porous region is symmetric around the centre of the channel. The flow in the channel is thermally and hydro-dynamically fully developed and laminar. The fluid is assumed to be Newtonian and incompressible.

As seen in Figure 9.15, dimensionless normalized velocities versus Y-axis are plotted for four different porous thicknesses and four different Darcy numbers for each porous thickness. In Figure 9.15(a), the porous thickness in the channel is *0.4*. As seen in this figure, for the lower Darcy numbers such as *Da=0.001* and *Da=0.01*, the porous effects become important and although the porous region is very small relative to the channel length, porous region slows down the fluid velocity, significantly. For the flow of *Da=0.001*, the fluid velocity in the porous region is almost zero and the velocity gradient at the surface is relatively higher than the other media with higher Darcy numbers. When the Darcy number increases, the flow resembles to that in clear channel and there is no effect of the porous region on fluid velocity. For the flow of *Da = 1*, there is no certain difference between the clear and the porous regions. In Figure 9.15(b), the porous thickness is *0.8*, and for *Da=0.001*; a smooth velocity profile is observed as in a turbulent flow. As seen in Figure 9.15(c), for both flows with *Da=0.001* and *Da=0.01*, the smooth velocity profiles in porous region can be observed. When the porous length increases, the velocity gradients at the surface for all the flows except the flow with *Da=1*, increases. For the flow with *Da=1*; the changes of the porous length do not affect the velocity profile, significantly.

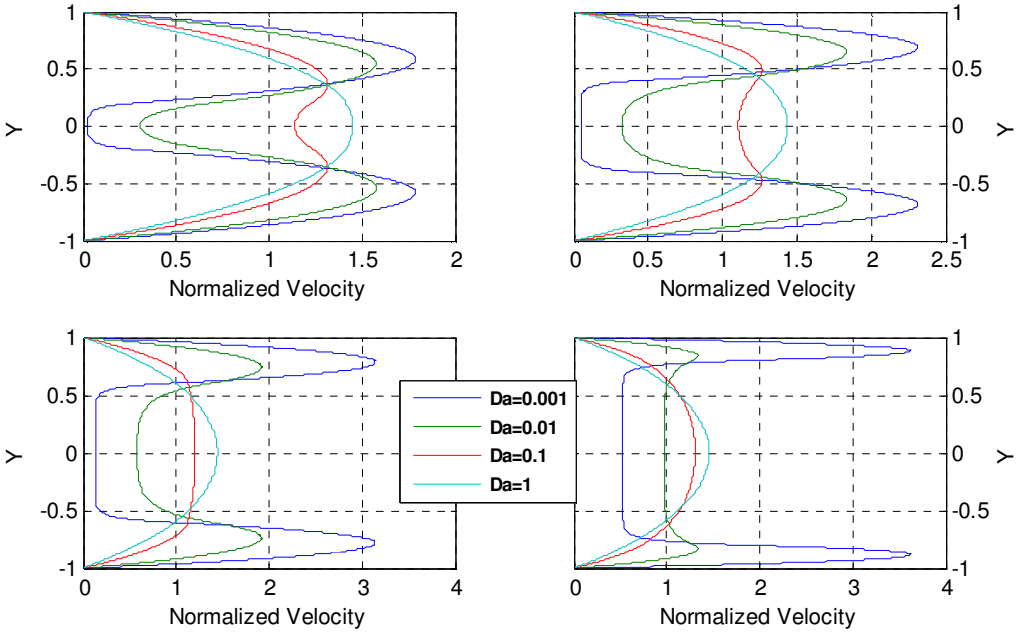

Figure 9.15. Normalized velocity profiles for four different darcy numbers, (a) ξ=0.2, (a) ξ=0.4, (a) ξ=0.6, (d) ξ=0.8

Table 1 lists the Nusselt numbers for flows with four different Darcy numbers of 10^{-5}, 10^{-4}, 10^{-3}, and 10^{-2}, respectively, for a constant conductivity ratio (k_r=1). Table 9.1(a) is for the viscosity ratio of *1.1* and Table 9.1(b) is for *10*. The Nusselt number is not highly changed with thermal conductivity and viscosity ratios for $Da = 10^{-5}$, 10^{-4}, and 10^{-3}. On the other hand, for the flow with $Da = 10^{-2}$, the Nusselt number is affected by the viscosity ratio, particularly for porous layer thickness of *0.2H.*It is clearly seen in the table that the larger porous media in a channel means larger heat transfer to the fluid. In addition, smaller Darcy number also means higher Nusselt numbers. This fact can be seen in Figures 3 and 4, too. Among the presented results, the dimensionless temperature gradient at the surface takes maximum values for $Da=10^{-5}$. For $\xi=0.8$, which indicates a larger porous medium contribution in the channel, a steeper gradient is clearly observed.

Table 9.3. Nusselt numbers for flows in various media (a) M=1.1, (b) M=10

M=1.1	**ξ**	**Da=10^{-5}**	**Da=10^{-4}**	**Da=10^{-3}**	**Da=10^{-2}**	
k_r=1	0.00	4.12	4.12	4.12	4.12	**Nu**
	0.05	5.65	5.61	5.46	4.85	
	0.10	5.96	5.92	5.76	5.19	
	0.25	7.15	7.08	6.84	6.00	
	0.50	10.70	10.52	9.78	7.27	
	0.65	15.23	14.76	12.46	7.17	
	0.75	21.19	19.83	13.10	6.40	
	0.90	46.05	16.89	7.00	5.29	
	0.95	22.99	7.63	5.89	5.15	
	1.00	5.66	5.13	4.43	4.16	

(a)

M=10	**ξ**	**Da=10^{-5}**	**Da=10^{-4}**	**Da=10^{-3}**	**Da=10^{-2}**	
k_r=1	0.00	4.12	4.12	4.12	4.12	**Nu**
	0.05	5.66	5.64	5.51	4.87	
	0.10	5.98	5.96	5.85	5.24	
	0.25	7.17	7.14	6.98	6.09	
	0.50	10.74	10.64	10.01	7.05	
	0.65	15.31	14.99	12.58	6.63	
	0.75	21.35	20.16	12.55	5.99	
	0.90	46.33	15.60	6.69	5.41	
	0.95	21.33	7.30	5.87	5.27	
	1.00	5.13	4.43	4.16	4.12	

(b)

In Figure 9.16, the dimensionless temperatures along the Y-Axis are plotted for the flows with four different porous thicknesses and four different Darcy numbers for each porous thickness. The conductivity ratio is *10000*. In Figure 9.16(a), the porous thickness is *0.4* and as seen in the figure, the maximum dimensionless temperature gradient at the surface (the Nusselt number) is for the flow with *Da=0.001*. When Darcy number increases, the Nusselt number decreases and the least heat transfer between the wall and the fluid is observed for the flow with *Da=1*. This result can also

be seen in Figures 3(b,c,d). In these figures, the Nusselt numbers can be seen as increasing when the porous thickness increases. In Figure 9.16(d), there are constant dimensionless temperatures are observed in the porous region because of very high conductivity.

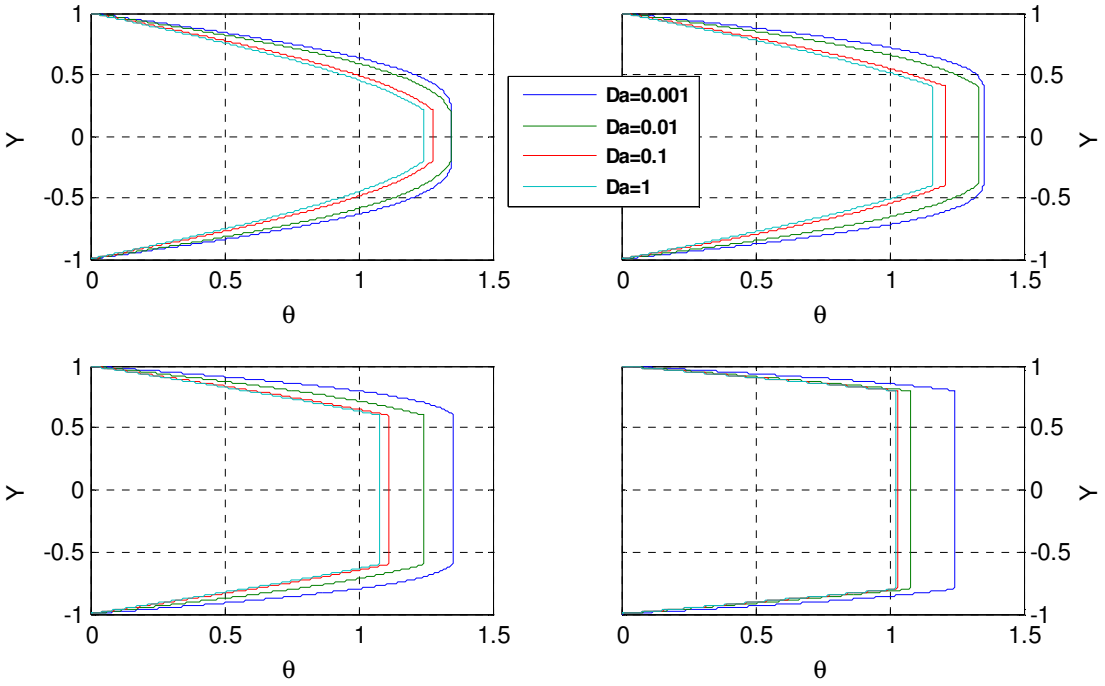

Figure 9.16. Dimensionless temperature profiles for four different Darcy numbers, (a) ξ=0.2, (a) ξ=0.4, (a) ξ=0.6, (d) ξ=0.8 , (k_r=10000)

The porosity, φ, is defined as the ratio of fluid volume and total volume for a selected control volume in a porous media. The effective conductivity can be calculated by using porosity $(k_{eff}=\varphi k_f+ (1-\varphi)k_s)$.These concepts are explained in detail in Chapter 2.In Table 2, conductivity ratios of different fluid-solid combinations for two different porosities are listed. This list is written under the assumption that the porosity is uniform through the channel.

Table 9.4. Conductivity ratios for specified fluid-solid combinations (Incropera and DeWitt, 1996)

Fluid-Solid Combination	**k_r**	
	φ=0.35	**φ=0.70**
water-Al (pure)	251.66	116.69
water-Cu (pure)	425.55	196.95
water-Rubber, rigid Foamed	0.38	0.72
water - Polyamide-Nylon 6	0.61	0.82
air-Al (pure)	5858.00	2704.10
air-Cu (pure)	9911.00	4574.80
air-Rubber, rigid Foamed	1.14	1.07
air - Polyamide-Nylon 6	6.28	3.44

In Figure 9.17, Nusselt number ratio changes with porous thicknesses are plotted for four different conductivity ratios. In Figure 9.17(a), the conductivity ratio is *0.1* and clearly seen in the figure, for all flows with Darcy numbers of 10^{-5}, 10^{-4} and 10^{-3}, the Nusselt number ratios have peaks at some point near $\xi=1$. At these points, the heat transfer reaches its maximum. Beyond this point, the Nusselt number decreases with increasing porous thickness. Therefore, for the sake of enhancing heat transfer in a parallel plate channel, it is better to fill it by porous media to this specific thickness that makes the Nusselt maximum, rather than fully fill it.

The flow with Da=10^{-5} has the greatest Nusselt number ratio for all cases. For the flow with $Da=10^{-2}$, the change of Nusselt number with porous thickness is relatively small, because this flow looks more like to clear one. Increases in conductivity ratio cause the maximum Nusselt number to increase for the flows with all Darcy numbers, and these maximum points approach to *1* much more than the lower conductivity ratio cases.

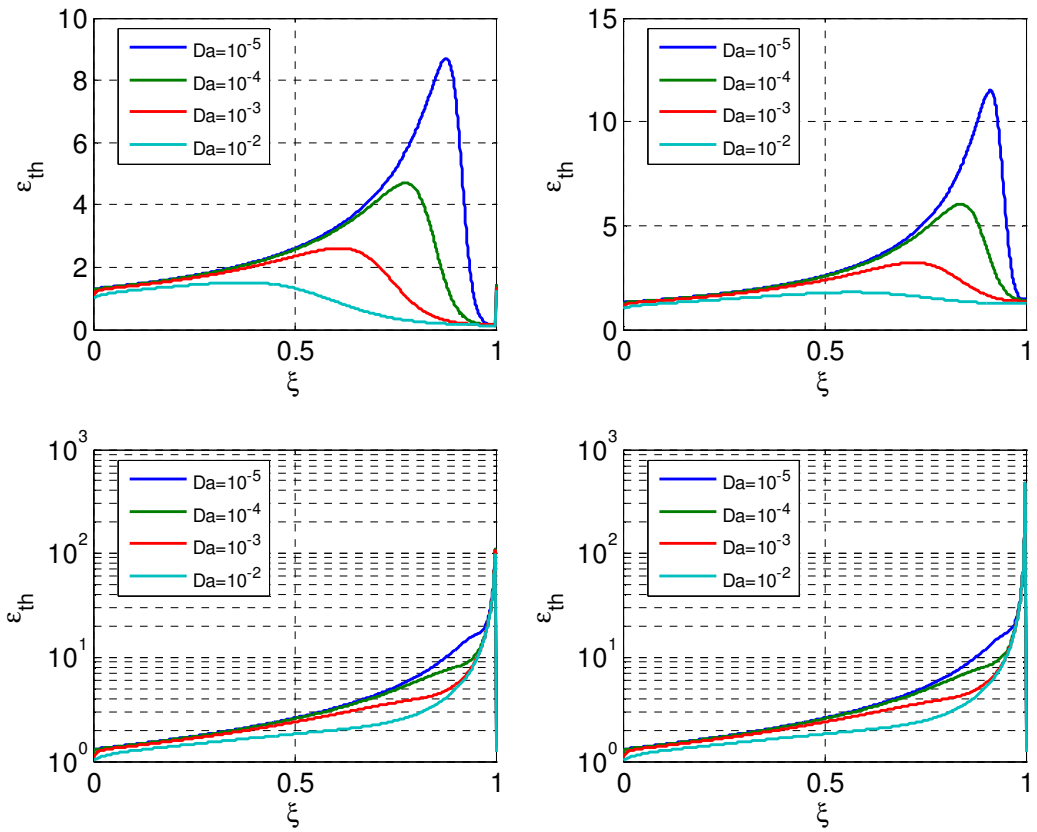

Figure 9.17. The heat transfer increment ratio for four different darcy numbers, (a) k_r=0.1, (a) k_r=1, (a) k_r=100, (a) k_r=10000

Although, significant heat transfer enhancement is provided by using porous media, there is a strong drawback for using it. This drawback is called as pressure drop. The fan (or pump if the working fluid is in liquid state) needs power which is directly proportional to pressure drop; more pressure drop implies more power input.

In Figure 9.18, the pressure drop increment ratio is observed for the flows with all Darcy numbers. The pressure drop for the flow with $Da=10^{-2}$ for fully filled porous channel is almost *40* times that of the clear flow. This ratio is approximately *350*, *3500* and *35000* for the flows with Darcy numbers of 10^{-3}, 10^{-4} and 10^{-5}, respectively. For a channel with porous thickness of *0.4* ($\xi=0.2$), the pressure drop ratio changes between *5* and *8*.

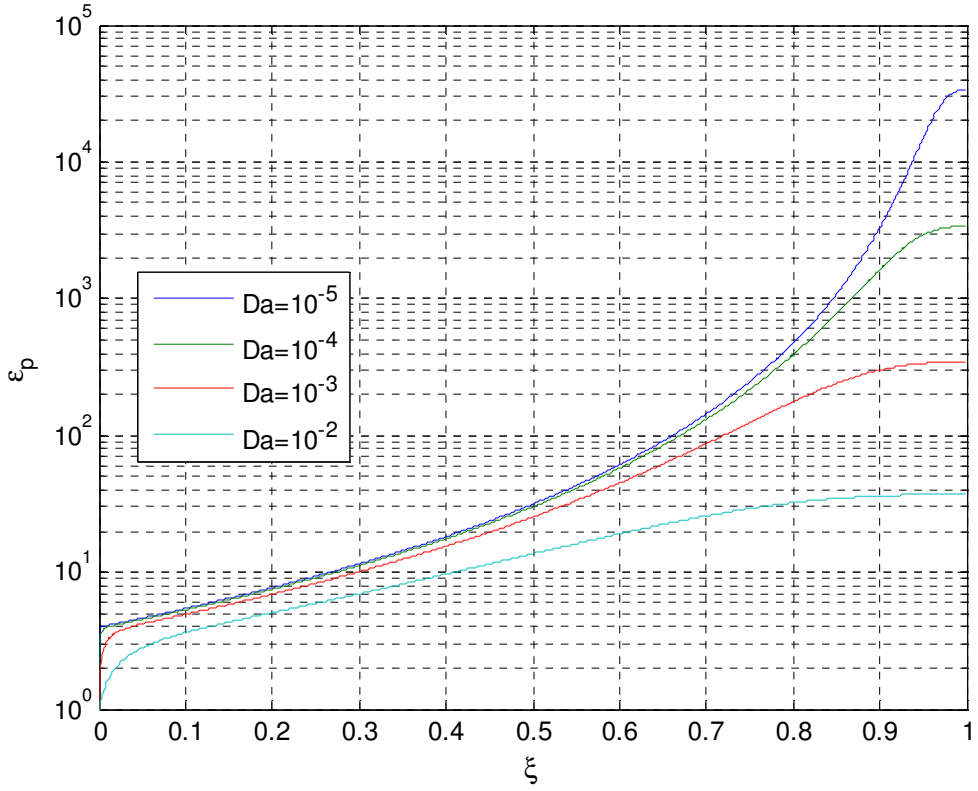

Figure 9.18. The pressure drop ratio for four different darcy numbers

In Figure 9.19, ratio of the Nusselt number and pressure drop ratios is plotted versus the porous length for four different conductivity ratios. Figures 9.19(a), (b), (c) and (d) are plotted for the conductivity ratios of *0.1*, *1*, *100* and *10000*, respectively. As seen in Figure 9.19(a), for the conductivity ratio of *0.1*, the pressure drop becomes dominant when the porous thickness increases. The ratio of ε_{th} and ε_p has its minimum value at full porous case. This result is not changed in Figure 9.19 (b), which is plotted for the conductivity ratio of 1. In both these cases, the ratio of the Nusselt number and

pressure drop ratios have not values greater than one. In Figures 9.19 (c) and 9.19 (d) (the conductivity ratios are *100* and *10000*, respectively), this ratio has greater numbers. Therefore, it can be said that as the conductivity ratio increases, the ratio of the Nusselt number and pressure drop ratios decreases. However, between the Figures 9.19 (c) and 9.19 (d) there is no sharp difference. In these two figures, it can be observed that, when $\xi > 0.99$, then $\varepsilon_{th} / \varepsilon_p$ has a value greater than *1*.

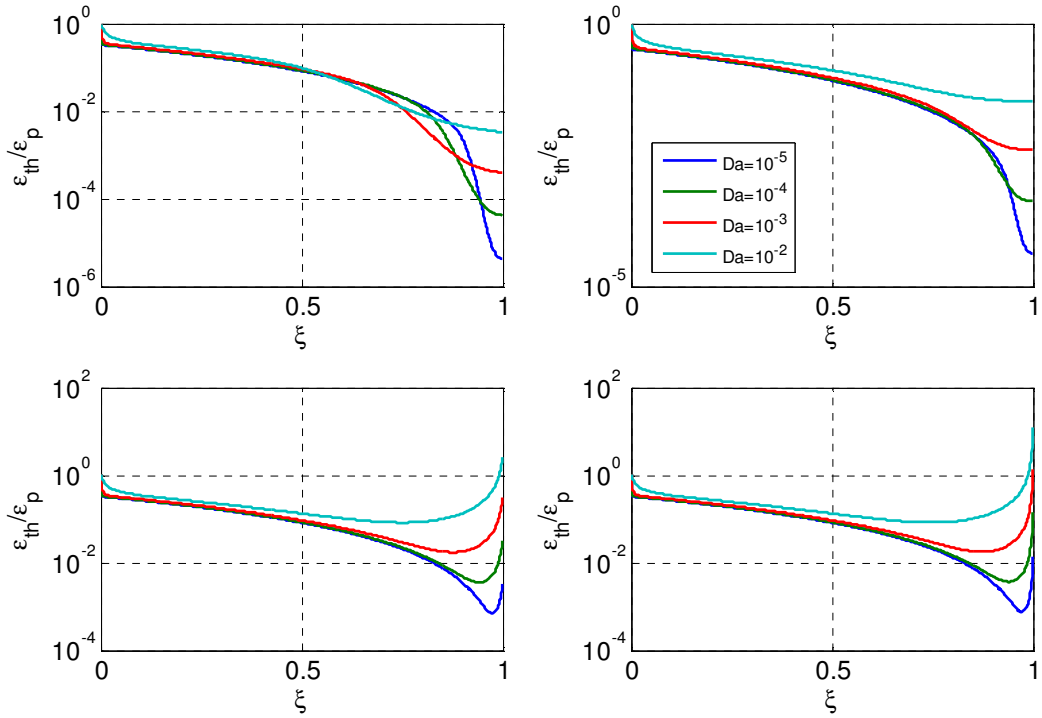

Figure 9.19 Theoverall performances for four different darcy number flows, (a) k_r=0.1, (b) k_r=1, (c) k_r=100, (d) k_r=10000

In Figure 9.20, the Nusselt number ratio versus the conductivity ratio is plotted. As seen in the figure; for the flow with $Da=10^{-5}$, the Nusselt ratio is constant after the point where the conductivity ratio is equal to *10*. Hence, there is no need to use another porous media whose conductivity ratio is larger than *10* for this flow. For the flow with $Da=10^{-4}$; the critical point for the conductivity ratio is *100* and the critical conductivity ratio is increasing with increasing Darcy number.

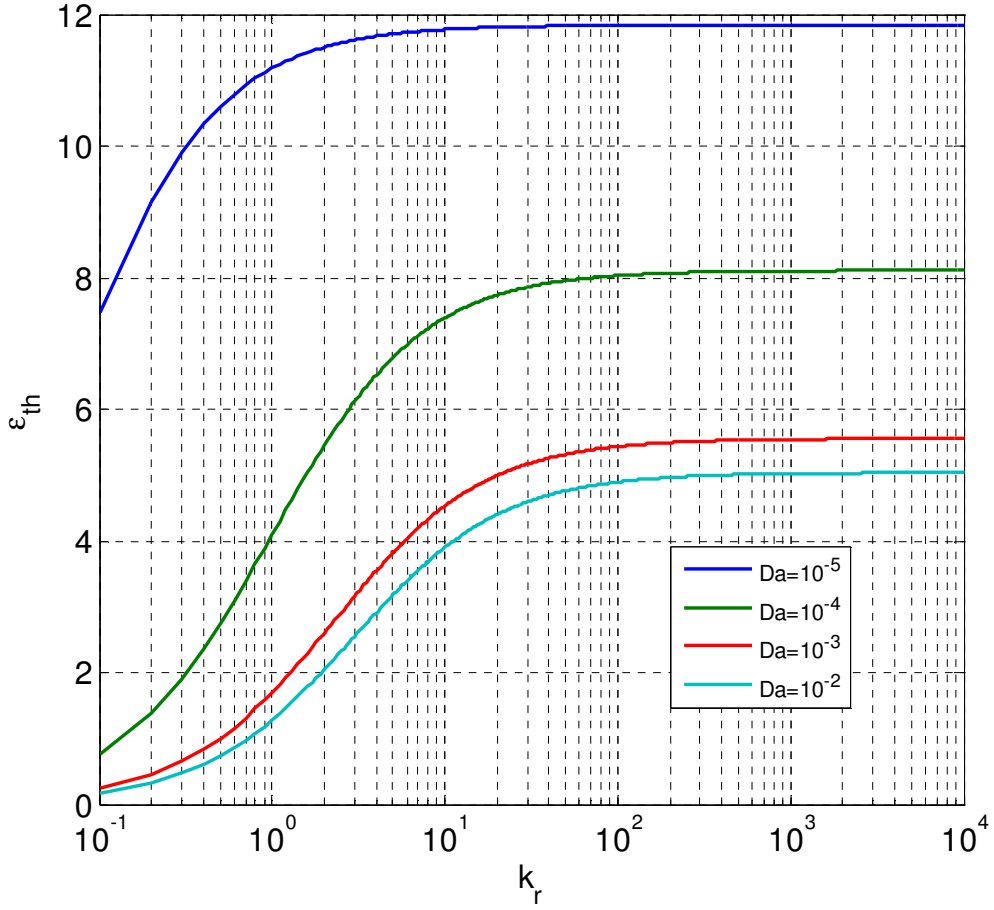

Figure 9.20. The heat transfer increment ratio against the conductivity ratio for flows with four different Darcy numbers

The overall performance $(\varepsilon=\varepsilon_{th}/\ \varepsilon_p)$ is plotted in Figure 9.21. For the flow with $Da=10^{-2}$, ε increases significantly with increasing conductivity ratio till $kr=500$. After that point, there is no effect of conductivity ratio on r. For the flow with $Da=10^{-3}$, there is a slight increase in r with increasing conductivity ratio, till $k_r=30$. After that point, r remains constant with changing k_r. For the flows with $Da=10^{-4}$ and $Da=10^{-5}$, there is no effect of conductivity ratio on ε, as observed in Figure 9.21.

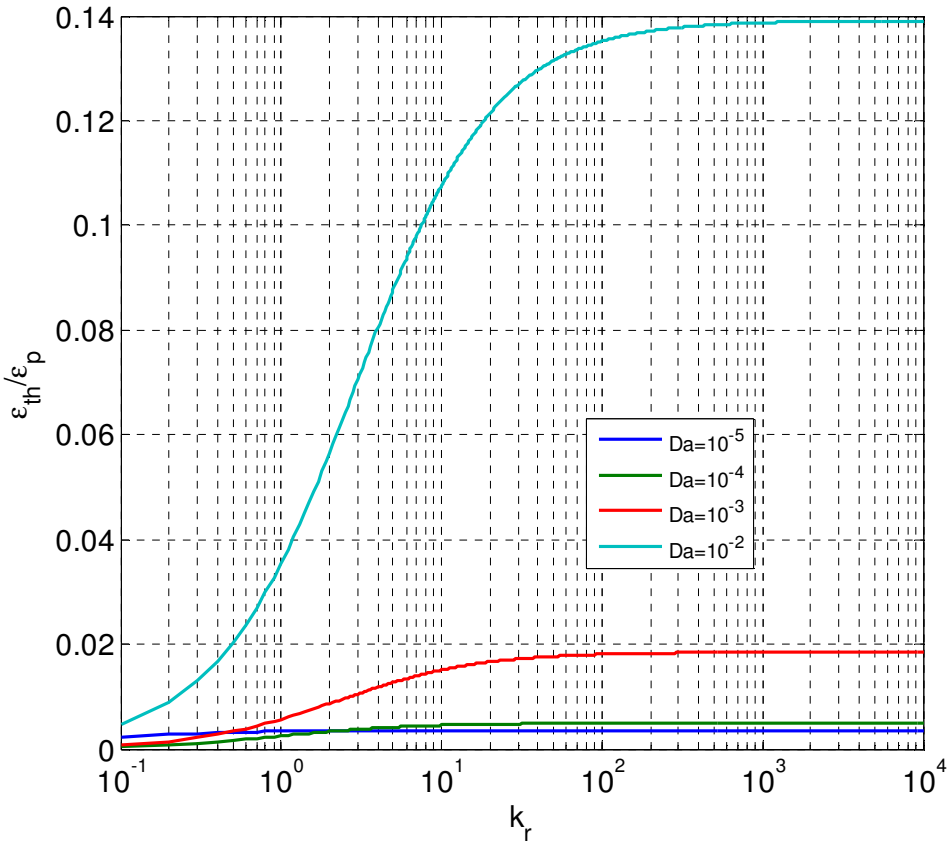

Figure 9.21. The nusselt number ratio over pressure drop ratio against the conductivity ratio for flows with four different Darcy numbers

9.5. Results for Flow in an Asymmetrically Filled Partial Porous Channel

In this part, some example normalized velocity distributions, which are obtained by two methods, namely Darcy-Law, and Brinkman extended Darcy-Law, are shown for comparison. The changes of dimensionless temperature gradients at both walls and the overall Nusselt number with the porous medium location are investigated.

As it is mentioned in Chapter 3, Darcy equation does not include the effects of the shear stresses near the boundaries. Assuming the pressure gradient is constant along the x-axis and the thermo-physical properties of the fluid are uniform, the velocity distribution in the porous region is constant. In dimensionless form, the value of dimensionless velocity is equal to the value of Da number. However, addition of the Brinkman term into the Darcy equation makes the frictional effects at the boundaries be considered. Since the flow velocity in a porous medium with low Darcy number is

extremely low, then these shear effects inside the porous media can be neglected. These facts are demonstrated in Figures 9.22 and 9.23.

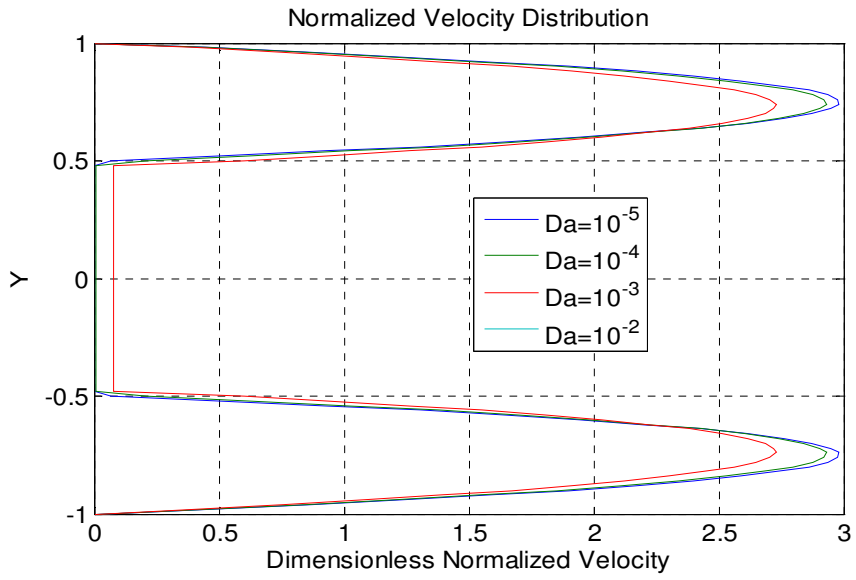

(a)

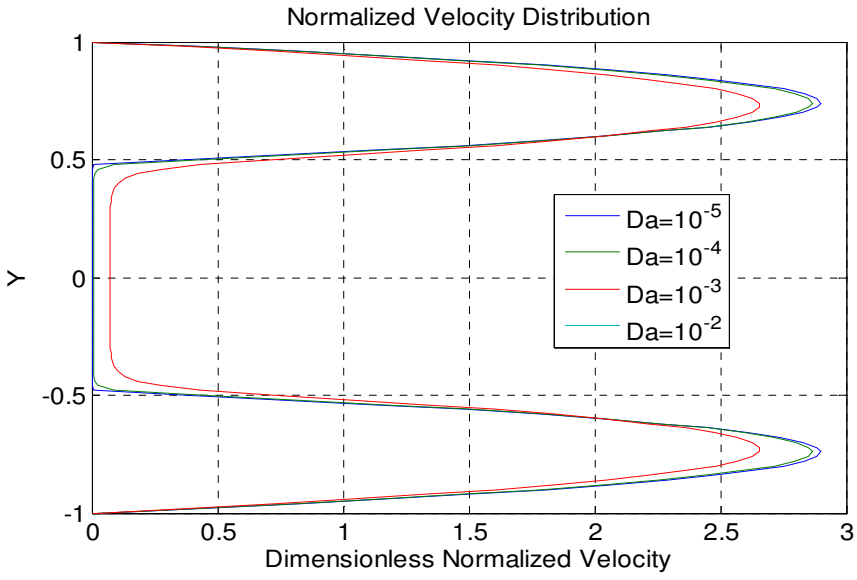

(b)

Figure 9.22 Normalized velocity distribution for M=1.1, ξ_1=0.5 and ξ_2=0.5 by (a) first approach: Darcy's Law (Beaver-Joseph boundary conditions are used at the interfaces), and (b) second approach: Brinkman Extended Darcy's Law (Shear stresses are accepted to be equal at the interfaces)

In our second approach, as expected; the constant velocities are observed in porous region. Furthermore, sharper velocity distinctions can be seen at the porous medium – clear medium interfaces. It can be clearly seen that, these approaches are more similar, when the Darcy numbers are small (when the porous effects are more significant). Since the **Beaver-Joseph** condition is used for the porous-clear region

interface in the second approach, there is a little slip occurs at these interfaces. This condition is known as **slip condition**. For high values of Darcy numbers, this interface condition is not applicable.

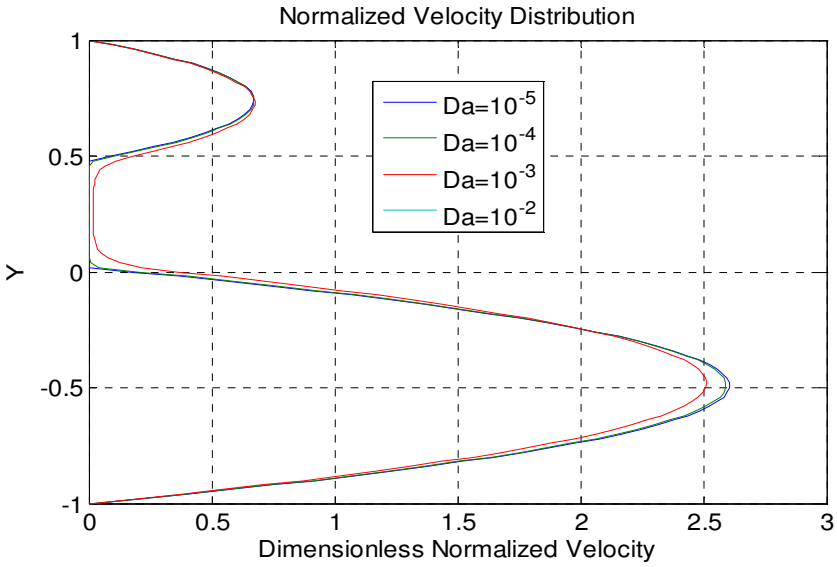

(a)

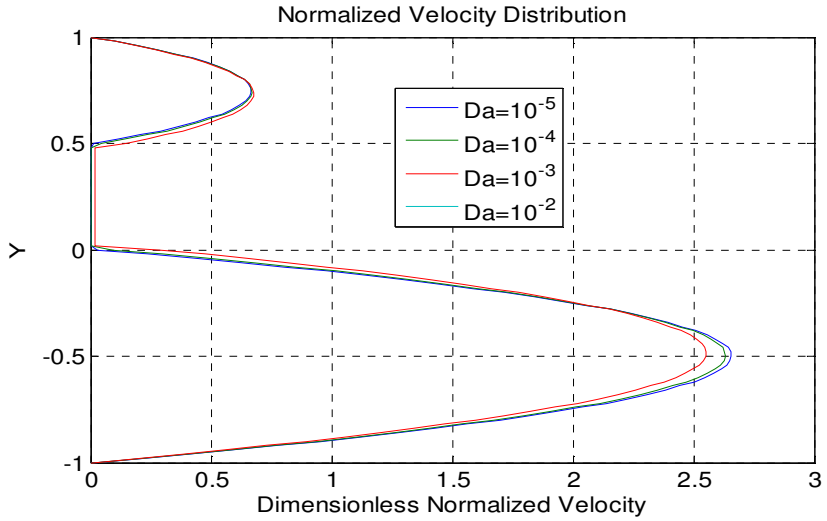

(b)

Figure 9.23. Normalized velocity distribution for ξ_1=0.5 and ξ_2=1 (a) first approach (b) second approach

Table 4 shows the lower wall, upper wall, and overall Nusselt numbers for different porous layer locations for dimensionless porous length of 1 when Darcy number is 10^{-5}, viscosity ratio is 1.1, and the conductivity ratio is 1. The overall Nusselt number is maximum when the porous layer is symmetrically located. However, the maximum value of individual Nusselt numbers and their locations are not only different

than overall Nusselt number but also different from each others. As an example; for ξ_1 = 0.4084 0 and ξ_2 = 0.5916, Nusselt number of the lower plate is maximum. It can be seen that, in this case the dimensionless temperature gradient is the greatest for the flow in the porous medium with Darcy number of 10^{-3}.

Table 5 demonstrates the same comments, but for the dimensionless porous thikness of 0.5.

Table 6 shows the overall Nusselt number variation with the conductivity ratio for ξ_1=0.4 and ξ_2=0.6. The Nusselt number increases with the conductivity ratio, because more energy is transferred by conduction heat transfer between the two sides of the porous medium, in y-direction.

Table 9.5. Nusselt numbers for various porous medium locations for dimensionless porous length of 1

	ξ_1	ξ_2	**Nu**	**Nu_u**	**Nu_l**
$Da=10^{-5}$	0.1	0.9	2.62	-1.53	9.19
	0.2	0.8	2.66	-1.51	11.21
	0.3	0.7	3.13	-1.70	19.70
M=1.1	0.4	0.6	5.37	-2.75	109.78
	0.5	0.5	10.70	-10.70	10.70
	0.6	0.4	5.37	-109.78	2.75
k_r=1	0.7	0.3	3.13	-19.70	1.70
	0.8	0.2	2.66	-11.21	1.51
	0.9	0.1	2.62	-9.19	1.53
Dimensionless Porous Length = 1					

Table 9.6. Nusselt numbers for various porous medium locations for dimensionless porous length of 0.5

	ξ_1	ξ_2	**Nu**	**Nu_u**	**Nu_l**
$Da=10^{-5}$	0.15	1.35	3.08	-2.06	6.10
	0.30	1.20	3.02	-1.92	7.07
	0.45	1.05	3.35	-2.04	9.30
M=1.1	0.60	0.90	4.84	-2.96	13.27
	0.75	0.75	7.15	-7.15	7.15
	0.90	0.60	4.84	-13.27	2.96
k_r=1	1.05	0.45	3.35	-9.30	2.04
	1.20	0.30	3.02	-7.07	1.92
	1.35	0.15	3.08	-6.10	2.06
Dimensionless Porous Length = 0.5					

Table 9.7. Nusselt numbers for various conductivity ratios for dimensionless porous length of 1

ξ_1=0.4	$\mathbf{k_r}$	**Nu**
ξ_2=0.6	1.0	5.37
M=1.1	1.5	6.18
	2.0	6.68
	2.5	7.02
	3.0	7.27
	3.5	7.46
	4.0	7.60
	4.5	7.72
	5.0	7.82

Finally, Figures 9.24, 9.25, and 9.26 show the variations of two individual Nusselt numbers at the walls and the overall Nusselt number with the porous medium location. The dimensionless porous thickness of porous medium is *1*. As seen in the figures, the maximum value of the overall Nusselt number occurs when the porous medium is symmetrically located and it increases with the viscosity ratio, *M*.

The individual Nusselt number of a wall has their maximum value when the porous part location is ξ=*0.4084* far from the other wall as seen in the Figures 9.24, 9.25, and 9.26. The meaning of these results can be embodied in real life. Assume that, we have two metallic chips to cool and the porous part is located in the channel as ξ_1 = *0.4*, and the porous length is *1*. If we submerge one of our chips into the upper part of the porous media and the other into the lower region, then; the chip at the lower part will cool faster, because; the Nusselt number at the lower wall is significantly higher than at the lower one. The main reason of this result seems to be that the high velocities of the fluid at the lower part of the porous region. Normalized velocity profile for that case is plotted in Fig. 9.27.

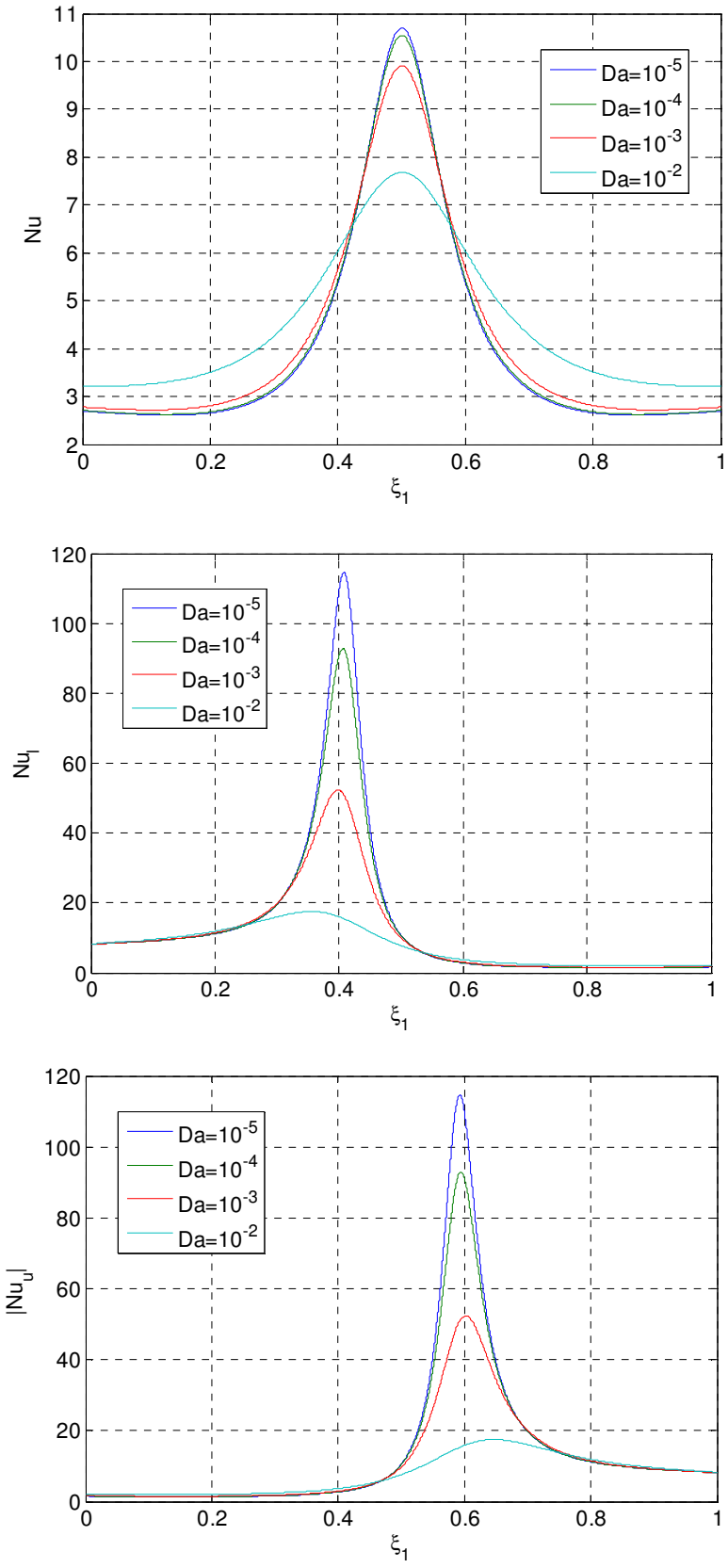

Figure 9.24. Two individual and overall Nusselt number variation with porous location when M=1.1 and porous length=1

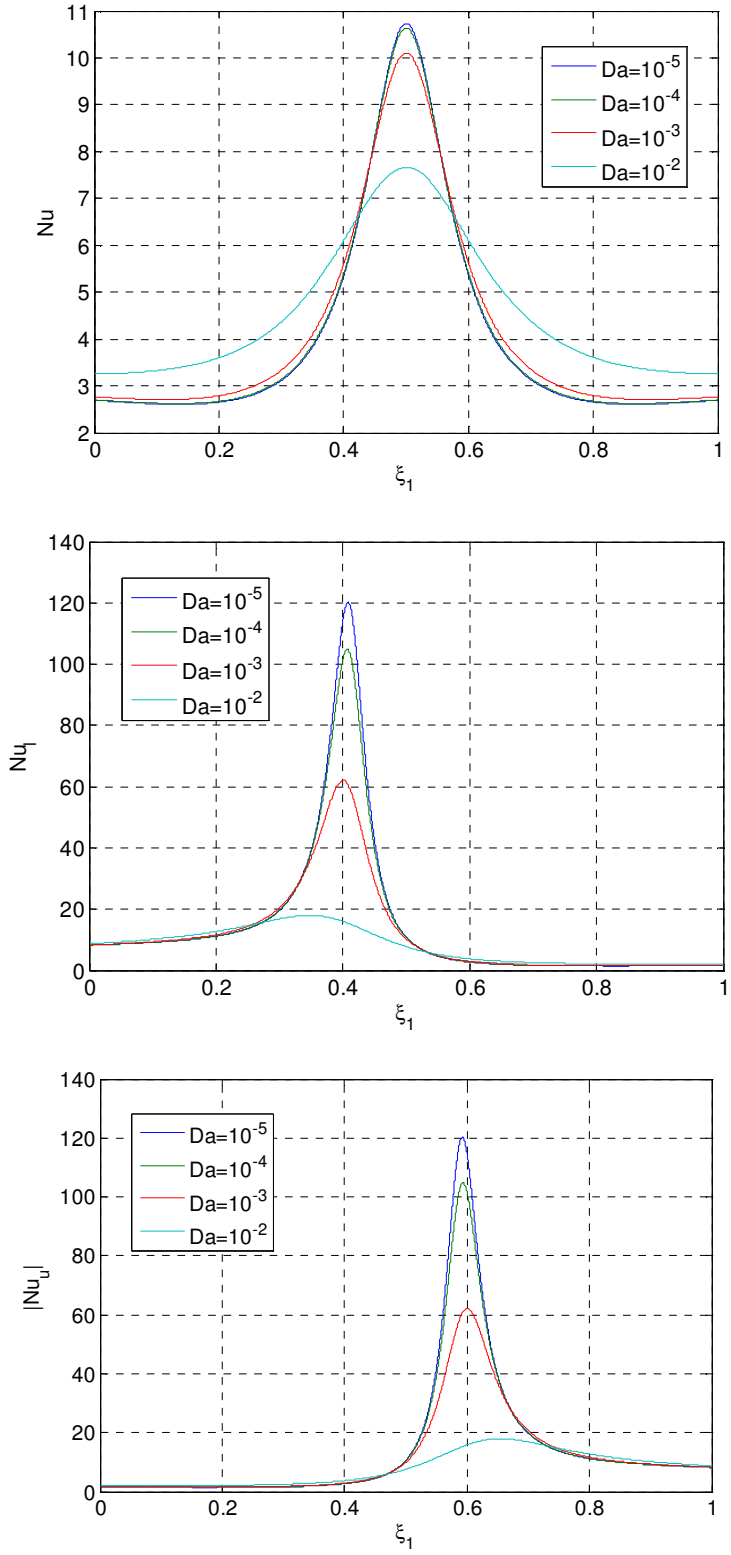

Figure 9.25. Two individual and overall Nusselt number variation with porous location when M=5 and porous length=1

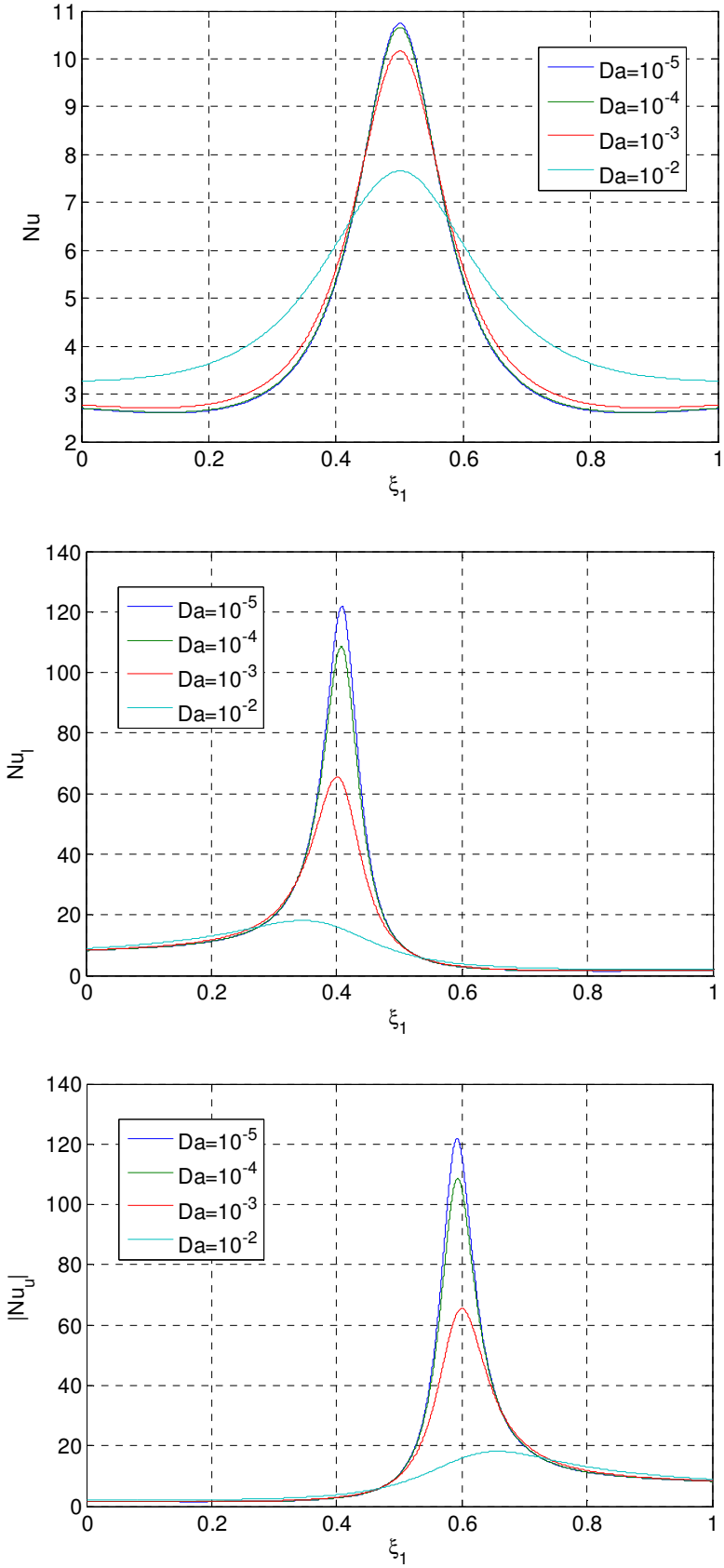

Figure 9.26. Two individual and overall Nusselt number variation with porous location when M=10 and porous length=1

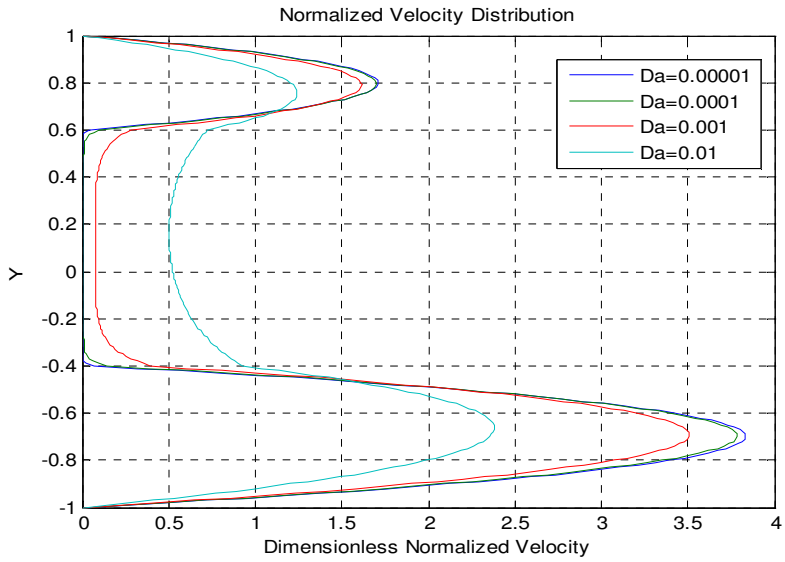

Figure 9.27. The velocity distribution in the case of the maximum lower plate Nusselt number

9.6. Results for Flow in a Solar Air Heater

In Chapter 8, the heat transfer enhancement by using porous media is investigated for a solar air heater.

The velocity distributions for three different Darcy numbers are shown in Figure 9.28(a). This flow has the following properties; $\xi=0.5$, $Nu_o=0.01$, $k_r=10$, $\alpha_r=1$. The bottom part of the channel, with a thickness of *0.5,* is porous. The remaining part with the thickness of *1.5* is clear medium. In upper region of the channel, the clear flow velocity profiles are observed whereas in porous region, the velocities reduce significantly. Especially, for the flow with *Da=0.01*; the flow velocity decreases, significantly.However, as it can be seen in the figure clearly, for *Da=1*, the porous media effects are almost negligible. This flows characteristics are similar to a flow in a clear channel. In other words, the flow does not affected by the porous medium layer.

In Figure 9.28(b), the dimensionless temperature distribution for the flow with *Da=0.01* is shown. Equating $Nu_o$to *0.01*, makes the upper wall almost insulated. This can be seen by observing the isothermal lines at the upper wall, which are almost perpendicular to the surface. Furthermore, temperatures at the porous layer seem to be larger than the clear parts of the fluid in the channel.

In Figure 9.28(c), the mean temperature variation with X-axis is shown. In this case, the Darcy number of the porous region is set to be *0.01*. The mean temperature

variation along the channel is almost linear as in the insulated case. Since there is a little energy transfer from the fluid to the outside of the channel, in other words; since there is a little energy loss, the fluid temperature is increasing linearly.

In Figure 9.28(d), the outlet temperature variation with Y-axis is demonstrated for *Da=0.01*. The outlet temperature has its maximum value in porous layer, and in this layer, there is no significant temperature change along Y-axis because of the high conductivity. This figure is just the line where *X=10*, in Figure 9.28(b).

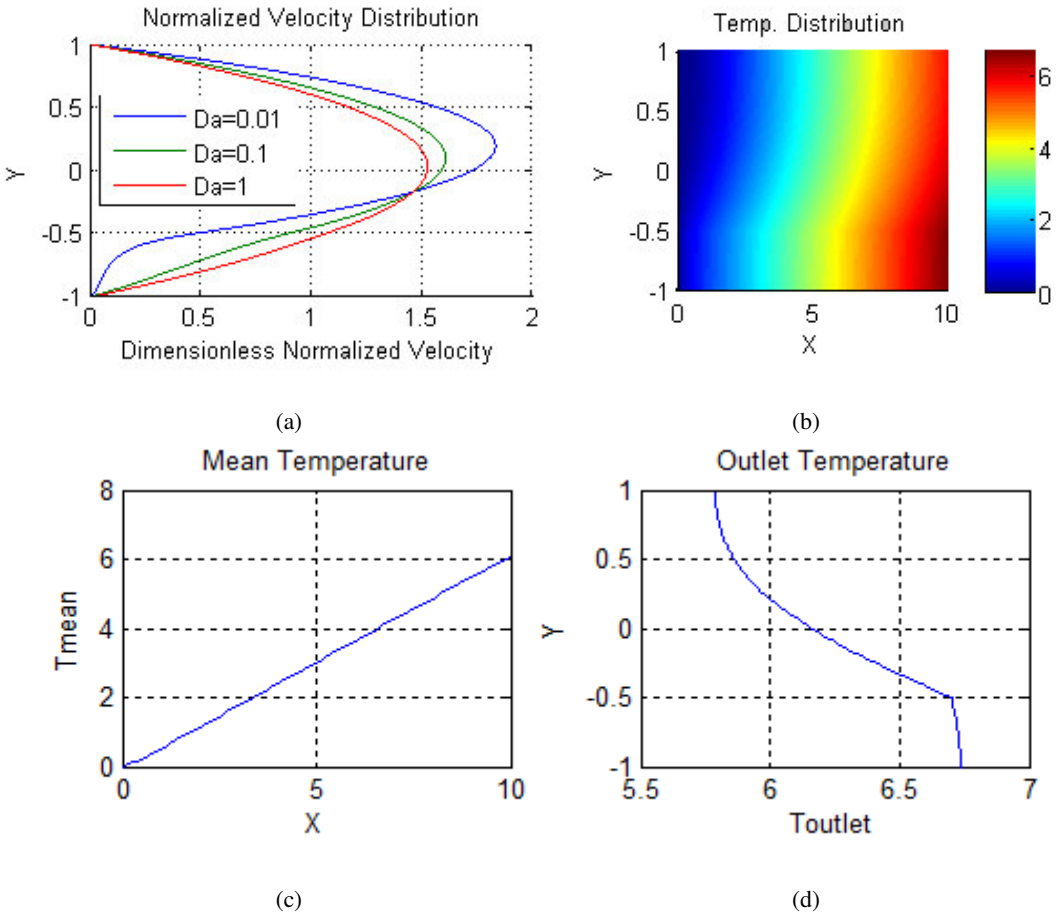

Figure 9.28. (a)Velocity distributions for three different darcy numbers, (b) temperature distribution for Da=0.01, (c) mean temperature along the X-axis for Da=0.01, (d) outlet temperature distribution along the Y-axis for Da=0.01

In Figure 9.29, outlet temperatures of the flows with three different Nusselt numbers are shown. In this flow Darcy number is 0.001 and lower half of the channel is filled with porous medium. The viscosity and conductivities are *1.1* and *1*, respectively. Decreases in the Nusselt numbers increase the outlet temperatures. For small Nusselt numbers, the upper wall insulation is greater. Hence, the energy losses are minimized. In Figure 9.30, Nusselt number effects on mean temperatures in the channel are

demonstrated for the same flow as Figure 9.29. For greater Nusselt number flows, the mean temperatures have some constant values after specific points. After these points, the flow becomes thermally fully developed. When *Nu=0.01,* the flow is held in the thermally developing region.

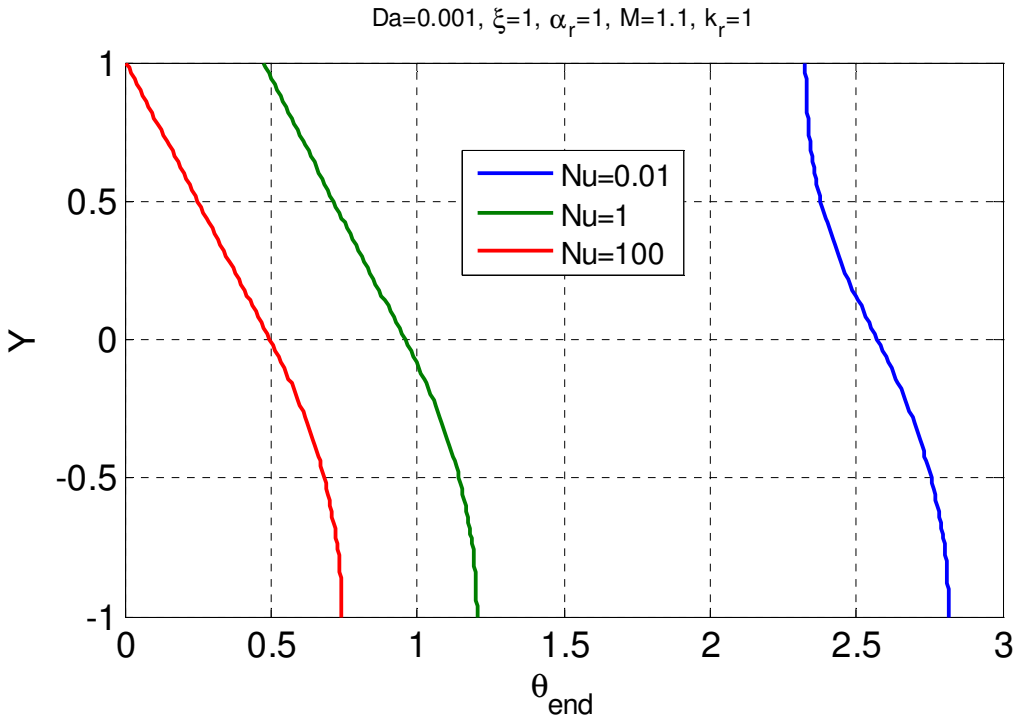

Figure 9.29. Comparison of outlet temperatures with three Nusselt number flows

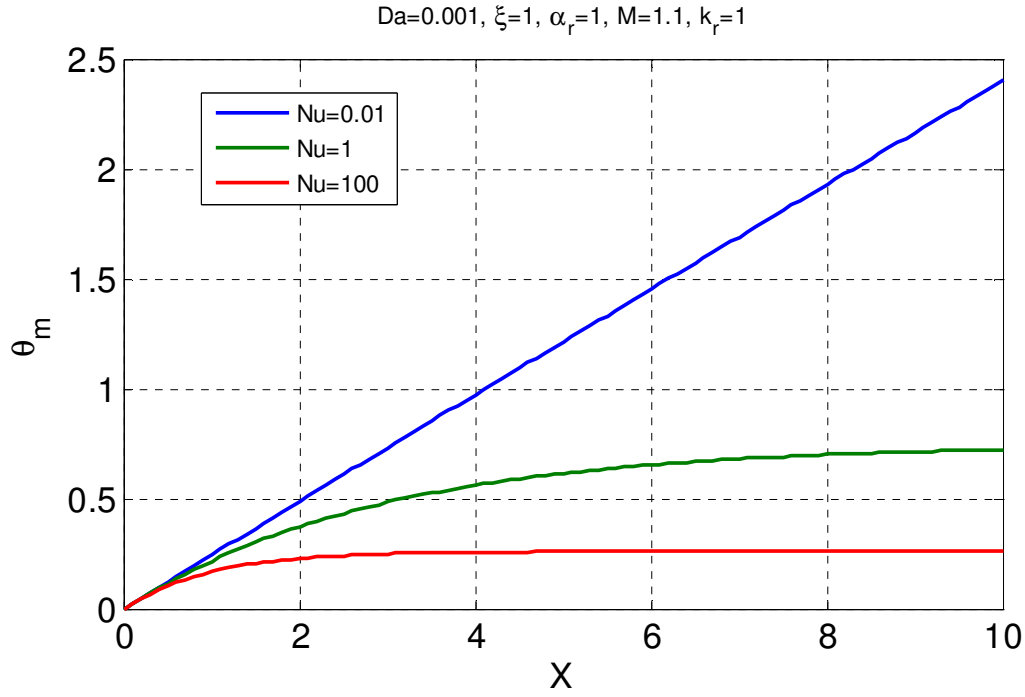

Figure 9.30. Comparison of mean temperatures with three Nusselt number flows

In Figure 9.31, the conductivity effects on outlet temperatures are investigated for the flows with specified porous thickness, *Nu*, and *Da*. In this case, the lower half of the channel is filled with porous media and *Nu* and *Da* are *0.01* and *0.001*, respectively. The viscosity ratio is *1.1*. It is obvious that, using porous medium with conductivity ratio of lower than *1*, is not appropriate for the solar air heater collector, since the clear fluid flow provides greater outlet temperatures. However, using porous layer with high conductivity ratio increases the outlet temperature, significantly. This conclusion is also applicable for the mean temperature distribution along the X-axis, as shown in Figure 9.32.

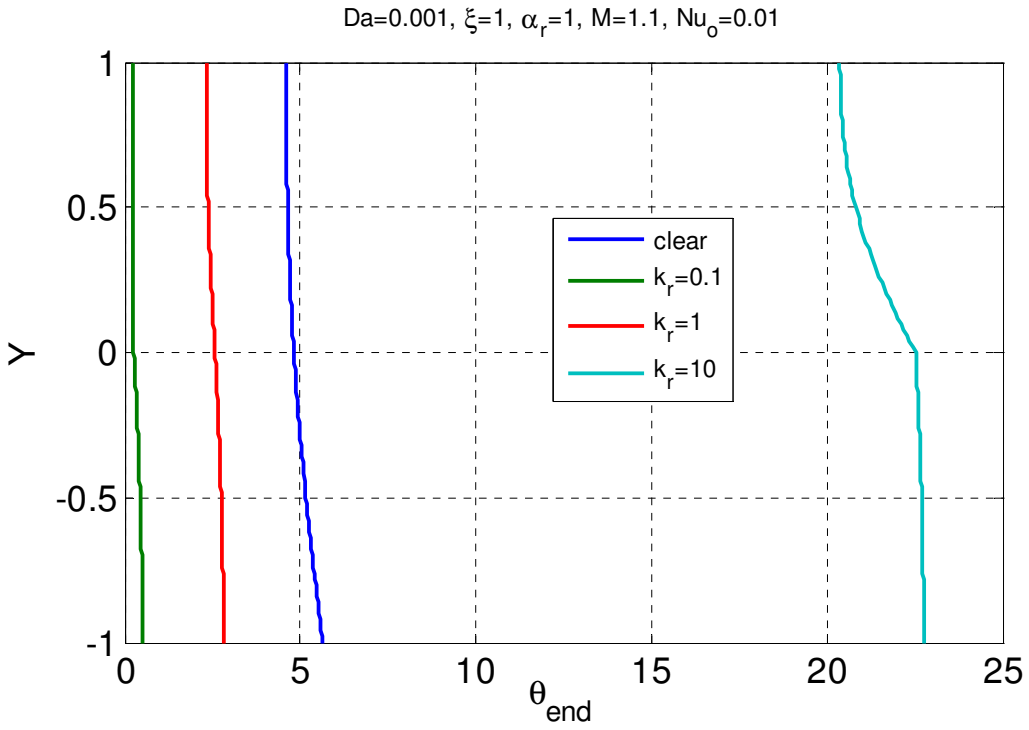

Figure 9.31. Comparison of outlet temperatures with three porous media with different conductivity ratios (Nu=0.01)

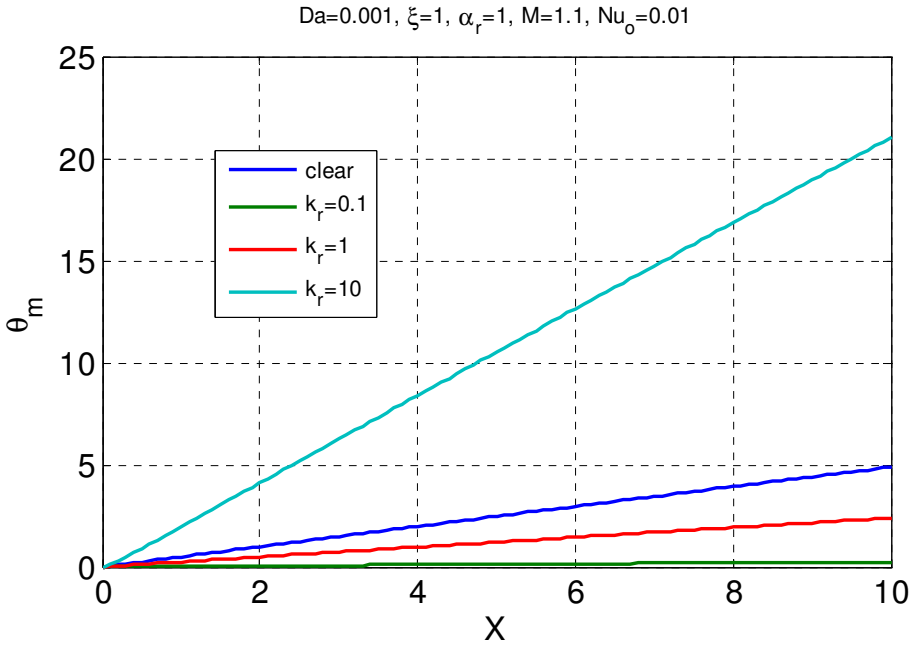

Figure 9.32. Comparison of mean temperatures with three porous media with different conductivity ratios (Nu=0.01)

In Figures 9.33 and 9.34, the effects of the porous thickness on temperature profiles are shown. The conductivity ratio is set as *10* and the Darcy number is *0.001*. The upper wall is almost perfectly insulated, such as the Nusselt number at the upper wall is *0.01*. It is clear that, for the thicknesses smaller than *0.5*, using porous medium is not applicable. For $\xi=1$, the outlet temperatures increase considerably, and further porous layer addition will increase the temperature, significantly. The outlet temperature of the fluid flows in a solar air heater collector increases with the thickness of the porous medium.

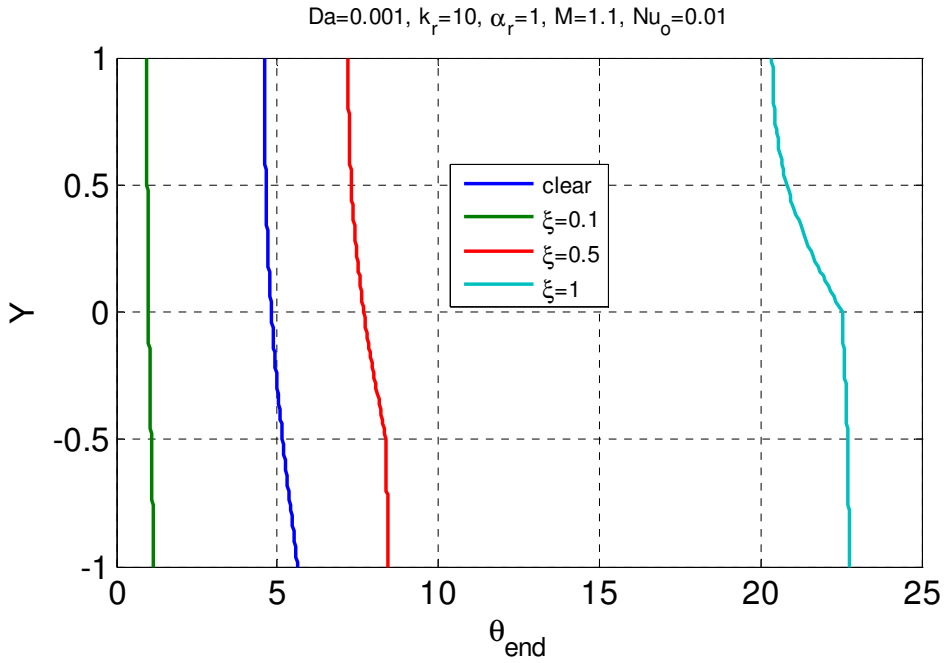

Figure 9.33. Comparison of outlet temperatures with three different porous media thicknesses

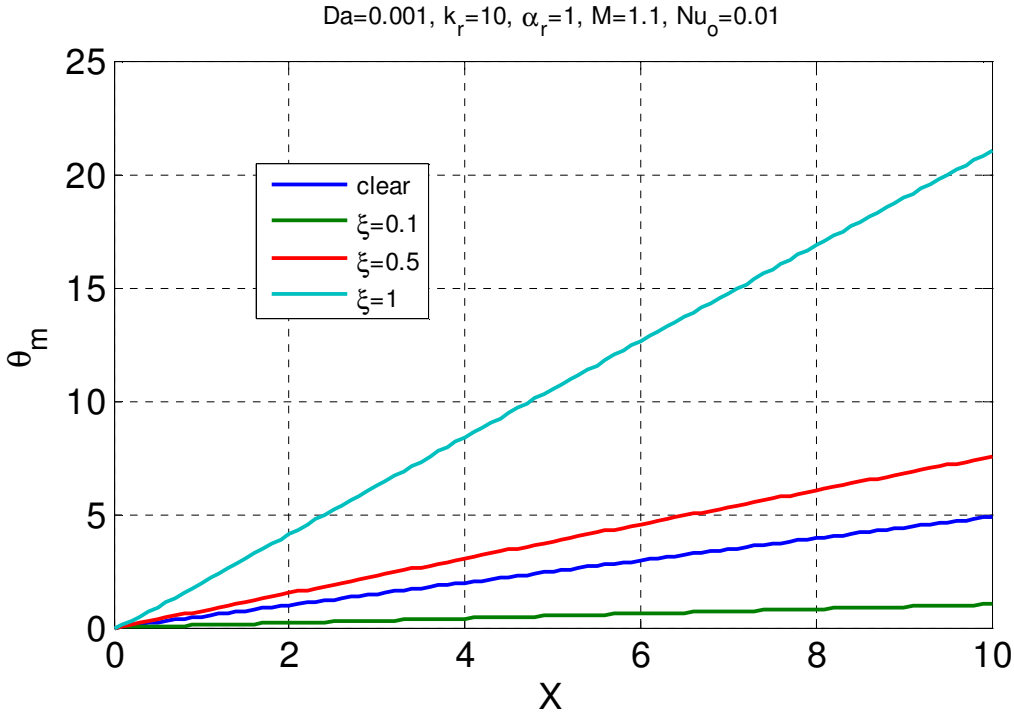

Figure 9.34. Comparison of mean temperatures with three different porous media thicknesses

In Figure 9.35, the heat transfer increment ratio, the pressure-drop increment ratio and overall performance are plotted against the porous thickness in a solar air heater collector. In this case, the thermal conductivity ratio is *10000* and the Darcy number is *0.001*. As seen in the Figure 9.35(a), thermal performance of the air solar

heater collector is investigated by plotting the heat transfer increment ratio versus the porous layer thickness. For the porous thicknesses from zero to 0.6,ε_{th} increases almost linearly and it has its maximum value where the porous thickness is about *0.6*. After that point, it decreases. In Figure 9.35(b), the change of the need in fan power is investigated by plotting the pressure-drop increment ratio versus the porous layer thickness. Since, the flow velocity is decreased by using porous media, it is expected that the pressure-drop will increase if the channel is assisted with porous media. As expected, it can be clearly seen in Figure 9.35(b) that, if the porous layer thickness increases, so does the pressure-drop along the channel. Finally, a combined thermal-hydraulic analysis is performed by plotting the overall performance against the porous layer thickness and it is found that the overall performance has its maximum value where the porous layer thickness is about 0.4. After that point, ε decreases, and for porous layer thicknesses larger than about *1.3*, the pressure-drop effects become dominant.

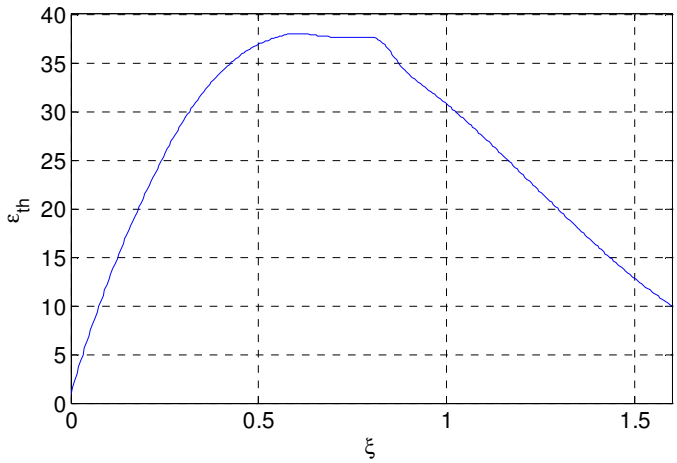

(a)

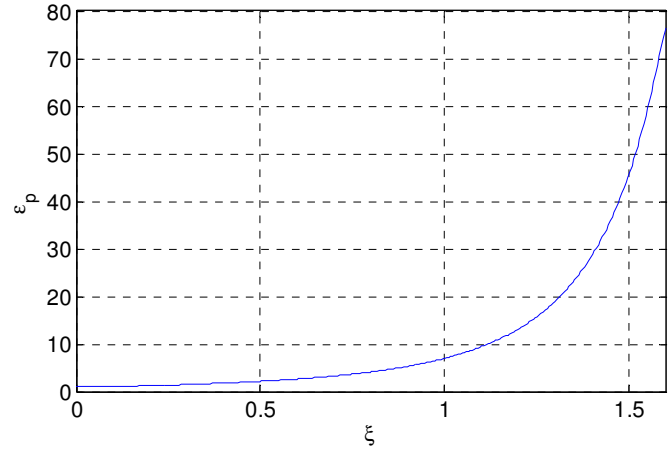

(b)

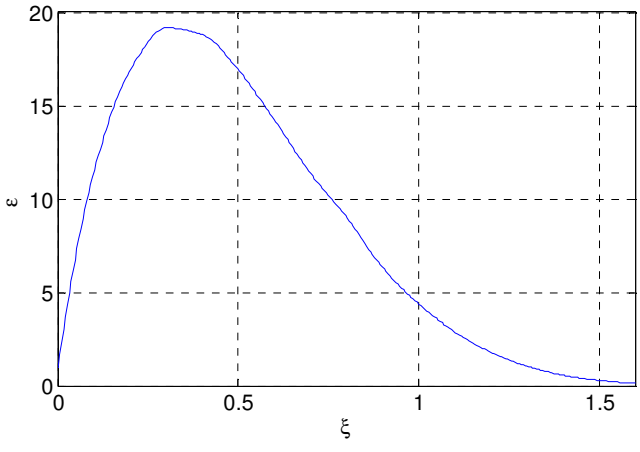

(c)

Figure 9.35. Performance analysis of the solar air heater collector assisted by a porous medium with kr=10000. (a)Heat transfer increment ratio against the porous thickness ($0 \leq \xi \leq 1.6$) (a)Pressure drop increment ratio against ξ, (c)Overall performance against ξ

CHAPTER 10

CONCLUSION

In this study; heat transfer enhancement by using porous media is investigated for a solar air heater collector. The study is started with heat and fluid flow analysis for a flow in a clear fluid channel. The channel walls are subjected to equal heat fluxes. The dimensionless heat transfer coefficient, the Nusselt number, was found 4.1176. The friction factor, $f\,Re$, is found *24* for clear flow. Then, the channel was fully filled by porous medium. Fluid and heat flow analyses were performed for four different dimensionless permeabilities (Darcy numbers). It is found that the increasing Darcy number makes the flow resemble to clear one. While increasing the Darcy number, the Nusselt number approaches to 4.1176. For the porous medium with a very high Darcy number, it becomes exactly 4.1176. When Darcy number decreases, the Nusselt number increases and more heat transfer will be achieved. Three new parameters are introduced as heat transfer increment ratio, pressure drop increment ratio and the overall performance. Both the heat transfer increment and pressure drop increment ratios increased with decreasing Darcy number. The overall performance remains less than *1* for all Darcy number flows in full porous channel.

In Chapter 5, asymmetric heat fluxes were subjected to both walls. It is concluded that the overall Nusselt number, hence the total heat transfer rate, does not been affected by the asymmetry of the heating. On the other hand, bottom and top wall Nusselt numbers are defined to determine heat transfer ratenear the boundaries. They are found that heat transfer rate from the pale is considerably affected from the heat flux ratio. There are some critical points in which the heat transfer directions are changed.

A porous medium is located at the centre of the channel symmetrically in Chapter 6. The porous length is changed and the Nusselt number has a maximum value for specific thicknesses. For instance, for a channel with $Da = 10^{-5}$, the maximum heat transfer can be achieved by locating the porous layer with a thickness of 0.92 at the centre of the channel. After that point, further porous structure addition to the channel will decrease the Nusselt number and it falls to 5.13, which is the dimensionless convective heat transfer coefficient for the full porous case. Therefore, it would be logic

to fill the 92% of the channel with that porous structure (with $Da=10^{-5}$) instead of fully filling it. The overall performance remains less than *1* for all porous layer thicknesses.

In Chapter 7, the porous medium was located asymmetrically in the channel. The channel walls were subjected to equal heat fluxes. As in Chapter 5, two individual Nusselt numbers for both walls were investigated. For the porous length of 1; for both walls, Nu has its maximum value, where the porous medium location is 0.6 units far from the wall whose heat transfer coefficient was investigated.

In Chapter 8, heat and fluid flow in a solar air heater collector is investigated. It is assumed that all the radiation is absorbed by the porous medium. The effects of the porous layer thickness, the upper wall Nusselt number (the energy loss), and the ratio of the effective conductivity and the conductivity of the fluid on outlet and mean temperatures are investigated. It is concluded that, the temperature increases with increasing porous layer thickness, decreasing the Nusselt number, and increasing the conductivity ratio. For relatively high conductivity ratios; the heat transfer increment ratio becomes dominant to pressure drop increment ratio when porous layer thickness is between *0.5* and *1.3*. Furthermore, using a porous medium-fluid pair which has a conductivity ratio less than *1* will not help the heat transfer enhancement.

REFERENCES

M.K. Alkam and M.A. Al-Nimr, Transient non-Darcian forced convection flow in a pipe partially filled with a porous material, hf. J. Heat Mass Transfer. Vol. 41, No. 2, pp. 347-356, (1998)

M.K. Alkam, M.A. Al-Nimr, M.O. Hamdan, Enhancing heat transfer in parallel-plate channels by using porous inserts International Journal of Heat and Mass Transfer 44 931-938 (2001)

M.A. Al-Nimr and M. K. Alkamm. A modified tubeless solar collector partially filled with porous substrate, Renewable Energy, Vol. 13, No. 2, pp. 165-173, (1998)

G. Alvarez, J. Arce, L. Lira, M.R. Heras, Thermal performance of an air solar collector with an absorber plate made of recyclable aluminum cans, Solar Energy 77 107–113(2004)

M.M. Awartani,M.M., M.H. Hamdan, M.H.:Fully developed flow through a porous channel bounded by flat plates. Appl. Math. Computation 169,749-757 (2005)

A.P.M. Baede, E. Ahlonsou, Y. Ding, D. Schimel, "Natural Forcing of the Climate System, Chapter 1: The Climate System: an Overview". Intergovernmental Panel on Climate Change. Retrieved 2007-09-29 (2007)

A. Bejan, A.D. Kraus, Heat Transfer Handbook, Wiley (2003)

A. Bejan, I. Dincer, S. Lorente, A.F. Miguel, A.F. Reis, Porous and Complex Flow Structures in Modern Technologies. Springer, New York (2004)

D. Degan, S. Zohoun, P. Vasseur, Forced convection in horizontal porous channels with hydrodynamic anisotropy. Int. J. Heat Mass Transfer 45, 3181-3188 (2002)

DOE (Department of Energy), “Independent Statistics and Analysis - U.S. Energy Information Administration Website - 2011”, (http://tonto.eia.doe.gov/)

D.A. Nield and A. Bejan, Convection in Porous Media, Springer, New York, (2006)

S.D. Harris, D.B. Ingham, I. Pop, Mixed convection boundary-layer flow near the stagnation point on a vertical surface in a porous medium: Brinkman model with slip.Transport Porous Media **77**, 267-285 (2009)

K. Hooman, A perturbation solution for forced convection in porous-saturated duct. J. Comput. Appl. Math. 211, 57-66 (2008).

K. Hooman, A.A. Ranjbar-Kani, Forced convection in a fluid-saturated porous-medium tube with isoflux wall. Int. Comm. Heat Mass Transfer 30, 1015-1026 (2003)

K. Hooman, A.A. Ranjbar-Kani, A perturbation based analysis to investigate forced convection in a porous saturated tube. J. Comput. Appl. Math. 162, 411-419 (2004)

D.B. Ingham, I. Pop (eds.), Transport Phenomena in Porous Media. Elsevier, Oxford (2005).

F.P. Incropera, D.P. DeWitt, Introduction to Heat Transfer, John Wiley and Sons (1996)

M. Kaviany, Laminar flow through a porous channel bounded by isothermal parallel plates. Int. J. Heat Mass Transfer 28, 851-858 (1985)

A.V. Kuznetsov, D.A. Nield, Thermal instability in a porous medium layer saturated by a nanofluid: Brinkman model. Transport Porous Media, DOI 10.1007/s11242-009-9413-2. (2009)

A.V. Kuznetsov, D.A. Nield, Forced convection in a channel partly occupied by a bidisperse porous medium: Asymmetric case, International Journal of Heat and Mass Transfer 53, 5167–5175 (2010)

M. Najjari, S.B. Nasrallah, Effects of latent heat storage on heat transfer in a forced flow in a porous layer, International Journal of Thermal Sciences 47, 825–833 (2008)

A. Nakayama, PC-Aided Numerical Heat Transfer and Convective Flow, Taylor Francis Inc, United States (1998)

P. Naphon, Effect of porous media on the performance of the double-pass flat plate solar air heater, International Communications in Heat and Mass Transfer 32, 140-150 (2005)

D.A. Nield, Forced convection in a parallel plate channel with asymmetric heating. Int. J. Heat Mass Transfer 47, 5609-5612 (2004)

D.A. Nield, Erratum to “Forced convection in a parallel plate channel with asymmetric heating”. I. J. Heat Mass Transfer 51, 2108 (2008)

D.A. Nield, A.V. Kuznetsov, M. Xiong: Effects of viscous dissipation and flow work on forced convection in a channel filled by a saturated porous medium. Transport Porous Media 56, 351-367 (2004)

Y. Ould-Amer, S. Chikh, K. Bouhadef, G. Lauriat, Forced convection cooling enhancement by use of porous materials, International Journal of Heat and Fluid Flow 19 , 251±258 (1998)

I. Pop, D.B. Ingham, Convective Heat Transfer: Mathematical and Computational Modeling of Viscous Fluids and Porous Media. Pergamon, Oxford (2001)

S.B. Prasad, J.S. Saini, Krishna M. Singh, Investigation of heat transfer and friction characteristics of packed bed solar air heater using wire mesh as packing material, Solar Energy 83, 773–783 (2009)

V.V. Satyamurty, D. Bhargavi, Forced convection in thermally developing region of a channel partially filled with a porous material and optimal porous fraction, International Journal of Thermal Sciences 49, 319–332 (2010)

R.K. Shah, A.L. London, Advances in Heat Transfer, Supplement 1. Academic Press, New York (1978)

K. Sopian, Supranto, W.R.W. Daud, M.Y. Othman, B. Yatim, Thermal performance of the double-pass solar collector with and without porous media, Renewable Energy 18, 557±564 (1999)

K. Sopian, M.A. Alghoul, E.M. Alfegi, M.Y. Sulaiman, E.A. Musa Evaluation of thermal efficiency of double-pass solar collector with porous-nonporous media, Renewable Energy 34, 640-645 (2009)

A. Sreekumar, Techno-economic analysis of a roof-integrated solar air heating system for drying fruit and vegetables, Energy Conversion and Management 51 2230–2238(2010)

S. Tada, K. Ichimiya, Analysis of laminar dissipative flow and heat transfer in a porous saturated circular tube with constant wall heat flux. Int. J. Heat Mass Transfer 50, 2406-2413 (2007)

N.S. Thakura, J.S. Sainib, S.C. Solankib, Heat transfer and friction factor correlations for packed bed solar air heater for a low porosity system, Solar Energy 74, 319–329 (2003)

P. Vadasz (ed.), Emerging Topics in Heat and Mass Transfer in Porous Media. Springer, New York (2008)

K. Vafai (ed.), Handbook of Porous Media (2nd edition). Taylor & Francis, New York (2005)

(Chapter 3, by Liu, S., Masliyah J.H., pp. 111)

K. Vafai, Porous Media: Applications in Biological Systems and Biotechnology. CRC Press, Tokyo (2010)

C. Yang, W. Liu, and A. Nakayama, Forced Convective Heat Transfer Enhancement in a Tube with its Core Partially Filled with a Porous Medium, The Open Transport Phenomena Journal, 1, 1-6, (2009)

APPENDIX A

THE COMPATIBILITY CONDITION

The compatibility condition results from the definition of the mean temperature, which is written in Eq. A.1.

$$T_m = \frac{\int_{-H}^{H} \rho c_p u T dy}{\int_{-H}^{H} \rho c_p u dy} \tag{A.1}$$

Since the thermo-physical properties are accepted to be constant, and then the density and the constant pressure specific heat of the fluid can be taken out of the integrals. After a little manipulation, Eq. A.1 becomes into the form as follows.

$$T_m = \frac{\int_{-H}^{H} u T dy}{\int_{-H}^{H} u dy} \tag{A.2}$$

Another description for the denominator of Eq. A.2 can be derived by using the definition of the mean velocity written below.

$$u_m = \frac{\int_{-H}^{H} u dy}{\int_{-H}^{H} dy} = \frac{\int_{-H}^{H} u dy}{2H} \Rightarrow \int_{-H}^{H} u dy = 2Hu_m \tag{A.3}$$

Inserting the Eq. A.3 into the equation A.2, the following result is obtained.

$$T_m = \frac{\int_{-H}^{H} u T dy}{2Hu_m} \tag{A.4}$$

After some manipulations shown in Eq. A.6 and using the definition of the normalized velocity (Eq. A.5), Eq. A.7 is obtained.

$$\widehat{u} = \frac{u}{u_m} \tag{A.5}$$

$$2HT_m = \frac{\int_{-H}^{H} uTdy}{u_m} = \int_{-H}^{H} \frac{u}{u_m} Tdy = \int_{-H}^{H} \hat{u}Tdy \tag{A.6}$$

$$2HT_m = \int_{-H}^{H} \hat{u}Tdy \tag{A.7}$$

At this point, the temperature and *dy* in the integral should be converted to the dimensionless ones, which are defined as in Eq. A.8 and after further manipulations Eq. A.9 is obtained.

$$\theta = \frac{T - T_w}{T_m - T_w}, \quad Y = \frac{y}{H} \tag{A.8}$$

$$\begin{aligned} 2HT_m &= \int_{-H}^{H} \hat{u}\left[\theta(T_m - T_s) + T_s\right] d(HY) \\ 2HT_m &= H\int_{-1}^{1} \hat{u}\left[\theta(T_m - T_s) + T_s\right] dY \\ 2T_m &= \int_{-1}^{1} \hat{u}\left[\theta(T_m - T_s) + T_s\right] dY \\ 2T_m &= (T_m - T_s)\int_{-1}^{1} \hat{u}\theta dY + T_s\int_{-1}^{1} \hat{u}dY \end{aligned} \tag{A.9}$$

The last term on the right hand side of the Eq. A.9, contains the integration of the normalized velocity. This integration results as *2*, as shown below.

$$\int_{-1}^{1} \hat{u}dY = \frac{\int_{-1}^{1} udY}{u_m} = \frac{\int_{-1}^{1} udY}{\frac{\int_{-1}^{1} udY}{2}} = 2 \tag{A.10}$$

After applying this result to Eq. A.9, the equation called the compatibility condition is obtained as written in Eq. A.11.

$$\int_{-1}^{1} \hat{u}\theta dY = 2 \tag{A.11}$$

APPENDIX B

THE NUMERICAL SOLUTION PROCEDURE

In this study, numerical results are also obtained for the governing equations for energy and momentum. Finite difference method under the given boundary conditions is used. However, the following transformation is used for compatibility condition. The function of is defined such that;

$$\psi = \frac{\theta}{Nu} \tag{B.1}$$

The overall Nusselt number is constant for fully developed flow in a channel. Hence, a new form of dimensionless heat transfer equation and boundary conditions based on ψ function can be obtained as in Eqs. B.2 and B.3, respectively.

$$\frac{d^2\Psi}{dY^2} + \frac{1}{2}\hat{u} = 0 \tag{B.2}$$

and

$$\Psi(-1) = \beta / Nu, \quad \Psi(1) = -\beta / Nu \tag{B.3}$$

These boundary conditions are used for the asymmetric cases. In symmetric cases, at the boundaries the dimensionless temperatures are zero.

Furthermore, the new form of the compatibility condition is:

$$\int_{-1}^{1} \Psi \hat{u} dY = 2 / Nu \tag{B.4}$$

The boundary conditions of new form of heat transfer equation (Eq. B.4) depend on overall Nusselt number, which is unknown. The distribution of was found according to an initial guess value for overall Nusselt number. Then, a new value for Nusselt number is found by using the compatibility condition (Eq. B.4). The new value of overall Nusselt number was used to obtain new distribution of and consequently the new value for overall Nusselt number was found. The procedure continued until the

absolute difference between the new and old calculated Nusselt number became less than 10-9. The number of nodes in Y-direction was 200 in the performed numerical study.